Design, Implementation and Validation of an Exoskeletal Robot for Locomotion Studies in Rodents

ARCHIVES
MASSACHUSETTS INSTITUTE OF TECHNOLOGY
JUN 28 2012
LIBRARIES

by

Yun Seong Song

M.S., Carnegie Mellon University (2006)
B.S. and B.S.E., Seoul National University (2004)

Submitted to the Department of Mechanical Engineering
in partial fulfillment of the requirements for the degree of

Doctor of Philosophy

at the

MASSACHUSETTS INSTITUTE OF TECHNOLOGY

June 2012

© Massachusetts Institute of Technology 2012. All rights reserved.

Author . . . .
Department of Mechanical Engineering
May 11, 2012

Certified by . . . .
Neville Hogan
Professor
Thesis Supervisor

Accepted by . . . .
David E. Hardt
Chairman, Department Committee on Graduate Students

Design, Implementation and Validation of an Exoskeletal Robot for Locomotion Studies in Rodents

by

Yun Seong Song

Submitted to the Department of Mechanical Engineering
on May 11, 2012, in partial fulfillment of the
requirements for the degree of
Doctor of Philosophy

Abstract

Growing interest in robotic treatment of patients with neurological injury motivates the development of therapeutic robots for basic research into recovery. Though humans are the ultimate beneficiaries, basic research frequently involves rodent models of neurological injury, which motivates robotic devices that can interact with rats or mice. Currently, available apparatus for locomotion studies of rodents is built upon treadmills, which simplify the design and implementation but also restrict the scope of possible experiments. This is largely due to the treadmill's single-dimensional movement and the lack of accommodation for natural or voluntary movement of the animal.

In order to open up new possibilities for locomotion studies in rodents, this work introduces newly developed apparatus for locomotion research in rodents. The key concept is to allow maximal freedom of voluntary movement of the animal while providing forceful interaction when necessary. Advantages and challenges of the proposed machine over other existing designs are discussed. Design and implementation issues are presented and discussed, emphasizing their impact on free, voluntary, movement of the animal. A live-animal experiment was conducted to verify the design principles. Unconstrained natural movement of the animal was compared with movement with the overground robot attached. The compact, overground design and back-drivable implementation of this robot allow novel experiments that involve open-space, free (or interactive) locomotion of the animal.

Thesis Supervisor: Neville Hogan
Title: Professor

Acknowledgements

There was a time when I was imagining the moment of completing my thesis and writing this acknowledgement, full of self-confidence and pride. Now, being present at that very moment, I have realized how this work could not have been possible without the support from great many people around me. I can only mention a few here – but I thank everyone.

Meeting Neville Hogan is probably the most wonderful thing that will have happened in my academic life. I am privileged to have had the opportunity to work with him. As a thesis advisor, his keen physical insight and clear, objective thoughts were always inspiring. He was a sharp advisor, an enthusiastic discussion partner, and a lethal critic that never fails to hit the mark. As a mentor, he was always open to concerns of his students and provided humble advices that resonated. As a person, he has quite an interesting character that I could only get a glimpse of. I wish I had the chance to talk to him outside of work.

Professors Russell Tedrake, Sangbae Kim and Richard Marsh constituted a superb committee. Coming from distinct disciplines, these experts helped shape my thesis the way it is now. They were available to provide invaluable insights on the apparatus design, control implementation and animal locomotion – and in every other aspect. It was always a humbling and exiting experience to discuss my work with them, individually or as a group.

I would like to thank the past and present Newman Lab members for making my days at MIT memorable. Dr. Hermano Igo Krebs was always an excellent source of information on hardware implementation. Laura Dipietro was very supportive of my work and my career in general, and I always enjoyed the conversations we had on vast array of topics. Jooeun Ahn has been a good friend of mine since before joining this group – and will continue to be so. Hyunglae Lee and Dan Klenk were especially helpful with animal experiments. Where help was needed, they were

superb technical assistants. Everywhere else, they were always a good company to have. Past members of the lab, namely Mohammad, Panagiotis, and Seungjae, are my respectful academic seniors with whom I had the pleasure to discuss my work with. I would also like to thank the newer, north-mezzanine members, Tyler Susko, Will Bosworth and Konstantinos Michimizos, for being a joyful presence in the lab. Finally, Marjorie Joss has been very helpful and patient as I placed a large numbers of orders through her.

As the apparatus design evolved, the focus shifted towards conducting animal experiment. On rat experiments, Dr. Matthew Wilson provided critical advices that greatly influenced the experiment design. Dr. Simon Giszter of Drexel University, PA, welcomed inquiries through emails and in person. Dr. Gang Song shared a lot of his time to help me initiate my very first animal experiment. Dr. Allison Hayward gladly served as an overseeing animal expert throughout the experiments. Catrina Wong, a veterinarian, was a very pleasant person to work with who were always offering helping hands.

I give my big thanks and love to my parents who are in Korea. I am sure they are as relieved to see this thesis as I am now. I cannot thank them enough for the amount of support and encouragement throughout my life. Yun-jeong is my sister, my life-long friend and a mentor to whom I owe a lot. Thank you, my sister, mom, and dad.

And finally, I thank my true companion, Sangeun. Through all the challenges and years of hardship, she has been on my side strong and patient. She was the one who truly understood and supported my views and actions in the past few years. Her presence made me rethink what happiness in life is about. Thank you, Sangeun.

This work was supported by New York State Center of Research Excellence CO19772, the Eric P. and Evelyn E. Newman Fund, Gloria Blake fund, and Samsung Scholarship.

Contents

Abstract 3

Acknowledgements 4

1 Introduction 23

1.1 Spinal Cord Injury 24

1.1.1 Number of Patients 25

1.1.2 Severity of Injury 25

1.1.3 Life Expectancy and Lifetime Cost 26

1.2 Methods to Aid Recovery from SCI 28

1.2.1 Conventional Methods 28

1.2.2 Current Progress in the Field 29

1.3 Using Therapeutic Robots 35

1.3.1 Upper Extremity Robotic Therapy for Stroke 35

1.3.2 Lower Extremity Robots for Neurological Injuries 36

1.4 Summary, Goal and Thesis Organization 37

2 Central Nervous System and Locomotion 39

2.1 Motor Function-related Anatomy of the CNS 39

2.1.1 The Spinal Cord 40

2.1.2 Corticospinal Tract 40

2.1.3 Sensory Inputs to the Brain 41

2.2 Sensory Information on Interlimb Coordination 42

2.2.1 Studies in Cats 43

2.2.2 Studies in Other Animals 44

2.2.3 Studies in Humans 44

2.2.4 Implications for Recovery from SCI 46

2.3 Studies on Neonatal Rats and Rat Embryos 46

2.3.1 Locomotor studies on the neonatal spinal cord, *in vitro* preparation 46

2.3.2 Locomotor studies in rats, *in vivo* preparation 47

2.3.3 Development of the rat spinal cord 48

2.3.4 Implication for Recovery from SCI 50

2.4 Spinal Network Models 51

2.4.1 Interlimb coordination 51

2.4.2 Lower limb coordination 52

2.4.3 Implications for SCI research 54

2.5 Discussion 54

2.5.1 Using Animal Models 54

2.5.2 Implications for the Apparatus Design 54

3 Apparatus Concept and Requirements 57

3.1 Requirements for the Apparatus 57

3.2 Treadmill-based Apparatus 58

3.2.1 The Rat Stepper 59

3.3 Design Concept 62

3.3.1 Early Design Concepts 62

3.3.2 Current Design Concept 64

3.4 Technical Challenges 67

3.4.1 Interfacing with the Animal 67

3.4.2 Minimum Encumbrance to the Animal 68

3.4.3 Lack of Similar Precedents 69

4 Design and Implementation of the Rat Module 71

4.1 Design Consideration 71

4.1.1 Number of Actuated Degrees of Freedom 71

4.1.2 Actuator Selection 73

4.1.3 Discussion of Motor Selection 75

4.2 Detailed Configuration 78

4.2.1 Overall Design 78

4.2.2 Robotic Arm 83

4.2.3 Custom Force Sensor 85

4.2.4 Base and Cover Design 88

4.2.5 Biomechanical Coupling 89

4.3 Fabrication 92

4.4 Supporting Hardware 94

4.5 Summary and Discussion 95

5 Body-Weight Support System 98

5.1 Motivation 98

5.2 Body-Weight Support System (BWSS) 99

5.2.1 Configuration 99

5.2.2 The R19 Robot Arm 101

5.4 Vision Feedback 104

5.4.1 Why Use Vision Feedback? 104

5.4.2 Image Processing 106

5.4.3 Camera Attachment 110

5.5 Weight Bearing 110

5.6 Wiring 112

5.7 Performance 114

5.8 Discussion 116

6 Simple and Robust Method to Manage Uncertainties with Discrete-State Control 118

6.1 Difficulties due to the Current Selection of the Motor 119

6.1.1 Position Control in the Presence of Large Static Friction 119

6.1.2 Improving Back-Drivability 122

6.2 Using Discrete-State Control 127

6.2.1 The DSC-Scheme 127

6.2.2 Using DSC to Modulate Position 128

6.2.3 Using DSC to Improve Back-Drivability 129

6.2.4 Another Example - Torque Modulation with a Series Damper 130

6.3 Formulation of Discrete-state control 134

6.3.1 Formulation 134

6.3.2 Heuristic Method to Select the Parameters 135

6.3.3 Simulation Examples 139

6.4 Discussion 142

6.4.1 System order and DSC 143

6.4.2 Comparison with Sliding Mode Control (SMC) 146

6.4.3 Other remarks 148

6.5 Conclusion 150

7 Validation Experiments with Rodents: Part I 152

7.1 Motivation 152

7.1.1 Questions Addressed in the Experiments 153

7.2 Methods 154

7.2.1 Experiments Using a 'Mockup' 154

7.2.2 Powered Device on an Anesthetized Animal 156

7.2.3 Rat Module with Force Feedback 157

7.2.4 Addressing Anxiety of the Animal 158

7.3 Results 159

7.3.1 Coupling Strategy 159

7.3.2 Kinematic Constraint 160

7.3.3 Apparatus Function 160

7.3.4 Animal Anxiety 162

7.4 Discussion 164

7.4.1 Anxiety was Reduced through Training 164

7.4.2 Coupling Strategy and Kinematic Constraint 164

7.4.3 Apparatus Function 165

7.4.4 Other Remarks 168

8 Validation Experiments with Rodents: Part II 170

8.1 Experiment Setup 170

8.1.1 Encouraging Forward Locomotion 172

8.2 Results 175

8.2.1 Observed Movements 175

8.2.2 Stride Length 175

8.2.3 Stride Duration 175

8.2.4 Swing Duration per Stride Duration (Duty Cycle) 176

8.2.5 Interaction Force 179

8.2.6 End Effector Trajectory 181

8.3 Discussion 182

9 Conclusion 188

9.1 Implication for the Field of Research 188

9.2 Future Prototypes 189

9.3 Summary 191

A Linkage Forward Kinematics and Jacobian 193

B Programming the R19 Robot 198

B.1 Roboforth 198

B.2 Position Control of R19 199

C Experiment Procedure 206

References 214

List of Figures

Fig. 1-1. Step training with weight support and manual assistance on a treadmill [**5**]. 29

Fig. 1-2. Schematic illustrating changes of inhibitory synapses (gray dots) around the extensor (labeled as E) or flexor (F) neuron groups in cats under various motor training conditions. Before injury (A), the number of inhibitory synapses in each neuron group is small. After the spinal transection (ST), the populations of the inhibitory synapses vary depending on the types of training. It can be seen that the training of a certain locomotion task decreases the number of inhibitory synapses in the neuron group that is responsible for that specific task. [**26**]. 33

Fig. 2-1. Schematic of the spinal cord, cross-section, simplified. 1: Spinal Ganglion. 2: Dorsal root. 3: White matter. 4: Gray matter, dorsal horn. 5: Gray matter, ventral horn. 6: Ventral root. 41

Fig. 2-2. Schematic of corticospinal tract. The neurons originate from the motor cortex (top). 80% of them decussate to the contralateral side in the medulla oblongata (middle). These neurons make synaptic connections to interneurons or directly to motoneurons within the gray matter (bottom). 41

Fig. 2-3. A photo of a thymidine radiogram of an embryonic rat spinal cord [**78**]. The cell nuclei are clearly visible. 49

Fig. 2-4. Diagram of the spinal cord, muscle and relevant neurons. 50

Fig. 2-5. Schematic of a postulated variation of neural movement control during different motor tasks [**83**]. Depending on the task, the brain may a) inhibit interlimb coordination, or b) promote cross-talk while minimizing its control over the upper limb. 53

Fig. 2-6. Left: Schematic of the half-center model of Brown and Lundberg. Each of the two centers (blue circles on the top corners) mutually inhibits the other. Right: The Haken-Kelso-Bunz (HKB) potential described by $V(\varphi) = a\cos\varphi - b\sin\varphi$, where φ is the relative phase between the motion of the two limbs. The parameter b/a is related to the movement frequency. 53

Fig. 3-1. A rodent treadmill from Panlab (www.panlab.com). 59

Fig. 3-2. Earlier designs of the Rat Stepper. (A) In the first version in 2000 haptic devices simulated virtual ground [**88**]. (B) A subsequent version in 2002 used a treadmill [**89**]. 60

Fig. 3-3. Current configuration of the Rat Stepper[**87**]. 61

Fig. 3-4. Conceptual sketch of a tentative apparatus (sketch by prof. Neville Hogan). 63

Fig. 3-5. Early prototypes of the wireless configuration. Each prototype weighed more than 2 kg and was taller than 25 cm. (The dark-orange components on the top of the left figure and in the middle of the right figure are the onboard batteries.) 64

Fig. 3-6. Current concept of the system, consisting of the Rat Module, BWSS, and an external computer for control, DAQ and power. The animal is free to move inside the circular 4'-diameter "arena". 67

Fig. 4-1. Advantages and disadvantages of many or few actuators. 71

Fig. 4-2. Body planes and DOFs of the hip and knee of the rat hindlimb. The arrows represent the axes of rotation for each joint. The solid red arrows indicate the two DOF that are normal to a sagittal plane, responsible for hindlimb motion in a sagittal plane. (The 3D model is taken from Turbosquid.com) 73

Fig. 4-3. Rough estimate of required power for the motors. 74

Fig. 4-4. Variations of Configuration #2 and #5. The white cylinders represent the motors, black bars depict the linkage mechanism, and the large gray cylinders represent the animal's lower back. 81

Fig. 4-5. First prototype with configuration (A) from Fig. 4-4. (1) CAD model. (2) first prototype fabricated in plastic. The flexible connectors to the motors (brown) emerge from both sides of the mechanism. 82

Fig. 4-6. One of the later prototypes with configuration (C) from Fig. 4-4. (1) A CAD model with the motors depicted as brown cylinders, and (2) an early prototype with motors placed on an actual-size rat doll. Note that the flexible connectors are all facing upwards and are easy to access. 83

Fig. 4-7. Figure from [**95**] showing the normal gait profile of a rat on a treadmill (left), and a plot from the linkage calculation (right). The two red dots represent the location of the two motor axes, and the blue area denotes the reachable end points of a certain 5-bar linkage configuration (Fig. 4-8 on the right). The red line is the ankle position with respect to the hip joint as derived from [**95**]. 84

Fig. 4-8. A selection of alternative linkage configurations. The design on the right with grey background is the final design. 85

Fig. 4-9. Final linkage dimensions. Triangle DAC forms one rigid link. 85

Fig. 4-10. Custom force sensors. (A) configuration and (B) actual photo of one force sensor. The two bundles of wires are for each force measurement direction. The strain gages were placed on the inner surface of the ring, forming two independent Wheatstone bridges. 87

Fig. 4-11. Exploded view of the base, two covers and the four motor assembly. 89

Fig. 4-12. A belt-type harnesses on the animal. (Top-left) the cloth belt was put on the animal while the rat was anesthetized briefly. (Top-right) the rat module was placed on the belt using Velcro tape. This cloth belt easily slipped off the rat's body. (Bottom) the Elastikon® tape around the animal's waist. The tape remained secure on the animal's fur. 91

Fig. 4-13. Photo of the Rat Module placed on a plastic block. Features of this device are enumerated and explained in the table. 93

Fig. 4-14. Supporting hardware items were fixed onto the utility cart. The cart could easily be transported between labs. 94

Fig. 5-1. R19 robot from ST-Robotics. Left: photo of the robot (a) and the controller box (b). Right: actuated degrees of freedom. 102

Fig. 5-2. Illustration of the idea of using a force sensor to measure the position error between the BWSS and the animal. The force sensor measures the shear force in a compliant medium, whose compliance is presumed known. 106

Fig. 5-3. Video camera used in the BWSS (Logitech Quickcam Pro 9000). 107

Fig. 5-4. Examples of processed images acquired from the video camera. The yellow pixels are those detected as 'true green' using the algorithm presented above. All pictures are 320 pixels by 240 pixels. (a) Rat Module on a rat doll. This is a typical view from the camera. (b) through (d) are cases when the video system may work less efficiently. (b) In rare cases, the wires may be tangled and partially block the view of the Rat Module. (c) The rat may be moving quickly, blurring the image. (d) The animal may rear up such that the Rat Module is slanted relative to the image plane. 109

Fig. 5-5. Camera mount for coupling the video camera to the R19 robot. Left: CAD drawing of the mount. Right: Attachment to R19. 110

Fig. 5-6. Weight supporting cord and tension spring attached to the BWSS and the Rat Module. 111

Fig. 5-7. Wire connections. See text for explanations. 112

Fig. 5-8. Experiment setup viewed from above. The body-weight support system was mounted on a low-profile wooden cart. The animal, initially anesthetized, was placed in the trapezoidal rat arena. 115

Fig. 5-9. Data from an experiment showing the animal's movement in the rat arena. See text for details. 115

Fig. 6-1. Schematic of the system used. A miniature brushless DC motor (Maxon EC6,...... 120 diameter 6 mm) was connected to a load through a planetary gearhead (57:1 reduction). An encoder was mounted on the motor shaft. The current into the motor was determined by a trans-conductance servo-amplifier (Copley Controls, Accelnet), which was driven by a control signal from a computer, in which different control schemes were programmed and tested.

Fig. 6-2. Open-loop velocity responses of the system in Fig. 1 to a quasi-static ramp...... 121 input. The input rose from 0 V to 10 V over 10 seconds. The velocity responses from four different trials are shown. The voltage at which the system first responded with non-zero velocity was different from trial to trial (by as much as 10% of the maximum control effort of 10 V). Once moving, the system reached its maximum velocity of 51,000 rpm after less than a 0.2 V increment of the input.

Fig. 6-3. Behavior of the plant of Fig. 6-1 when driven by a PID controller to modulate...... 122 the position of the motor shaft. Plotted are the gear-reduced, expected positions and error of the shaft outside of the gearhead, assuming no backlash. (A) Position tracking. The system response (blue) deviated from the commanded trajectory (red). (B) Time history of position tracking error. The error was largest at low velocities and varied substantially from cycle to cycle.

Fig. 6-4. The 2-DOF manipulator using two motors described in section 4-1. A 2D force...... 123 sensor measured the x and y interaction forces at the tip.

Fig. 6-5. (Left) Kinematic model of the system in Fig. 6-4. M1 and M2 are the two...... 124 motors with poor back-drivability, and A is the point of interaction which is the tip of the force sensor in Fig. 6-4. (Right) The force feedback scheme used in this study (right).

Fig. 6-6. Trajectories and interaction forces while manually back-driving the system in...... 126 Fig. 6-4. Top row: Open-loop measurement with no controller. The trajectory consisted almost entirely of arcs, characteristic of only one motor back-driven at a time due to significant static friction of the other motor. The peak interaction force was in excess of 1.3 N. Bottom row: Force feedback using a PI controller. The back-drivability is enhanced, although interaction force could occasionally exceed 0.5 N.

Fig. 6-7. Response of the system of Fig. 6-1 to DSC with $V = 5$ V, $M = 0.0125$ rad....... 129 Plotted are the gear-reduced, expected positions and error of the shaft outside of the gearhead, assuming no backlash. (A) Position tracking. The commanded input (red) and the response (blue) of the plant in Fig. 6-1 to a DS-controller. The two curves are on top of each other. (B) Time history of error (blue), a substantial improvement over the performance with PID control (red).

Fig. 6-8. Force feedback using DSC. Back-drivability is enhanced with a peak...... 130 interaction force substantially less than 0.2 N.

Fig. 6-9. The DC motor with gearhead is connected in series with a rotary damper. The...... 132 right side of the damper is the torque sensor. The torque reading is determined by the velocity of the motor shaft.

Fig. 6-10. Torque modulation with DSC. (A) Without the damper in series and in 2 kHz...... 133 sampling rate. (B) Damper is in series and with 200 Hz sampling rate. RMS error was 0.007 V. (C) Damper in series and with 2 kHz sampling rate. RMS error was 0.005 V In all cases, V = 10 V, M = 0.01 V.

Fig. 6-11. System $F(u)$ modulated by the controller G. 134

Fig. 6-12. Function D(e) used in (a). 135

Fig. 6-13. Step response of a system and the maximum slope S. 137

Fig. 6-14. An example where undesired bouncing of x can occur. 139

Fig. 6-15. DSC on a lightly damped 2nd order system ($\zeta = 0.087$ in Table 6.3). Top:...... 144 Command (red) versus the response with DSC control (blue) after 5% settling time (5 sec). Bottom: error. RMS value over this time window is less than 5% of the amplitude of the sine input.

Fig. 6-16. DSC on a system in Fig. 6-15 with an added zero at -10. Despite the...... 145 similarity in the step response, DSC performs much better when a zero is added. Top: Adding a zero at -10 does not drastically improve the system response to a step input. Middle: DSC performs well. Command (red) and response (blue) are indistinguishable. Bottom: error. RMS value after transient response (before t = 1s) is 0.23% of the amplitude of the sine input, an improvement of more than 95% improvement over the no-zero case in Fig. 6-15.

Fig. 6-17. (A) A motor-load system can usually be modeled as a 2nd order system with...... 146 no zero for $F = \omega/V_{in}$. (B) A damper in series with the load introduces a zero to the transfer function of $F = \omega_l/V_{in}$.

Fig. 6-18. Left: The saturation function often used in SMC. Right: DSC may be...... 148 considered to use an alternative function with more aggressive suppression of control action within the boundary layer.

Fig. 7-1. 1D-arena used in the experiment. 156

Fig. 7-2. Experiment setup. 158

Fig. 7-3. Collection of movements commonly observed in this experiment. 160

Fig. 7-4. Trajectory of the left and right leg ankles plotted over the entire workspace of...... 161 the 5-bar linkages. The yellow dotted circle represents the area in which the ankle position would be expected in normal (sober) conditions.

Fig. 7-5. Magnitude of the force measured at the left hindlimb ankle. 162

Fig. 7-6. Stride length (left) and stride duration (right) compared between 1: an animal...... 165
with coupling attachments only, and 2: identical animal trained in mockup.

Fig. 7-7. Recorded force vectors are plotted on top of the trajectories of the ankles...... 166
shown in Fig 7-4. The vectors are plotted at 100 ms intervals. Force vector of length 1 (mm) represents the force magnitude of 0.1 N. Regions inside the red-dotted circle are where the ankles were for most of the duration of the experiment.

Fig. 8-1. Addressing back-drivability of the Rat Module (these figures were presented...... 171
in chapter 6.) Trajectories and interaction forces while manually back-driving the right side of the Rat Module. Top row: Open-loop measurement with no controller. The trajectory consists of arcs, characteristic of only one motor back-driven at a time due to significant static friction on the other motor. The peak interaction force is over 1.3 N. Bottom row: with force feedback. Back-drivability is enhanced with peak interaction force of 0.2 N.

Fig. 8-2. The animal was trained to respond to and walk through the dark 'hallway'. A...... 173
side wall was transparent to allow video recording of the locomotion.

Fig. 8-3. Snapshots from a live animal experiment. Top: The Rat Module mounted on...... 174
the animal. 1-Waist coupling. 2-Ankle coupling. 3-Wires for the sensors and actuators. 4-Compliant elongation springs for partial weight support. Right: snapshots from the video recorded while the animal performed self-paced, forward locomotion.

Fig. 8-4. Stride Length data. Left: Mean ±STD. There is no significant difference...... 178
between cases. Right: Data histograms.

Fig. 8-5. Stride Duration data. Left: Mean ±STD. Significant differences from the...... 178
unconstrained case are marked with * ($p < 0.05$). Right: Data histograms.

Fig. 8-6. Ratio of swing duration to stride duration (Mean ±STD). No significant...... 179
difference from the unconstrained case were observed.

Fig. 8-7. Time-averages of interaction force magnitude during forward locomotion...... 180
(blue), and the average peak interaction force. The left side showed larger interaction forces.

Fig. 8-8. End effector trajectories derived from encoder recordings during nine...... 182
occurrences of forward locomotion are superimposed.

Fig. 9-1. An alternative design. Two robotic arms placed outside the area of activity...... 191
(arena) are coupled to the ankles of the animal.

Fig. B-1. Coordinate frames of the BWSS robot in the “home-position”. The x-y frame (black), also called the robot frame, is the fixed coordinate for the position of the end-effector of the robot. The x’-y’ frame (brown) is attached to the end-effector. The x”-y” frame is also attached to the end-effector (more specifically, to the camera attached at the end-effector). The positive y” axis is opposite to the positive y’ axis. In this “home-position”, the x’-y’ frame is offset 360 mm in the y-direction from the robot frame...... 201

List of Tables

Table 1.1 Life Expectancy of SCI Patients for Persons Surviving At Least One Year Post-Injury [3] 27

Table 1.2 Lifetime Costs of SCI Patients [3] 27

Table 2.1 Apparatus Design Considerations 55

Table 4.1 List of Motors Considered 75

Table 4.2 Motor and Gearhead Specification 76

Table 4.3 Candidate Configurations 80

Table 5.1 Possible BWSS configurations 100

Table 6.1 DSC performance on $F = 10/(s+10)$, $L = 0.001$ s and $x_c = \sin(2\pi t)$ 141

Table 6.2 DSC performance on $F = 24/(s^2 + 10s + 24)$, $L = 0.001$ s and $x_c = \sin(2\pi t)$ Performance evaluated after 5% settling time (0.6 sec) 141

Table 6.3 DSC with 2nd order systems. $F = \omega_0^2/(s^2 + 2\zeta\omega_0 s + \omega_0^2)$ where $\omega_0^2 = 50$ Command = $1\cdot\sin(2\pi\cdot t)$, Frequency = 1 kHz 144

Table 8.1 Stride Length 177

Table 8.2 Stride Duration 177

Chapter 1

Introduction

Every living organism's instincts drive it to pursue a longer and healthier life. Humans are no exception, as we have long been seeking the panacea for every illness, disease or injury, with the hope of extending life. For a long time in human history, the available remedies for illness or injury were limited to naturally available substances that were taken orally or applied to the skin surface. While the first record of medicine in the west is dated at 420 BC, other forms of medical technology that are available today did not exist, and even those that did remained in their infancy until much later. Surgery was in a primitive state until the early 19th century, when new solutions could better address the major problems of controlling bleeding, pain, and infection. Vaccinations and the injection of drugs became more effective only after the industrial revolution.

In the 20th century, advances in science and engineering have led to advances in medical technology, such as new diagnostic methods or treatment options. Synthetic drugs became widely popular by the 1950's [1]. The first human kidney transplants were performed in 1954. Magnetic Resonance Imaging (MRI) and Computed Tomography (CT) technology were developed in 1971, leading to the first commercial MRI machine in 1980. Surgical robots emerged in the 1980's, while robots for rehabilitation became available in the 1990's. As a result of these advances and many others, the life expectancy at birth in the United States increased from around 50 years in the 1900's to over 70 years in the 1990's [2]. Further, as of 2011, identifying breast cancer in its early stages gives patients an excellent prognosis, with the same life expectancy as the general population.. Today, stem cell research, artificial organs, and gene therapy are a few technologies in development that have potential to drastically alter the field of medicine.

Despite the general trend towards longer and healthier life, humans are still challenged by numerous forms of illness and injury. For example, neurological injuries or illness such as Alzheimer's disease, stroke, or spinal cord injury are receiving more attention than in the previous century as researchers are enthusiastic to find a cure. Patients with these injuries suffer decreased or even completely absent sensory-motor functions in their legs, arms or sometimes the whole body below the neck. As the number of patients with such injury continues to grow, their lowered quality of life as well as the financial burden of their care adds to the motivation to find effective methods for recovery.

This thesis is in line with the ongoing quest to find effective treatments to aid the recovery of patients with lost sensory-motor functions due to neurological injuries. In particular, the focus is on spinal cord injury and lower extremity function, as well as the neural circuitry associated with the biomechanics of locomotion. As a large volume of research in neurological injuries is done in animal models, this work focuses on developing and validating a new tool for animal locomotion research related to spinal cord injury.

1.1 Spinal Cord Injury

Spinal Cord Injury (SCI) is a neurological disorder described as a disturbance of the spinal cord that results in loss of sensation and/or mobility. The main causes of the injury include motor accidents (40%), falls (28%), violence (15%) or sports-related injuries (8%) [**3**]. Depending on the severity and location of the injury, the patient may suffer various degrees of sensory-motor deficit such as being paraplegic or tetraplegic, and cases of full-restoration of functionality are extremely rare.

1.1.1 Number of Patients

There are more than 11,000 new patients each year in U.S., where less than 1% of the new patients fully recover their sensory and motor functions. The total number of patients keeps growing from 210,000 in 2002 to 250,000 in 2006, and the total is estimated to have reached 265,000 in 2011 [**4**][**3**]. The average age when an SCI occurs has been gradually increasing, from 28.7 years during the 1970's to 40.7 years in 2005. The increase in these numbers is in part due to the higher survival rate of the patients after the incident that caused the injury, which may also account for the increasing trend in the number of the SCI patients.

1.1.2 Severity of Injury

Persons with legions at a higher level of the spinal cord (namely in the cervical segments) become tetraplegic, while patients with a lower injury site (thoracic, lumbar, or sacral segments) become paraplegic. At hospital discharge, it is reported that 39.5% of patients are incomplete tetraplegic, 22.1% are complete paraplegic, 21.7% are incomplete paraplegic, and 16.3% are complete tetraplegic [**3**]. Less than 1% of patients recover full sensory-motor functions at discharge.

The ASIA scale is an SCI impairment assessment scale developed by the American Spinal Injury Association. It defines the level of spinal cord injury as follows:

A: **Complete**: No motor or sensory function is preserved in the sacral segments S4-S5.

B: **Incomplete**: Sensory but not motor function is preserved below the neurological level and includes the sacral segments S4-S5.

C: **Incomplete**: Motor function is preserved below the neurological level, and more than half of key muscles below the neurological level have a muscle grade* less than 3.

D: **Incomplete**: Motor function is preserved below the neurological level, and at least half of key muscles below the neurological level have a muscle grade* of 3 or more.

E: **Normal**: motor and sensory functions are normal.

(* Muscle grade of 3: subject can hold a limb against gravity but no additional pressure can be tolerated.)

A 'complete' injury is declared if the patient has a level below which no sensory-motor functions remain at all. An 'incomplete' injury is every other situation except being normal (ASIA E level as described above).

1.1.3 Life Expectancy and Lifetime Cost

The life expectancy of SCI patients continues to increase as well. The specific expectancy varies with several factors, such as the severity of injury and the age at injury. While the mortality of SCI patients is higher than in normal persons, patients whose age at injury was 20 are expected to live on average another 17 years (Table 1.1). The life-long expenses for these patients are very high, as can be seen in Table II. Note that these figures do not include indirect loss of income from loss of productivity. In order to increase their general quality of life as well as reduce the patients' financial burden, partial to full recovery from loss of sensory-motor function in these patients is of great interest in this field of study.

Table 1.1
Life Expectancy of SCI Patients for Persons Surviving At Least One Year Post-Injury [3]

Age at Injury	Individuals Without Injury	Motor Functional at Any Level	Paraplegia	Low Tetraplegia (C5-C8)*	High Tetraplegia (C1-C4)*	Ventilator Dependent Any Level
20	58.6	53.0	45.8	41.0	37.4	23.8
40	39.4	34.5	28.2	24.2	21.2	11.4
60	22.4	18.0	13.2	10.4	8.6	3.2

*C1, C4, etc. refers to the injury location at the spinal cord, where higher number refers to lower site of lesion.

Table 1.2
Lifetime Costs of SCI Patients [3]

Severity of Injury	Average Yearly Expenses (USD)		Estimated Lifetime Costs by Age at Injury (USD)	
	First Year	Each Subsequent Year	25 years old	50 years old
High Tetraplegia (C1-C4)*	985,774	171,183	4,373,912	2,403,828
Low Tetraplegia (C5-C8)*	712,308	105,013	3,195,853	1,965,735
Paraplegia	480,431	63,643	2,138,824	1,403,646
Incomplete Motor Functional at Any Level	321,720	39,077	1,461,255	1,031,394

*C1, C4, etc. refers to the injury location at the spinal cord, where higher number refers to lower site of lesion.

1.2 Methods to Aid Recovery from SCI

1.2.1 Conventional Methods

While potential therapeutic strategies under research in animal models include cell implants, pharmacological interventions, and locomotor training, current rehabilitation methods applicable to human patients are limited to compensatory strategies for accomplishing mobility or strengthening muscles above the level of lesion until early 21st century [**5**][**6**]. In the past 10 years, physical therapies motivated by findings in animal studies have shown partial success in human patients. For example, a young patient has scored a lower ASIA level after receiving physical therapy motivated by findings from animal research [**5**]. This may be possible because the spinal cord below the lesion still maintains functional neural circuits and can respond to sensory inputs. While physical therapy is currently the only available option to improve motor functions in human patients, the mechanism behind its partial success is still largely unknown and calls for further studies. Other methods such as cell implants are not mature enough for human trials at this point, but show significant potential in animal studies.

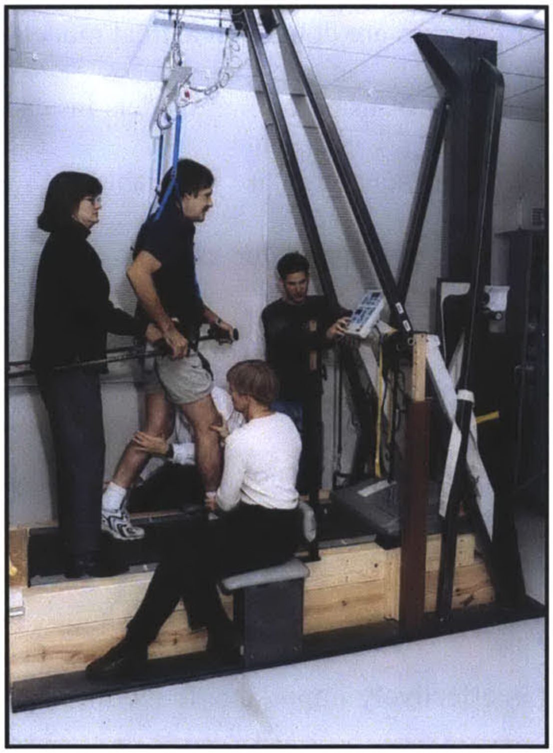

Fig. 1-1. Step training with weight support and manual assistance on a treadmill [**5**].

1.2.2 Current Progress in the Field

Research in SCI reports observations regarding the functionality (or automaticity) present in the spinal cord that may play a significant role in locomotion when supra-spinal control is compromised due to injury. Functional recovery after SCI may be possible, because 1) the spinal cord has the automaticity to perform certain tasks, and 2) the spinal cord has an ability to adapt to any imposed activity (functional plasticity). As mentioned previously, there are a number of different research pathways to improve recovery from SCI. Most of the attempts to facilitate recovery from SCI listed in this section show modest results at best, but the ultimate goal may be reachable by combining these therapies.

Note that a large volume of studies are done with animal models of SCI, and especially with rats. There are a number of benefits of using animal models instead of human subjects for this research. Firstly, the range of experiments that are justifiable with animals is much wider than those that can ethically be done with humans. For example, one can prepare decerebrated cats (intact animals in which connections between the spinal cord and cerebral hemispheres have been severed) to study the effect of functional isolation of the spinal cord from the brain. Also, one can use pharmacological agents that are not approved for use with humans but may be justifiable for animal research. Secondly, in animal studies, one can control important factors of the SCI such as the intensity of injury, lesion site, days since injury or even genetic homogeneity of the subject population. It is effectively impossible to recruit human SCI patients with such a homogeneous intensity of injury, lesion site, etc.

1.2.2.1 Relevant Observations

There are three major observations after SCI that affect locomotor function. 1) Loss of coordination between motorneuron pools, 2) deficits in activation of specific motorneuron pools, and 3) atrophy of skeletal muscle. At present, there is evidence that 1) motorneuron pools can become more effectively coordinated [**7**][**8**], 2) the level of activity in specific motorneuron pools can be elevated [**7**][**8**][**9**], and 3) the amount of muscle atrophy can be at least partially and perhaps fully recovered [**10**][**11**][**12**][**13**][**14**]. In spite of this evidence, there has been no full recovery from SCI in humans. However, in cats, almost full recovery is reported.

Spinal automaticity remains even after the absence of supra-spinal input. After a complete transection or injury, automaticity in the spinal cord can be attributed to two components: a Central Pattern Generator (CPG) [**15**][**16**], and the sensory input to the spinal cord. When they work in synergy, relevant patterns of locomotion can emerge. The temporal patterns of ensembles of peripheral inputs may have to be matched with that of the CPG for locomotion to continue effectively. In other words, only the specific sensory input patterns (such as those generated by walking) may generate appropriate motor patterns in the CPG.

Some examples of conserved automaticity in the spinal cord are shown in both human and cat studies. In an ASIA A subject (complete SCI), muscle activation patterns for supporting load can occur at the appropriate timing within the step cycle [**17**]. Similar loading-related responses have been described in cats whose spinal cord is completely transected at a low-thoracic level [**18**]. Also, a series of experiments on spinal cats demonstrated that a stimulus to the dorsum of the paw of a spinal cat during the swing phase would induce ipsilateral flexion and contralateral extension [**19**].

In addition, voluntary initiation of locomotion can be observed in SCI patients. For example, an ASIA A subject standing with bilateral weight support can initiate stepping by shifting body weight, extending the hip of the contralateral leg, and then leaning forward [**20**]. By shifting the weight of the upper body and therefore unloading a limb at the end of the stance phase of a step, one can facilitate the initiation of the swing phase of that leg [**21**]. This observation is in agreement with the load-related human experiments mentioned in the previous section.

1.2.2.2 Various Facets of Research

Motor Training

In humans, combinations of motor training that involve body-weight supported treadmill training as well as overground training were reported to enhance the level of motor pool activation and the coordination of motor pools and reduce muscle atrophy, although progress is slow [**9**]. Some of the early animal studies reported that in spinal cats, full weight bearing treadmill training for 2-3 weeks results in close-to-normal EMG behaviors in the muscles [**22**][**23**]. Trained cats, compared to non-trained cats, can produce accurate timing of toe-off and paw-contact even at higher treadmill speeds [**22**]. Also, it has been shown that motor training can markedly change the physiological, biochemical and pharmacological state of the spinal cord. (See figure 1-2.) Presumably, motor training works to repetitively activate the appropriate extensor and flexor networks in a specific temporal/spatial pattern so as to enhance the coordination of the motorneuron pools [**24**].

Sensory Stimulation

One can benefit from above-threshold sensory stimulation that may enhance a specific part of the cyclic pattern of neural activity that may be otherwise preventing normal steps. One example in humans involves stimulating the peroneal nerve at the end of the stance phase to induce a flexor reflex and therefore help the initiation of the swing phase. Subjects improved their walking speeds by 45% after a year of such training [**25**].

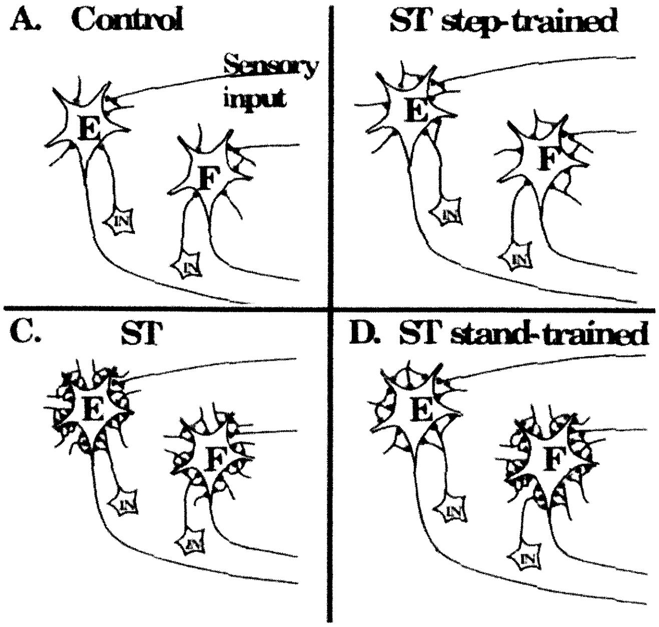

Fig. 1-2. Schematic illustrating changes of inhibitory synapses (gray dots) around the extensor (labeled as E) or flexor (F) neuron groups in cats under various motor training conditions. Before injury (A), the number of inhibitory synapses in each neuron group is small. After spinal transection (ST), the populations of inhibitory synapses vary depending on the types of training. It can be seen that the training of a certain locomotion task decreases the number of inhibitory synapses in the neuron group that is responsible for that specific task. [**26**].

Spinal Cord Stimulation

Direct stimulation of the spinal cord results in some positive improvement in motor function. For example, in intact cats under anesthesia, L3-L4 stimulation of the dorsum of the spinal cord induced hindlimb muscle group activation [**27**]. In an ASIA C human, an implanted electrode at the upper lumbar spinal cord (dorsum) significantly improved motor performance [**28**]. Although different frequency and amplitude of stimulation resulted in different physiological effects, a generalized, non-specific electrical stimulation of upper lumbar neurons may be sufficient to generate rhythmic stepping movements of the lower limb [**24**].

Pharmacological Stimulation

Some biochemical adaptation that degrades motor performance occurs after spinal cord injury [**17**]. Use of the right drugs can manipulate the 'state-dependence' of the degraded neural circuits within the spinal cord such that it may respond 'better' to appropriate stimulation. For example, when small doses of strychnine (glycine receptor antagonist) were given to adult spinal cats, they showed some weight-bearing, alternating steps even without any previous motor training [**29**]. There are multiple neurotransmitters and neuromodulatory systems that can facilitate or degrade motor performance. Hence, one must use the right combination of drugs to achieve a suitable physiological state for the spinal circuitry to respond to the relevant proprioceptive inputs.

Growth factors

A biochemical agent known as brain-derived neurotrophic factor (BDNF) could possibly stimulate axons to grow across the lesion of an injured spinal cord. The amount of BDNF in the spinal cord or in the muscles was increased in response to wheel running in rats [**30**][**31**][**32**][**33**], suggesting a positive role of BDNF in motor function recovery. The exact role of growth factor in these studies is only vaguely known at this point.

Cell Implants

There are four types of possible implants that may result in facilitation of lomocotor ability, which are listed here. They have all been reported to produce some positive preliminary results, especially in neonates.

- Peripheral nerves: for example, the intercostals nerves that are found around the ribcage are used.

- Fetal tissue: embryonic spinal cord tissues are used in SCI research in rats.
- Olfactory ensheathing cells (OECs): these cells are found in the olfactory mucosa and are responsible for the life-long growth of neurons in this region.
- Schwann cells: these cells provide myelin insulation to axons, and also promote regeneration of axons. Direct injection of these cells to the lesion site has resulted in some, although limited, functional reconnection in rats [**34**].

1.3 Using Therapeutic Robots

Therapeutic robots may greatly reduce the workload of therapists by providing similar physical assistance. These robots may be programmed to test and provide novel locomotor training protocols. Moreover, they may also be used to study neurological disorders. Robotic therapy may even be used in conjunction with other promising therapies, such as shown in a study with rats [**35**]. In short, there is a great potential for the use of robotic devices for therapy and basic research on neurological injuries.

1.3.1 Upper Extremity Robotic Therapy for Stroke

Rehabilitation of the upper extremity in stroke patients is the earliest and primary example of the significant advantages that robotic therapy has to offer to patients with neurological disease or injury. An upper extremity robot, the MIT-Manus, was used in a number of studies involving both acute [**36**] and chronic stroke patients [**37**][**38**]. In both cases, robotic therapy showed measurable benefits over manual conventional therapy. The results with chronic patients were particularly novel, since recovery in the chronic phase was thought to be absent. This robot has been used later in attempts to identify other forms of robotic therapy, such as an EMG-triggered therapy [**39**], that may be of greater benefit. The success of MIT-Manus may have resulted, in part, because it was designed to be compatible with and take advantage of contemporary knowledge about neural control of upper extremity movement.

1.3.2 Lower Extremity Robots for Neurological Injuries

A number of robots have been developed for lower extremity rehabilitation after stroke or SCI, such as Lokomat [**40**], ALEX [**41**], or ARTHuR[**42**]. However, none of these robots have achieved a level of success similar to upper extremity robots. Although the machines exhibit excellent engineering design and implementation, they may have failed to be compatible with what little is known about lower extremity neural control during locomotion. For example, all current lower extremity therapy robots are built upon treadmills, while walking on a treadmill is known to be different from walking overground. Also, these robots restrain certain aspects of locomotion that may be important. For instance, the Lokomat does not permit weight shifting even though it is known that load-related sensory inputs play an important role in locomotion [**43**]. It is also common for these lower extremity robots to omit actuation at the ankle, despite the fact that this joint makes a major contribution to the propulsive force [**44**].

In short, the current lower extremity robots for rehabilitation appear to have been designed without properly considering what is currently known about lower extremity biomechanics and neural systems in locomotion. This is hardly surprising however – the current knowledge of neural control of human locomotion is sparse. Better understanding of human movement is necessary in order to design and implement useful rehabilitation robots.

1.4 Summary, Goal and Thesis Organization

This chapter can be summarized as follows:

- SCI is a neurological disorder whose complete cure is absent.
- SCI patients suffer reduced quality of life and significant financial burden .
- Current research to find a cure relies heavily on animal models (rats in particular)
- Promising research directions are 1) combinations of therapy that include motor training, 2) robotic therapy based on knowledge of the biomechanics and neural control of movement.

Motivated by these findings, the research reported in this thesis aimed to develop a robotic device for basic research into locomotion and therapy for its restoration after neurological injury in animal models. In particular, the device is expected to enrich basic research on hindlimb locomotion in rats, which may serve as a model of lower extremity locomotion in humans.

The following chapters provide further motivation for the development of such an apparatus. Chapter 2 reviews relevant motor neuroscience on lower limb locomotion. Chapter 3 details the specific requirements of the apparatus based on these findings. Also, the basic configuration of the apparatus is presented and justified by comparison with existing equipment. Chapters 4 and 5 detail the design and implementation of the several hardware modules. Chapter 6 presents the engineering challenges and the solution developed. Chapters 7 and 8 document animal experiments to evaluate the apparatus. The thesis is concluded in Chapter 9 by discussing implications of the developed apparatus for the relevant field of research.

Chapter 2

Central Nervous System and Locomotion

We have seen in the previous section that limited knowledge of how the human body works may lead to poorly designed robots that are ineffective for recovery after SCI or stroke. To build a more useful machine, it is important to review the current findings on locomotion and the neural circuitry involved. A well-designed machine should be compatible with the biomechanics and the neural control of movement.

This chapter is a survey of current research on the role of the Central Nervous System (CNS) in locomotion, including both animal and human studies. Of particular interest is the role of the spinal cord in the animal models. Relevant topics include the role of sensory inputs, interlimb coordination, spinal cord development in rats, and existing models of the spinal circuitry. Implications for recovery from SCI and/or on the development of the apparatus in this project are also provided.

2.1 Motor Function-related Anatomy of the CNS

In this section the anatomical features of the CNS that are relevant to motor function are summarized. Specifically, an introduction to the neural circuitry of the spinal cord and its connection to the brain is provided.

2.1.1 The Spinal Cord

The human spinal cord is composed of cervical, thoracic, lumbar and sacral levels which consist of 8, 12, 5 and 5 segments respectively. One such segment is shown in Fig. 2-1. In each segment and on each side, there are dorsal roots which are bundles of sensory neurons that carry information into the spinal cord (afferent signals), and ventral roots, which are bundles of motoneurons that carry neural signals generated by the CNS to the muscles (efferent signals). The dorsal roots neuron bodies are protected by nodules called dorsal root ganglions, or spinal ganglions. The two bundles of neurons make synaptic connections to interneurons (INs) within the spinal gray matter.

The gray matter contains INs that provide connections between not only the ipsilateral dorsal and ventral roots, but also between interneurons on both sides (left and right) of the gray matter. Spinal white matter is the pathway of axons that originate from higher CNS as well as those originating from the spinal cord. In other words, the white matter contains pathways of neurons communicating between the spinal cord and the brain, whereas the gray matter contains interneurons that provide communication between the dorsal and ventral roots within the spinal cord. Neurons in the white matter that originate from the brain terminate in the gray matter to make synaptic connections to interneurons, or directly to motoneurons.

2.1.2 Corticospinal Tract

The motor cortex in the brain sends motor commands to the periphery through the corticospinal tract (Fig. 2-2). It is a bundle of neurons that originates from layer V of the motor cortex (where the cell bodies reside) and descends into the spinal cord through a white matter tract, ending up making synaptic connections to interneurons or to motoneurons in the gray matter of the spinal cord. 80% of the neurons in the corticospinal tract decussate (cross over) to the contralateral side in the medulla oblongata before entering the spinal cord. The remaining 20% do not decussate and follow the white matter tract on the ipsilateral side.

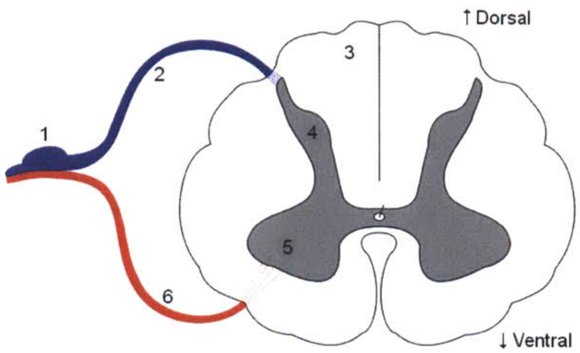

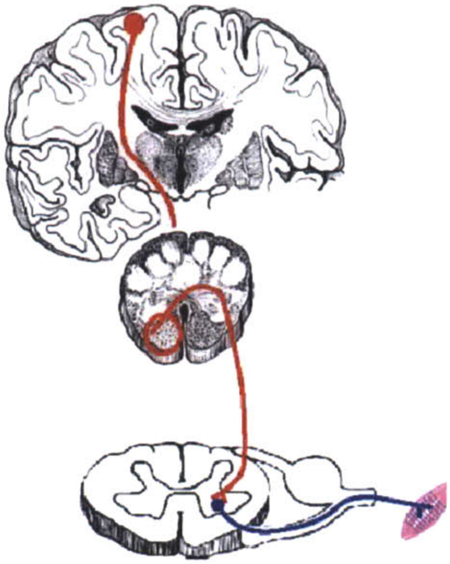

Fig. 2-1. Schematic of the spinal cord, cross-section, simplified. 1: Spinal Ganglion. 2: Dorsal root. 3: White matter. 4: Gray matter, dorsal horn. 5: Gray matter, ventral horn. 6: Ventral root.
Fig. 2-2. Schematic of corticospinal tract. The neurons originate from the motor cortex (top). 80% of them decussate to the contralateral side in the medulla oblongata (middle). These neurons make synaptic connections to interneurons or directly to motoneurons within the gray matter (bottom).

2.1.3 Sensory Inputs to the Brain

There are several pathways within the spinal cord that transmit the sensory information from the periphery to the higher CNS. For example, Spinothalamic tract transmits information about itch, pain, or temperature to the thalamus, while Posterior column-medial lemniscus pathway is responsible for transmitting fine touch or vibration. Of particular interest to human movement is the spinocerebellar tract. This pathway transmits information obtained from sensory receptors such as the Golgi tendon organs or muscle spindles to the cerebellum. That is, kinematic information such as position and velocity of body segments is carried to the brain through this the spinocerebellar tract within the white matter.

2.2 Sensory Information on Interlimb Coordination

This section reviews current findings in the literature regarding the influence of sensory input on motor output. A number of experiments have shown the role of the CNS, especially the spinal cord, in generating rhythmic movements such as gait as a result of appropriate sensory inputs. The neural circuitry responsible for this within the spinal cord is called a Central Pattern Generator (CPG). It is known that there are CPGs in mammals, particularly in rats and cats. Other types of animals such as turtles, lampreys or squids also are believed to have CPGs. Although the evidence of a CPG in humans is not as clear, the community is inclined to believe in its existence [**45**].

A lot of the studies mentioned in this chapter involve animal models such as cats or rats. Popular preparations include decerebration (the elimination of cerebral brain function in an animal by removing the cerebrum or cutting across the brain stem) or partial/complete spinalization (cutting across the neuron bundles in the spinal cord). Fictive locomotion studies are also popular, where 'fictive steps' refer to patterns of motoneuron output that would generate muscle activation for step-like movements. Fictive locomotion studies involve using isolated or exposed spinal cords taken from animals. These preparations offer useful insights particularly on the role of the lower spinal cord in locomotion. However, intentional application of such preparations in humans would be morally indefensible.

2.2.1 Studies in Cats

A large body of research reports on interlimb coordination in the presence of sensory inputs in cats. In spinalized cats, continuous flexion of one hindlimb blocks rhythmic motion of both hindlimbs [**46**]. De-afferentation of one hindlimb in spinalized cats disrupts not only ipsilateral stepping [**47**], but also contralateral stepping. It is also observed that there exists a fore-and-aft coordination of the limbs, both in intact and in spinal cats [**48**][**49**][**50**][**51**]. These experiments suggest that there is a spinal mechanism for interlimb coordination whose mechanism depends on sensory inputs.

Spinalized cats can, to some extent, adjust to a "split-belt" condition where different treadmill speeds are imposed on the two hindlimbs. Decerebrated cats can also adjust to the same condition [**52**]. This suggests that the adjustment to a rather non-trivial task can be made within the spinal cord without supraspinal control.

Spinalized cats can produce motor output patterns in the lower spinal cord similar to those seen in normal locomotion. This can be done by inducing a hip position-related afferent activity [**53**] [**54**][**55**], or by unloading the ankle extensor at the end of the stance phase [**21**]. However, the muscle activation patterns of fictive and normal locomotion were not identical, suggesting a role of stretch reflexes based on length and force related receptors such as muscle spindles or Golgi-tendon organs (GTO) [**56**][**57**][**58**] [**59**]. Still, it is argued in the same studies that the contribution of stretch reflexes to motion is restricted to particular muscles only, and their effect at a more general level is small.

Other studies in cats report fictive steps related to forelimb-hindlimb coordination. In high-level decerebrated cats, fictive step cycles of the two forelimbs were always strictly alternated. The phasing of the step cycles of either the two hindlimbs or pairs of homolateral or diagonal limbs were more variable. Also, the time interval between the onsets of flexor bursts of one of the two pairs of diagonal limbs was independent of the step cycle duration [**60**]. This suggests that in quadrupeds, forelimb motion is to some degree coupled to hindlimb motion. Hindlimb locomotion may be altered by the current state of the forelimbs.

2.2.2 Studies in Other Animals

It is stated in [**24**] that in rats, insects, crabs or lobsters, load conditions change gait patterns. For example, in cats and rats, unloading the leg at the end of the stance phase is essential to invoke the onset of the swing phase. It is also known that the load condition on one leg affects the motion of the contralateral leg. These findings agree with the results reported in cats.

2.2.3 Studies in Humans

Studies in humans suggest that the CPG found in cats or rats may also be present and play a similar role in humans. Various experiments mentioned in [**24**] show the relationship between sensory inputs and gait. One experiment on humans showed the interlimb interaction induced by motion of one leg [**59**][**61**]. In these studies, the subjects kept one leg outside the treadmill and kept that leg straight and stationary. The contralateral leg was on the moving treadmill with speed set to the subject's preferred gait speed. The researchers monitored the neural activities in the stationary leg while the other leg was moving. They observed a reflex in the biceps femoris (a hamstring muscle) in the stationary leg that is dependent on the phase of gait in the moving leg. This suggests that there is an interlimb interaction in gait motion. Another study, involving cycling of the legs, also suggested that motion of one leg facilitated motion of the other leg, even when that leg lacked sensory input that the pedaling leg received [**62**]. These two experiments suggest that rhythmic locomotor output on one side facilitates a rhythm on the other side. The sensory coupling between the two legs is fairly robust and persists in the presence of reduced sensory inputs.

Studies on humans that are of particular interest are those on the role of afferent inputs induced by loading and unloading. Various research studies on this topic were conducted with infants and adults, both loading and unloading the limb. Infants 2 to 11 months old show well-organized, phase-dependent and location-specific reflex responses to mechanical perturbation during walking in different directions, which require very different interlimb coordination [**43**][**63**][**64**][**65**]. Information about limb loading and hip position are powerful signals regulating stepping patterns [**43**].

In adults, some studies reported that even with increased cortical control (which can overrule spinal switching automatism), the loading/unloading reflex is preserved, suggesting a prominent role of a CPG and afferent inputs [**66**]. Also, there is a suggestion that the arm swinging motion during gait is produced by CPG centers within the spinal cord, rather than just being a counter action to pelvic motion. Adding mass to the arms during gait does not change the gait pattern or the frequency of the arm swing, suggesting that the effect of the mass of the arm on gait is minimal [**67**]. However, this may be a short-term result. In order to fully understand the effect of physical parameters of the arm such as the mass, long-term effect of changing such parameters must be addressed.

A study involving sudden perturbation of the loaded leg during walking showed that, when the stance leg was suddenly unloaded, a flexion reflex in the ipsilateral leg was observed as well as an extension reflex in the contralateral leg [**68**][**69**]. The role of this reflex is presumably to increase stability in the sudden unloading condition. In other words, humans produce a bilateral reaction in which interlimb coordination aims at recovering stability.

2.2.4 Implications for Recovery from SCI

Previous work presented in this section strongly suggests that there is a neural circuitry known as a CPG within the spinal cord that can generate locomotion-like motor output. The context of sensory input is important to induce movement in both the ipsilateral and contralateral limbs. If such a 'recipe' of sensory inputs can be consistently provided to SCI patients through therapy or through robotic technology, it may be able to induce useful motion in the legs to help facilitate stepping. On the other hand, if the sensory inputs are not well designed, they may be incompatible with outputs from the CPG and may impede natural walking.

2.3 Studies on Neonatal Rats and Rat Embryos

Studies on locomotion and the role of the spinal cord extend to neonatal rats, or rat embryos. The experiments are done both *in vivo* as well as *in vitro.*

2.3.1 Locomotor studies on the neonatal spinal cord, *in vitro* preparation

Neonate rats provide an excellent electrophysiological *in vitro* preparation for studying rhythmic behaviors, particularly due to the presence of rhythmic locomotor activity and the absence of myelin at this stage [**70**][**71**][**72**]. Several pharmacological agents can induce locomotor rhythms in this *in vitro* preparation, which include N-Methyl-D-Aspartate (NMDA), Serotonin, Acetylcholine, Dopamine, and excitatory amino-acids. Four CPGs have been identified in this preparation, two at the cervical level corresponding to movements of the forelimbs and two at the lumbar level corresponding to movements of the hindlimbs. The exact network structure connecting the CPGs is still largely unknown.

A left-right coordination mode in the lumbar CPGs is observed [**73**]. This was also seen in a study involving an embryo seven days prior to birth, but at a much lower frequency (1/10th of that observed at birth) [**74**]. Also, some functions relating to cervical level CPGs and their coordination with the lumbar spinal cord was observed. For example, forelimb extensor bursts were in phase with hindlimb flexor bursts but sometimes these relations were reversed [**73**]. If the cervical and lumbar spinal cords are isolated, the burst frequencies in the cervical and lumbar levels are different, suggesting that in the intact spinal cord, the cervical CPG interacts with the lumbar CPG. Also, it has been shown that rhythmic stimulation of the lumbar dorsal roots can induce entrainment not only of the lumbar CPG, but also of the medullary respiratory rhythm (located near the brainstem) [**75**].

2.3.2 Locomotor studies in rats, *in vivo* preparation

It is observed that during the first week after birth, the rats are blind, muted and can crawl only with their forelimbs. Even so, they can show gait-like motion when stimulated with the odor of their mother [**76**], suggesting the existence of a locomotor rhythm generator in the CNS at postnatal days 3-10 (P3-P10). However, this rhythm is slow and only becomes faster and more fluent at 2 weeks after birth when four-leg standing is possible. These observations suggest that at birth, the rat's CNS is composed of the main structures of the locomotor CPGs but they become functional only later when postural regulation develops.

Another experiment with neonatal spinalized rats showed that tail pinching can elicit long lasting sequences of rhythms which are not seen in the intact animal, but the left-right alternation pattern shown in the intact animal is absent in spinalized rats [77].

In summary, it has been shown experimentally that the development of the locomotor network takes place before birth and can be activated right after birth [76], but it takes time to become useful (1~2 weeks after birth when the rat is capable of 4-leg standing and when the sensory afferents are fully operational). This work suggests that sensory afferents may play an important role to 'turn-on' the spinal network.

2.3.3 Development of the rat spinal cord

Useful information about the rat spinal cord can be gained through visually observing how the features of the spinal cord develop in the rat embryo. One of the ways to do this is by using various types of thymidine radiographic preparations of the early spinal cord (Fig. 2-3). This preparation works in the following way: First, thymidine is injected to the mother rat carrying the embryo. After a certain time, the mother (and therefore the embryo) is sacrificed and the spinal cord of the embryo is studied by thin sectioning. The injected thymidine works in a way to give better visual picture. Since thymidine is found in DNA, it is speculated that this chemical marks the cell nucleus so to make it more visual apparent under the microscope. This way, one can observe the development of the spinal cord in the embryo, specifically between E12 and E19 (12th to 19th day after the fertilization).

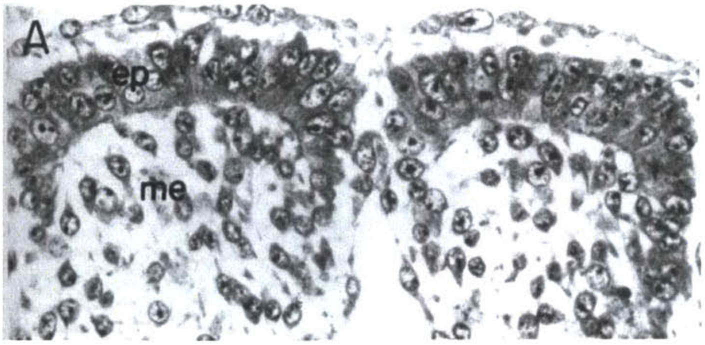

Fig. 2-3. A photo of a thymidine radiogram of an embryonic rat spinal cord [**78**]. The cell nuclei are clearly visible.

From these preparations, the order in which different nerves develop in the spinal cord may be determined, summarized as follows [**78**] (see Fig. 2-4):

- Ventral roots sprout first, at E12-E13, before the development of the dorsal roots or the interneurons within the spinal cord.
- Contralateral interneurons develop earlier than the ipsilateral interneurons. These events happen at around E15-16.
- Dorsal root afferents develop between E13-E17, but usually later than the development of the interneurons. This is in line with the observation that endogenous movement emerges earlier than reflexive (exogenous) movement.
- Spinal ganglions, small nodules on the dorsal root that contains cell bodies of afferent nerves, develop at E12-E15.
- Left and right alternation appears at E18~E19 [**74**]. If an alternating movement is a result of afferent inputs, the emergence of this motion can be attributed to the development of dorsal roots at E13~E17.

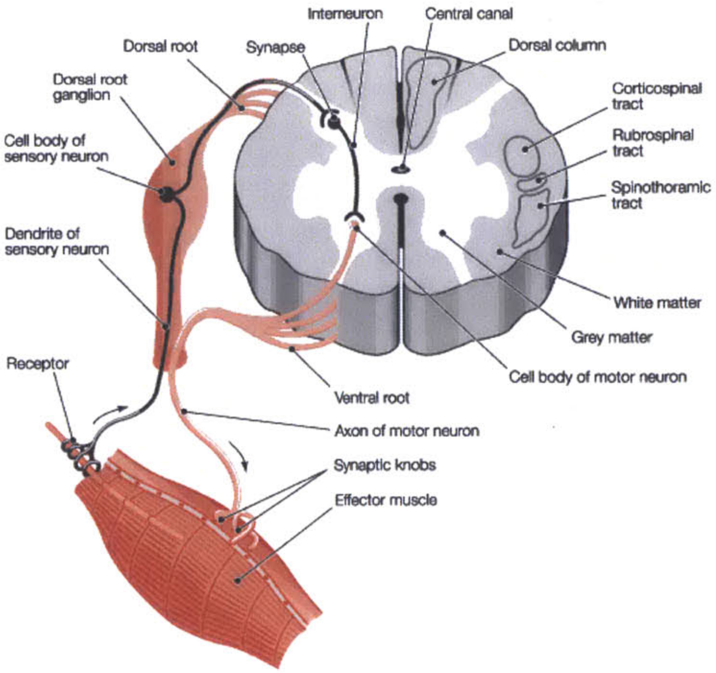
Interneuron
Central canal
Dorsal root
Synapse
Dorsal column
Dorsal root ganglion
Corticospinal tract
Cell body of sensory neuron
Rubrospinal tract
Spinothoramic tract
Dendrite of sensory neuron
White matter
Grey matter
Receptor
Cell body of motor neuron
Ventral root
Axon of motor neuron
Synaptic knobs
Effector muscle

Fig. 2-4. Diagram of the spinal cord, muscle and relevant neurons.

2.3.4 Implication for Recovery from SCI

Research on the spinal cord in these early development stages provides useful information about the neural circuitry in the mature spinal cord. For example, neural circuitry responsible for the features present in a 'young' spinal cord may still be present in maturity, although the behavior of this circuitry may be suppressed and the same features may not be observed in the mature spinal cord. If so, such circuitry may become useful in recovery after SCI.

Furthermore, observations of neonates are in agreement with the observation in adult rats and cats: the neural circuitry is sensitive to the sensory inputs. The findings in this section further reinforce the motivation to develop a robotic device capable of providing appropriately timed sensory inputs through forceful interaction.

2.4 Spinal Network Models

Coordination between similar limbs has been widely reported in the literature. Coordination of the motion of two legs is evidence of coupled neuronal systems (see section 2.2). Similar observations have been reported for the upper limbs in humans. For example, an obvious cross-talk between the two arm movements has been observed (the direction of movement of one hand affects the direction of movement of the other hand) [**79**][**80**]. Interlimb coordination between the arms and legs has also been observed. For example, a response of the arm to electrically stimulating the leg has been observed during walking. The 'mode' of interlimb coordination is task dependent [**81**].

2.4.1 Interlimb coordination

There are a number of interesting observations regarding interlimb coordination between arms and legs. For example, iso-directional movement between the hand and the foot is easier to conduct than the anti-directional movement ([**24**], pp.190-191). For cervical level SCI patients, interlimb coordination between contralateral limbs is still observed a few months after the injury. The higher the lesion site is, the more 'normal' the induced pattern is, suggesting that interlimb coordination is mediated in the spinal cord [**82**]. However, this does not mean that the role of supra-spinal control is negligible. For example, interlimb coordination may be encouraged or inhibited by the higher CNS depending on the task (Fig. 2-5) [**83**].

2.4.2 Lower limb coordination

A larger volume of research is available on lower limb coordination. Since the specific phase relation between the two legs while walking is thought to be induced by a CPG, these studies are essentially attempting to describe the CPG. Non-linear oscillators are often used as the basis of such models which try to explain some of the 'robust constraints' observed in human behaviors.

One prominent example is the half-center model, in which the CPG is described as two groups of neurons that govern the flexor and extensor muscles of a limb [**84**]. In this model the flexor group and extensor group inhibit each other (Fig. 2-6). Along with this mutual inhibition, there are positive feedback loops within this architecture such that the combination is a limit-cycle oscillator. There have been numerous modifications and additions to this model by the research community, but the concept of 'mutual inhibition' remains its essence. A useful aspect of this model is that the concept of inhibition or excitation is consistent with the properties of neurons. In other words, there is a biological reason why this model may be relevant.

Another model, possibly receiving less attention than the half-center model, is the Haken-Kelso-Bunz (HKB) model [**85**]. This is a non-linear mathematical model that attempts to explain the frequency-dependent phase preferences of two limbs (arms, legs, fingers). For example, it is not difficult to rotate two hands in the clockwise direction at low frequency. As frequency increases, the task becomes more and more difficult, and at some critical frequency, the phase relation between hands cannot be sustained and one hand rotates counter-clockwise. The HKB model establishes an HKB potential (Fig. 2-6), where the parameter b/a is assumed to be reciprocally related to the frequency of motion. The locally stable minimum at $\varphi = -\pi$ and b/a = 0.9 becomes unstable as b/a decreases (i.e. frequency increases) to 0.2. At this value of b/a, the only stable point condition corresponds to zero relative phase between the two limbs. This is a purely theoretical model with no biophysical motivation for its specific mathematical form. Nevertheless, it competently reproduces psychophysical observations.

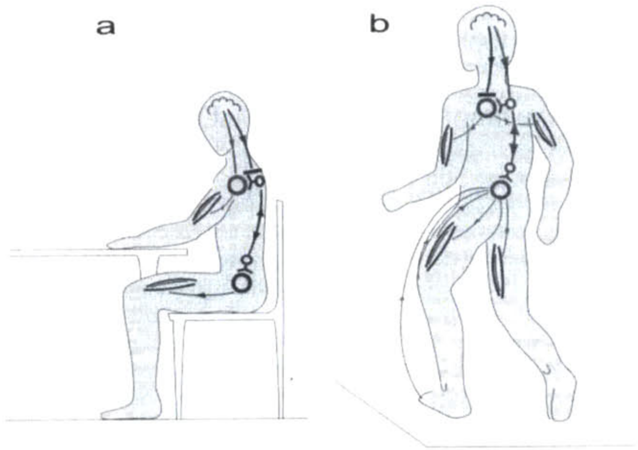

Fig. 2-5. Schematic of a postulated variation of neural movement control during different motor tasks [**83**]. Depending on the task, the brain may a) inhibit interlimb coordination, or b) promote cross-talk while minimizing its control over the upper limb.

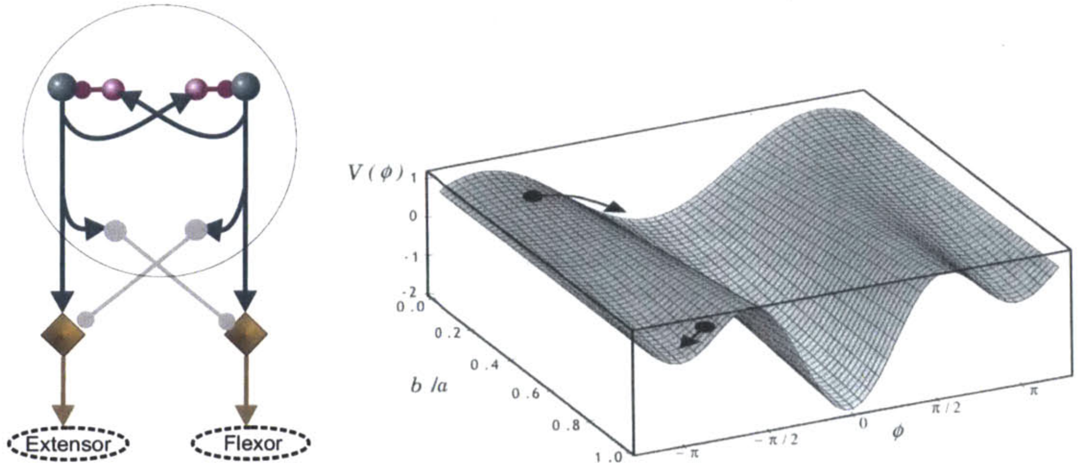

Fig. 2-6. Left: Schematic of the half-center model of Brown and Lundberg. Each of the two centers (blue circles on the top corners) mutually inhibits the other. Right: The Haken-Kelso-Bunz (HKB) potential described by $V(\varphi) = a\cos\varphi - b\sin\varphi$, where φ is the relative phase between the motion of the two limbs. The parameter b/a is related to the movement frequency.

2.4.3 Implications for SCI research

Spinal network models may be tested in software to provide deeper insight [**86**]. On the other hand, if a robotic system existed on which one might implement these models, one may be able to develop a CPG-controlled robot. Real, physical interaction may be possible with the environment to further study the implemented model. Furthermore, if a specific model of the spinal network proves to be promising, one may implement it in a robot, and then let the hardware drive the legs of a patient based on sensory inputs the robot (and the patient) receives.

2.5 Discussion

2.5.1 Using Animal Models

A large number of studies compare the human CNS with other animal's CNS. In all cases, basic features of the human CNS related to movement, such as the existence of synergies or interlimb coordination, were also present in the mammalian CNS. The anatomy of the human CNS, and the spinal cord in particular, is very similar to that of other mammals such as cats and rats. Thus the animal CNS makes a feasible and readily accessible model of the human CNS. The results of experiments with animal models can thus be useful in understanding the human CNS.

2.5.2 Implications for the Apparatus Design

Some understanding of the human or animal CNS is crucial to develop useful equipment that may contribute to research. The findings reviewed in this chapter indicate what is required. For example, since sensory inputs are important for generating locomotor patterns, the apparatus must be able to provide specific sensory inputs when required. In other words, the apparatus must be able to provide useful interaction.

Table 2.1 lists findings in the literature that may be relevant to the design of the new apparatus for research on locomotion after neurological injury.

Table 2.1
Apparatus Design Considerations

Reported in the Literature	Implication for the Apparatus Design
Animal models are widely used	Should be compatible with the animal species widely used in SCI research
Load related sensory inputs play an important role in locomotion	a. Should be able to provide varying weight support b. Should be strong enough to aid in loading/unloading of the foot from the ground
The timing of sensory input is important	Should be able to provide interaction with the animal's hindlimb when needed
CPGs play a role in interlimb coordination	a. Should allow all four limbs to be on the ground b. Should have enough sensing and actuation for the limbs
Models for CPGs exist	Should be able to simulate complex models of CPGs in the mechanical apparatus

Perhaps less evident in Table 2.1 is the fact that the machine should not impede the natural movement of the animal. As sensory inputs are of such importance, avoiding irrelevant sensory inputs is also very important. Thus, the 'default mode' of operation should be to provide little to no interaction force while the animal is as free as possible to move at will. This would allow investigation of animal locomotion 'as-is'.

Chapter 3

Apparatus Concept and Requirements

Following the last chapter, this chapter presents more detailed functional requirements of the apparatus. An existing device built upon a treadmill is introduced and evaluated against the requirements of the new apparatus. Early design concepts are discussed focusing on their contribution to the current design. This chapter concludes by presenting the challenges associated with the current choice of the apparatus configuration.

3.1 Requirements for the Apparatus

Further expanding Table 2.1, the new apparatus is expected to achieve the following:

A. Interface with a widely used animal model in SCI research: A large volume of research on cell implants, pharmacological stimulation, or sensory stimulation both *in vivo* and *in vitro* is based on rodent models. More specifically, adult Sprague-Dawley rats are widely used in SCI research. The apparatus must be able to interface with this animal.

B. Permit a wide range of voluntary overground movement: It is beneficial to be able to examine various modes of locomotion, especially when they might be important aspects of overground quadrupedal behavior (turning, rearing up, etc.). Also, voluntary movement should be permitted as much as possible in order to address the role of specific experimental manipulations (e.g. new pharmacological agents) whose effect may result in sustained and changed features of voluntary locomotion.

Mechanical loads and kinematic constraints imposed on the animal should be minimal. To reduce inertia, the number of hardware elements moving with the animal should be minimized. All other elements may be placed further from the animal. The apparatus near the animal should be compact in size. The output mechanical impedance of the machine must be small for sufficient back-drivability. Movement constraints should be minimal. For example, constraining body parts of the animal is strongly discouraged, as it would restrict voluntary overground movement.

C. Provide various modes of physical interaction: The apparatus is intended to allow experiments including, but not limited to, passively monitoring the animal's movement overground. For example, a new locomotor therapy protocol for patients with neurological injury may be implemented and tested with this apparatus. Specific sensory cues may be provided to the animal to evoke responses from the neural circuitry affecting locomotion. The apparatus may also be used to simulate unique, challenging locomotor conditions.

To provide physical interaction, the apparatus should have sufficient number of actuated and sensor-monitored degrees of freedom. Sufficient torque and power is also required. Robust coupling between the apparatus and the animal is crucial.

3.2 Treadmill-based Apparatus

To further motivate the functional requirements, existing devices for locomotion studies in rodents are reviewed. All of them are designed around a miniature treadmill for rodents.

A typical treadmill used in rodent locomotion studies is shown in Fig. 3-1. The user can manually change the speed of the treadmill or its degree of incline. Animals first exposed to this device do not understand that they have to walk on the belt at a predetermined speed; in order to train the animal to do so, a means to deliver an electric shock is placed at the end of the treadmill. The animal learns to step forward in order to avoid the shock.

Devices such as Fig. 3-1 do not provide any interaction with the animal's hindlimb except for the imposed speed and inclination of the treadmill. The range of aspects of locomotion addressable is thus substantially limited.

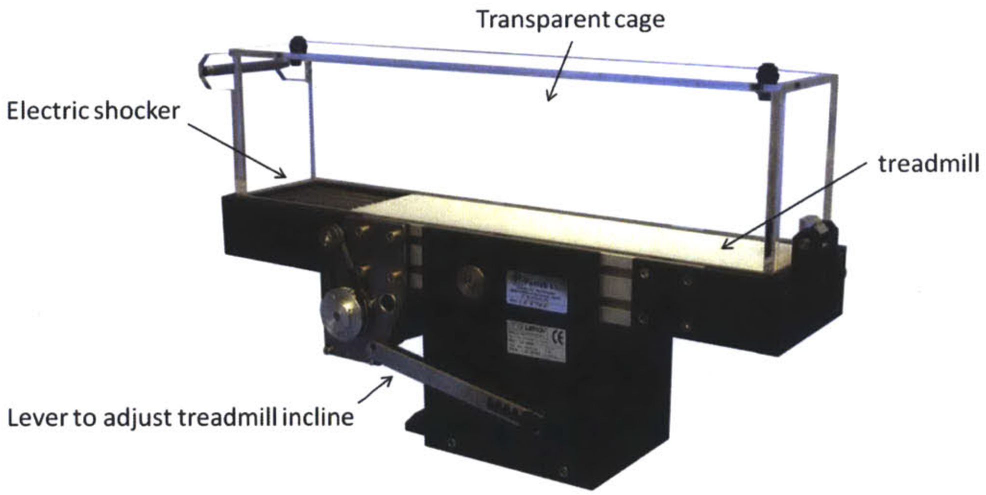

Fig. 3-1. A rodent treadmill from Panlab (www.panlab.com).

3.2.1 The Rat Stepper

3.2.1.1 Design Evolution

The Rat Stepper is a device that, in its present form, consists of a miniature treadmill for rodents, two 2-DOF manipulators, and an active body-weight support system (BWSS) [**87**]. In the early development of the Rat Stepper, it was first conceived to be a 'virtual treadmill' in which the animal was manually held while two PHANToM 1.0 haptic interfaces (SensAble Technologies, Inc.) coupled to the paws of the animal simulated virtual ground [**88**] (Fig. 3-2). Perhaps due to technical difficulties, subsequent designs moved away from the idea of simulating a virtual treadmill. Instead they incorporated a physical treadmill while haptic interfaces were coupled to the animal's hindlimb ankles [**89**]. The current design evolution is similar to that reported in [**87**] in which the haptic interfaces were replaced by custom-designed robotic arms (Fig. 3-3).

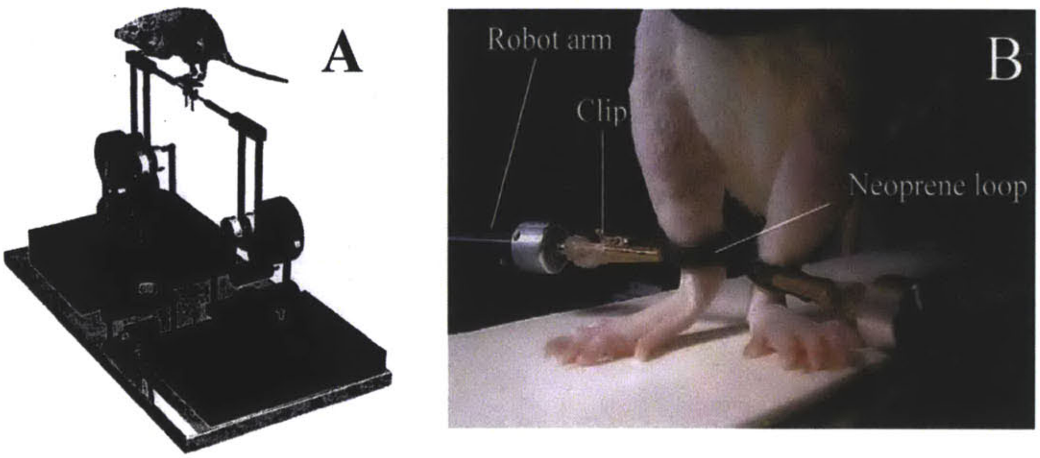

Fig. 3-2. Earlier designs of the Rat Stepper. (A) In the first version in 2000 haptic devices simulated virtual ground [**88**]. (B) A subsequent version in 2002 used a treadmill [**89**].

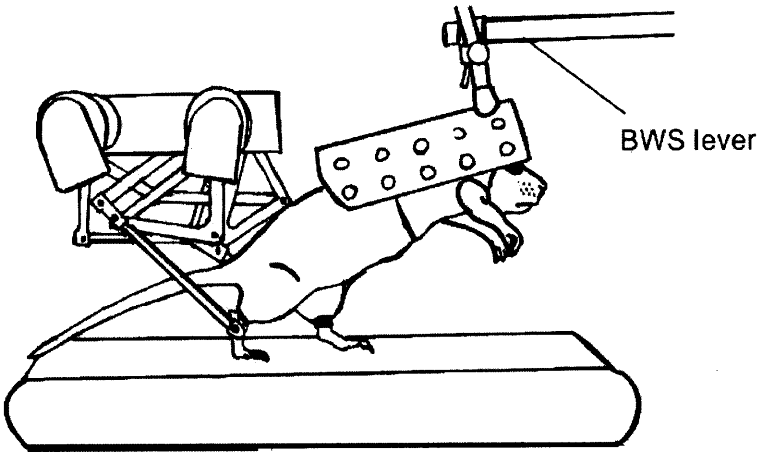

Fig. 3-3. Current configuration of the Rat Stepper [**87**].

3.2.1.2 Advantages and Shortcomings

As the Rat Stepper is built upon a treadmill, it possesses many design advantages. First of all, this configuration keeps the location of the animal essentially fixed in space. This allows the hardware to be stationary as well, located in close proximity to the animal. Large actuators can be used without concern for their weight and inertia. This allows the design to consider practically every actuator technology that is available. This is a significant advantage given that, in general, actuator technology is one of the most limiting factors in robot design [**90**]. In short, the current configuration of the Rat Stepper simplifies the design and implementation of the device.

On the other hand, this design also restricts the scope of possible experiments. For example, because voluntary movements such as turning or rearing up are not permitted, the contribution of these movements to quadruped locomotion cannot be addressed. Topics such as natural balance or fore-hindlimb coordination are also difficult to address in this apparatus. Only certain types of 'perturbation' can be applied, while the observable 'response' is also restricted to those possible on the treadmill belt. This is largely due to the treadmill's single-dimensional movement and the lack of room for any natural or voluntary movement of the animal. To better understand the bio-system, it is important to allow various modes of natural movement of the animal beyond those possible on a treadmill, especially because locomotion on a treadmill may differ significantly from locomotion overground [**91**].

In summary, the Rat Stepper assumes a design in which the implementation is simplified, but because of that design, limits voluntary movement and the scope of possible research.

3.3 Design Concept

In order to allow features of natural movement that may be relevant in the field of SCI research, high priority was set towards designing apparatus that allows the animal to move freely in an open space, or an 'arena'.

3.3.1 Early Design Concepts

As stated earlier, a new apparatus with an overground configuration is expected to offer greater benefits for locomotion research in rats. Allowing overground locomotion strongly constrains the design yet it still allows many different design paths to choose from. The design space is further reduced by considering other important requirements detailed in Chapters 4 and 5. Also, the current state of available technology affects the realization of any tentative designs.

Originally, the apparatus was conceived to be similar to Fig. 3-4. The emphasis was on 'compactness', so that the apparatus was small in size, near the animal, and without external wires or tethers. In this form, the design consisted of all of the following in one package: power, servo amplifier, actuators, sensors and wireless transmission. Data acquisition was envisioned to be performed by an external station communicating with the apparatus wirelessly. The control loop was to be closed either within the apparatus or via the external station. In short, this design can be summarized as un-tethered, wireless and self-contained (i.e. having as many features onboard as possible).

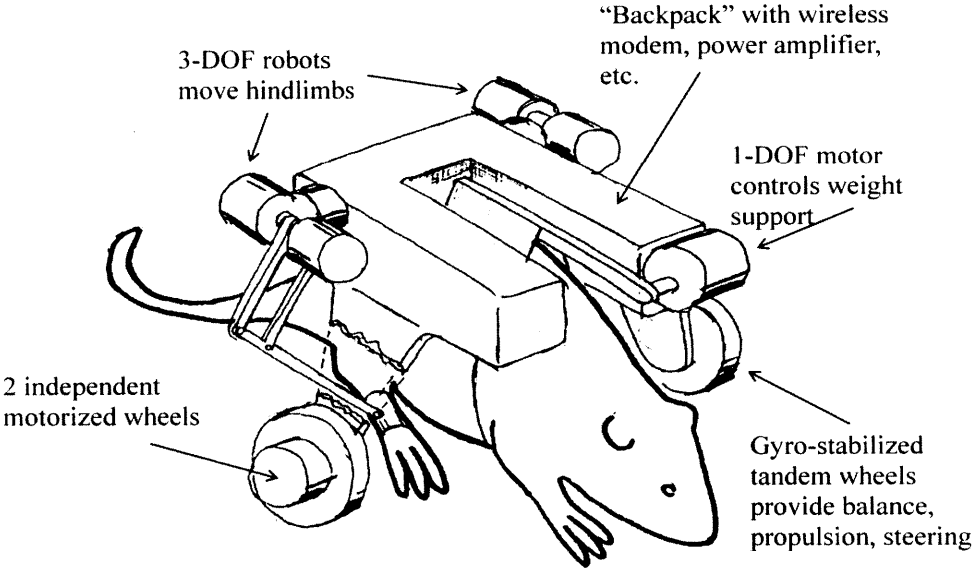
"Backpack" with wireless modem, power amplifier, etc.
3-DOF robots move hindlimbs
1-DOF motor controls weight support
2 independent motorized wheels
Gyro-stabilized tandem wheels provide balance, propulsion, steering

Fig. 3-4. Conceptual sketch of a tentative apparatus (sketch by prof. Neville Hogan).

A former graduate student of the Newman Laboratory, Joshua Young, worked on realizing this concept. The initial prototype deliberately omitted the two 3-DOF robot arms shown in Fig. 3-4 and focused on having power and wireless communication onboard, as well as implementing the two gyro-stabilized wheels. The robot arms and the weight support feature could then be added in subsequent design iterations. However, two initial prototypes (shown in Fig. 3-5) revealed some critical shortcomings of the wireless design. First, onboard power required multiple battery packs to be located on the prototype, drastically increasing the size and weight of the prototype. Lighter and more compact alternatives lacked the power necessary to run the two motors for the wheels as well as onboard electronics. Second, the lag of the wireless transmission system severely limited the quality of control. The resulting prototype weighed more than 2 kg and was unable to demonstrate feasibility. A substantial reduction in weight or improvement in data transmission seemed unlikely, quite aside from the challenge of implementing the robotic arms and active weight support. It was thus concluded that with technology available at the time, wireless, self-contained designs similar to Fig. 3-4 were unlikely to be realizable.

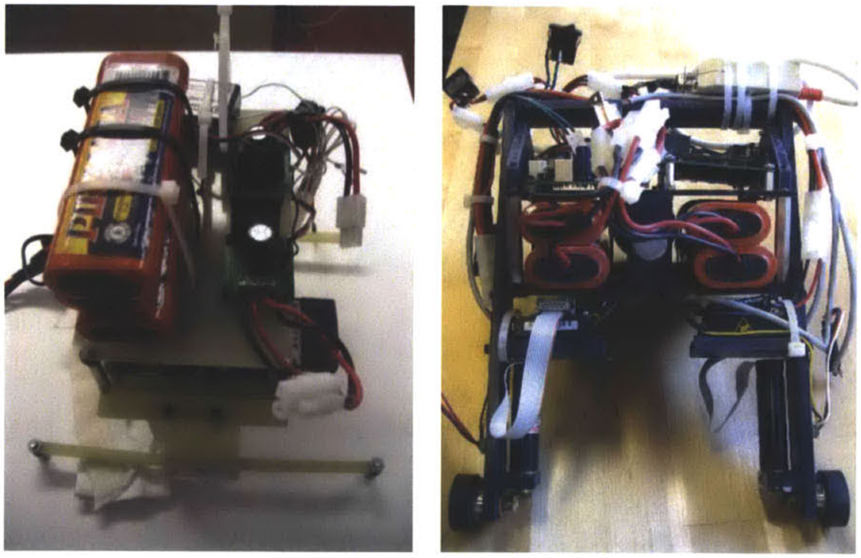

Fig. 3-5. Early prototypes of the wireless configuration. Each prototype weighed more than 2 kg and was taller than 25 cm. (The dark-orange components on the top of the left figure and in the middle of the right figure are the onboard batteries.)

3.3.2 Current Design Concept

Learning from the limitations of these previous designs, the current design is tethered. This allows better data transmission as well as avoiding encumbering the animal by placing larger and heavier components away from the animal. The system now consists of three separate modules described briefly below and in more detail in subsequent chapters, namely the Rat Module, the Body-Weight Support System (BWSS) and other supporting hardware such as a computer which implements the control system and also stores data (Fig. 3-5).

A. Rat Module

The Rat Module, colloquially known as the “Rat Backpack”, is a robotic device that operates in close proximity with the animal and physically interacts with its movement. While other elements such as the servo-amplifiers or power supply can be further away from the animal, at least the sensors and actuators are required to be within close proximity to the animal to ensure proper control. The Rat Module was conceived to be lightweight and compact to minimize its inertia, thereby to minimally encumber the animal, in order to maximize free, voluntary movements. The Rat Module works like an ‘exoskeleton’ for the animal’s hindlimbs.

B. Body-Weight Support System (BWSS)

Weight support is an important feature of the apparatus. In certain animal preparations (such as spinal transection), the animal may lack the ability to support its own weight. In order to provide necessary weight support and to relieve the animal of the weight of the Rat Module if necessary, a weight support feature is required.

The tethered design allows the BWSS to be a separate, external module that is remote from the animal. This, then, allows the BWSS to be larger and more powerful. A crane-type support from above was envisioned which maintains vertical force as shown in Fig. 3-6. The system covers a 4’-diameter arena in which the animal is free to move. This would allow the apparatus to be compatible with enclosures commonly used for rat locomotion studies which are the basis of a widely-used locomotor rating scale for rodents known as the Basso, Beattie and Bresnahan (BBB) Locomotor Rating Scale [**92**]. In this standard scale, the animal's locomotion is evaluated while it is free to move inside a 4~5'-diameter arena.

The BWSS also effectively serves as a 'wiring tower', a means whereby electrical communication (power and signals) between the Rat Module and other electronics remote from the animal travel through a bundle of adjacent wires supported by and guided through the physical structure of the BWSS.

C. Controller, Data Acquisition (DAQ) and Power

All sampling, computation and data storage is accomplished using a computer which is outside the animal's area of activity. With no limitations on its size or performance, this computer monitors and controls both the Rat Module and the BWSS in real time. Data stored in the computer can be used for subsequent analysis. Power for all active components in the system is provided by an external Power Supply Unit (PSU) also placed outside the animal's area of activity.

In summary, the current design is centered on having a compact and lightweight Rat Module carrying only the minimal necessary components onboard, while it communicates with other off-board components such as the BWSS or the main computer through wires. This general concept is the backbone of all hardware developed herein. The feasibility of this concept is assessed in the later part of this dissertation.

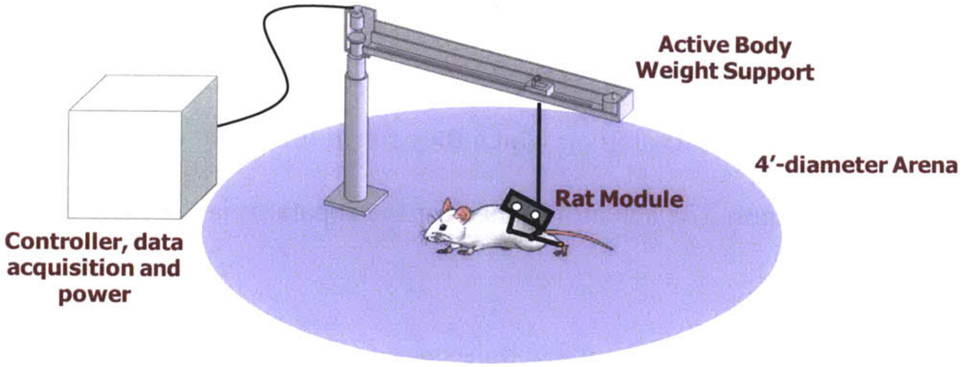
Active Body Weight Support
4'-diameter Arena
Rat Module
Controller, data acquisition and power

Fig. 3-6. Current concept of the system, consisting of the Rat Module, BWSS, and an external computer for control, DAQ and power. The animal is free to move inside the circular 4'-diameter "arena".

3.4 Technical Challenges

While assuming the overground, exoskeletal design is advantageous to address various modes of natural locomotion, it also poses significant technical challenges to the implementation of the apparatus.

3.4.1 Interfacing with the Animal

As with any other apparatus interfacing with the animal (such as the Rat Stepper), working in close proximity of rats can be quite challenging.

First of all, rodents are small, frail animals that weigh 200~300 grams on average when fully mature. Their leg bones are less than 5 mm in diameter and the surrounding muscles are also small. The magnitude of forces familiar to humans may easily injure the animal. Also, attaching to the animal is a non-trivial task. Their skin is extremely soft and loosely connected to their muscles or bones, making it difficult to interface the apparatus with their musculoskeletal structure. Their high flexibility also motivates a device with a large range of motion.

Rodents are also extremely fast and agile. Smaller breeds can run at 4 m/s [**93**], while larger species such as the Sprague-Dawley rats can walk at 80 cm/s, beyond which is considered 'running' [**94**]. Although the occasion on which they run at full speed may be rare, they often trot at 30-40 cm/s in their cages. The actuator choice for the apparatus is expected to comply with the speed of the animal.

Rats are a natural prey animal and are thus very sensitive to their surroundings. They may become timid as a result of changes in the ambient sound, large moving objects in their vicinity, changes in the hour of day experiments are performed, sudden changes in lighting, or excessive handling. They may become anxious about these changes and show signs of stress (excretion, shivering, reluctance to maneuver, etc.). When this occurs, the experiment would not be conducive to studying normal behavior. Hence it is necessary to validate that the apparatus does not intimidate the animal.

3.4.2 Minimum Encumbrance to the Animal

Unlike in the design of Rat Stepper, the proposed design requires that its actuators operate in close proximity to the rat and move along with the animal. This suggests that the Rat Module may have to carry a modest number of electromechanical components onboard. At the same time, it should be compact enough to minimize interference with the animal's movement, and light enough to minimize weight and inertia. The size and weight of the Rat Module then becomes a compromise balancing between the number of components onboard (and thus the complexity of the system) and the size and inertia of the equipment. Finding the 'sweet spot' may be difficult.

The robotic arms on the Rat Module must be sufficiently back-drivable. At the very least, the device must be able to provide a mode of operation in which the interaction force imposed on the animal is sufficiently small to enable expression of nearly normal behavior, though quantifying this criterion may be difficult. Ideally, actuators with low output impedances should be used to ensure back-drivability. If such actuators are not available, active impedance modulation with force feedback may be necessary.

3.4.3 Lack of Similar Precedents

Developing novel equipment with little previous references may be challenging. An advantage is the vast freedom of design and implementation possibilities. On the other hand, choosing the right design with little or no instructive examples may require a lot of speculation and estimation in the design process. In this regard, it will be useful to consider several design alternatives, fabricate them as prototypes and testing them on animals.

Chapter 4

Design and Implementation of the Rat Module

4.1 Design Consideration

4.1.1 Number of Actuated Degrees of Freedom

In the system shown conceptually in figure 3.5, the bulkiest components of the Rat Module are its actuators. The number of controlled degrees of freedom (DOF) equals the number of actuators needed for the machine. The number of actuators affects many aspects of the design, as illustrated in Fig. 4-1. The more controlled degrees of freedom available, the more agile the machine becomes. On the other hand, the complexity of implementation rises and the overall weight of the robot is also increased. Therefore the problem of choosing the number of controlled DOF is equivalent to answering the question "what is the minimum number of controlled DOF needed for the purpose?"

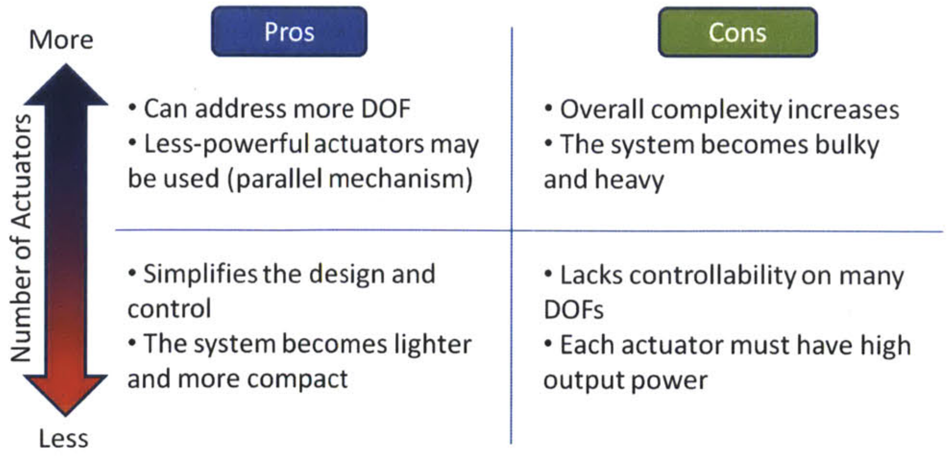
More
Pros
Cons
Number of Actuators
• Can address more DOF
• Less-powerful actuators may be used (parallel mechanism)
• Overall complexity increases
• The system becomes bulky and heavy
• Simplifies the design and control
• The system becomes lighter and more compact
• Lacks controllability on many DOFs
• Each actuator must have high output power
Less

Fig. 4-1. Advantages and disadvantages of many or few actuators.

The design is focused on investigating hindlimb locomotion rather than forelimb locomotion as the former is more related to human locomotion. Also, a prominent motivation for this machine is to support Spinal Cord Injury (SCI) research in rats, where the rodents are typically given surgery that removes the motor and sensory functionalities of the hind quarters only. Hence it is sufficient to consider only the hind quarters of the animal and how the apparatus can interact with them.

While the joints of the hindlimb allow movements away from the sagittal plane (e.g. abduction/adduction of the legs), hindlimb stepping occurs primarily in this plane [**87**] and thus it is reasonable to consider sagittal plane motion only (see Fig. 4-2). The kinematics of hindlimb locomotion are usually quantified using the hip, knee and ankle joint angles. One may consider interacting with all three of these DOFs. However, that would increase the number of actuators needed and also require interfacing with the foot of the animal. However, attachment to the foot is strongly discouraged since it may alter sensory feedback during stepping. Alternatively, one may consider interacting with the hip and knee joint only, by interfacing the apparatus with the lower tibia of the animal (the bone between the knee and ankle joint). This design would reduce the required actuators to two per limb and also clear the foot of the animal while sacrificing control of the ankle joint. To avoid complexity, the design adapted the option of interacting with the hip and knee joint only.

For the design presented here a total of four actuators were used to control 2 DOF sagittal plane motions of each hindlimb. Note that the Rat Stepper also uses 4 actuators to drive sagittal plane motion of each hindlimb [**87**]. This allows a reasonable comparison of that machine with the design presented here.

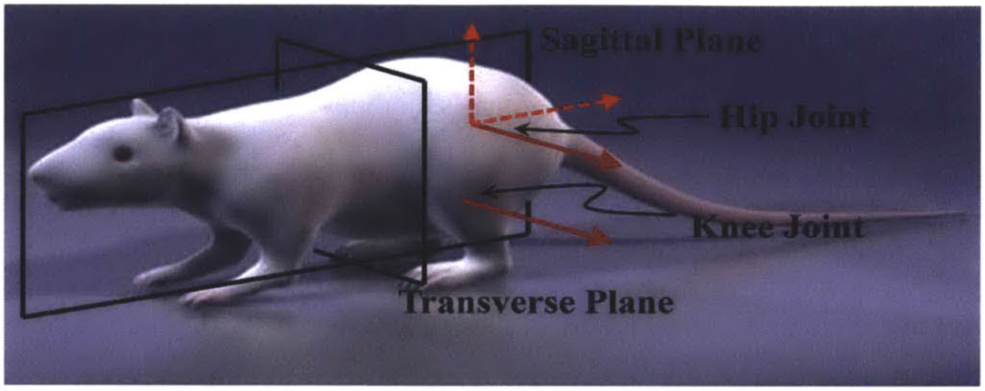

Fig. 4-2. Body planes and DOFs of the hip and knee of the rat hindlimb. The arrows represent the axes of rotation for each joint. The solid red arrows indicate the two DOF that are normal to a sagittal plane, responsible for hindlimb motion in a sagittal plane. (The 3D model is taken from Turbosquid.com.)

4.1.2 Actuator Selection

As the actuators may be the bulkiest and heaviest elements onboard the Rat Module, the choice of actuators greatly influenced the overall design. It was thus required to select the appropriate actuators first before considering different configuration options for the Rat Module.

Among all the actuator types available (piezoelectric actuators, shape memory alloys, linear motors, hydraulics, etc.), electric permanent-magnet (PM) rotary motors were the most suitable for this project [**90**]. PM motors available today can be small and lightweight yet powerful. Moreover, the characteristics as well as practical application techniques of PM electric motors are better established and have been studied for a longer time than the majority of other actuators. However, for rotary PM motors to be useful in this application, they should also be able to generate enough torque, be fast enough, and as light as possible.

To estimate the required power output (torque times angular velocity), we estimated the required force at the tip of the linkage that is attached to the ankle of the animal. A typical animal weighs 200~250 grams. We estimated that the maximum force generated by a leg on the ankle is about half the body weight of the animal, which is about 1N on each side. Assuming that the moment arms are of similar lengths to the animal's hindlimb, which is roughly 5 cm, the required torque on each robotic arm is 0.05 Nm (Fig. 4-3). Further, it was observed that the typical gait frequency of a healthy rat is no higher than 3 Hz. Given these numbers, the required total power output of the two motors on either side was calculated as

$$\text{(Torque)} \times \text{(Angular Velocity)} = 0.05 \text{ Nm} \times 20 \text{ rad/s} = 1 \text{ W},$$

then each motor would be required to produce at least 0.5 W of power.

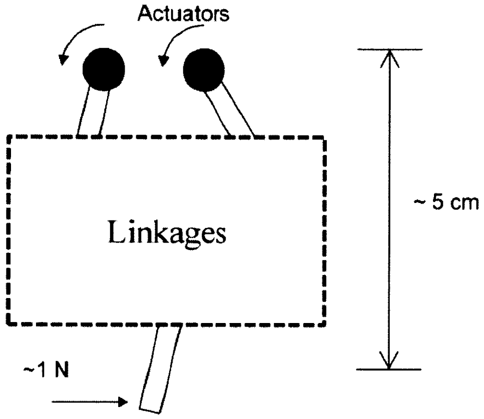

Fig. 4-3. Rough estimate of required power for the motors.

Typical PM motors operate at high speeds (maximum speed of 30,000 rpm is not unusual) and easily meet the speed requirements but not the torque requirements. For example, a motor capable of operating at 16,600 rpm and generating 0.8 W of mechanical power can only exert 1.3 mNm of torque at best. It is thus natural to add a gearhead to the motor so as to meet the torque requirement. Some portion of the mechanical power is dissipated within the gearhead, so it is also necessary to consider the efficiency of the gearhead.

Table 4.1 shows the list of motor and gearhead combinations that were considered. Among those that meet the requirement of generating 0.5 W power output, the one with the least weight was chosen (Maxon EC6 motors with 57:1 reduction gearhead). More detail on this selection is presented in the following section. Maxon (www.maxonmotor.com, Switzerland) was the only vendor that provided a motor suitable for this application. For example, motors from Yaskawa (www.e-mechatronics.com/en, Japan) or Mitsubishi Electronics (http://www.mitsubishielectric.com, Japan) were too heavy and bulky for the application. Miniature DC motors provided by Didel (didel.com, Switzerland) simply lacked the power output.

Table 4.1
List of Motors Considered

Model	Power (W)	Max. torque (mNm)	Max. speed (rpm)	Gearhead (ratio and efficiency)	Weight (gearhead + motor, grams)
Maxon A2516	0.8	1.3	16600	1:50 (70%)	23
Maxon EC6	1.2	0.5	36100	1:57 (70%)	5
Maxon EC14	1.5	3.54	21200	Not available	8.5
Maxon RE13	1.2	2.67	11200	Not available	12
GWS Pico Servo STD	0.2 (estimate)	7.0	900	Not necessary	5.4

4.1.3 Discussion of Motor Selection

Maxon EC6 motor is a 3-phase brushless motor which satisfies more design requirements than any other motor considered. Unfortunately, the motor still lacked the required torque output even after amplification with the 1:57 gear ratio. However, it was speculated that this would not preclude satisfactory performance, since the torque requirement was calculated by assuming maximum force at the tip of the linkage mechanism.

One of the greatest advantages of the EC6 motor was that it was very light even with the encoder and a gearhead provided by the manufacturer (around 5 grams total). Four of these motors weighed less than 20 grams total (less than 10% of the rat's body weight). The motor's largest diameter was 6.7 mm and it was 44 mm long from the tip of the shaft to the end of the motor casing. The length of two of these motors was comparable to the distance between the two hind paws. Another notable advantage of the EC6 motor was that it could be ordered with the encoder custom designed for and integrated to the motor (provided by the vendor). This simplified the design of the Rat Module as the motor-gearhead-encoder package was compact and robust.

Table 4.2
Motor and Gearhead Specification

Maxon EC6 Motor, model #250101	Maxon Planetary Gearhead, GP6, #199689
• Brushless, 3-phase DC motor	• Reduction ratio : 1/57
• Nominal voltage : 12V	• Number of stages : 3
• Power output : 1.2 W	• Maximum efficiency : 68 %
• Nominal speed : 11900 rpm	• Average backlash no load : 2.2°
• Stall torque : 0.402 mNm	• Recommended input speed : less than 40000 rpm
• Terminal resistance : 81.5 Ohms	
• Terminal inductance : 0.602 mH	
• Mechanical time constant : 5.48 ms	

* Total Length (gearhead + motor + encoder) = 38 mm. Total weight = 5 grams

To estimate the back-drivability of the motor + gearhead configuration, the effective output moment of the inertia and viscous damping is calculated as follows: (Items with * were taken from the motor/gearhead datasheet)

J_g : gearhead moment of inertia, 0.001 $g \cdot cm^2$ (*)

J_m : motor rotor moment of inertia, 0.005 $g \cdot cm^2$ (*)

N : gear reduction ratio, 57 (*)

τ : mechanical time constant of the motor, 0.0055 s (*)

B_g : viscous damping in the gearhead, unknown

B_m : viscous damping of the motor ~1 $g \cdot cm^2/s$, ($B_m = J_m / \tau$)

J_{eq} : equivalent output moment of inertia

B_{eq} : equivalent output viscous damping

The value of B_m was derived assuming a simple first order system without an elastic element, $J_m\alpha + B_m\omega$ = (external torque), whose time constant is $\tau = J_m/B_m$. (α is the motor shaft acceleration and ω is the angular velocity of the motor shaft.) Then,

$J_{eq} = J_g + N^2 J_m \approx 16\ g \cdot cm^2$ (similar to the moment of inertia of four quarter coins)

$B_{eq} = B_g + N^2 B_m \approx 3200\ g \cdot cm^2/s$, assuming $B_g \approx B_m$

The above value of B_{eq} produces about 0.4 N resisting force at the end of the tip when driven at 2 Hz. This is comparable to the estimated maximum force of 1 N that the animal can impose at the tip. Thus it may be difficult for animal to back-drive the two motors at 2 Hz speed. Feedback control with force sensors may resolve this issue.

Note that the static friction in the motor and gearhead was not considered in these calculations. With the chosen motors (Maxon EC6 with gearhead), essentially the only option at the time of Rat Module development, there existed significant static friction in the gearhead such that the output mechanical impedance of the manipulator arms was not negligible. A novel control scheme was developed to successfully overcome this issue. See chapter 6 for further detail.

4.2 Detailed Configuration

Once the bulkiest element onboard the Rat Module (the actuator) had been selected, the overall design of the Rat Module could evolve around the size and shape of the Maxon EC6 motor.

4.2.1 Overall Design

From the system concept presented in chapter 3, the design requirements for the Rat Module can be specified as follows:

Req. 1) Should be compact and lightweight.

Req. 2) The motors should be positioned close to the hind quarters of the animal to avoid long linkage lengths.

Req. 3) Should be able to provide body-weight support on its own, or allow interaction with an external body-weight support system.

Req. 4) Should minimally interfere with the animal's natural motion, including walking, running, or rearing up.

Req. 5) Simple design and fabrication is preferred

The four motors were the bulkiest component in the Rat Module. Their placement with respect to the animal's pelvic bone could be 1) At the bottom, 2) On the top, 3) On the sides, or 4) Behind. Out of these possible locations, 4) was ruled out because if the robot was behind the rat, it would interfere with the movement of the tail (which appears to be important for normal behavior). Also, the mechanism might interfere with the animal's ability to rear up on its hindquarters.

Table 4.3 shows candidate design configurations focusing on the location of the actuators with respect to the rat, and their ability to meet the requirements stated above.

Configuration #1 is advantageous in that it is compact and simple to make but it was discarded after learning that there is very little space underneath the animal between the two hindlimbs. Configurations #2 and #5 are advantageous in that they meet the functional requirements better, especially those that are emphasized in chapter 3 (req. 2, 3 and 4). Configuration #2 and #5 had the highest scores. Hence, Configuration #2 was preferred over other candidates that were considered, while #5 was also a viable option. Other options lacked compactness or would interfere with the animal more than configuration #2.

Configuration #2 admits a number of variations. For example, the exact location of the motors, the design of the manipulator arms, wiring, and attachment to the animal are all important details of the final design. Figure 4-4 shows possible variations of Configuration #2 and #5, focusing on the location of the four motors.

Table 4.3
Candidate Configurations

	General location where the actuators would be.	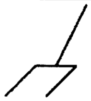	Manipulator arms.
	Wheels contacting the ground. The weight of the device is supported from below.		Weight-support string. The weight of the device is supported from above.

Design Candidate	Req. 1.	Req. 2.	Req. 3.	Req. 4.	Req. 5.	Total Score
#1 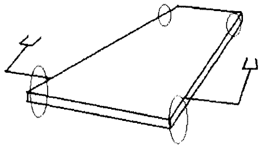	There is little room between hindlimbs Score: 3	The actuators are close to the ankle, but not to the pelvis Score: 6	BWS not needed, and non-adjustable Score: 7	Possible interference when rearing up Score: 5	Simple with no wheel actuation. (Complex otherwise.) Score: 9 (5)	30 (26)
#2 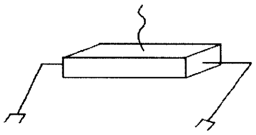	Small enough Score: 8	Very close to the pelvic bone Score: 9	Adjustable BWS Score: 9	Least interference other than its mass Score: 9	Simple, but attachment to the rat may be difficult Score: 6	41
#3 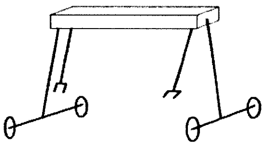	Bulky Score: 5	Constrained side and vertical motion Score: 4	Adjustable BWS within the robot Score: 8	Rearing up may be impeded Score: 6	Simple with no wheel actuation. (Complex otherwise.) Score: 7 (4)	30 (27)
#4 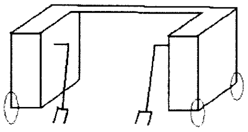	Bulky Score: 4	Constrained side and vertical motion Score: 4	No BWS Score: 3	Rearing up may be impeded Score: 6	Simple with no wheel actuation. (Complex otherwise.) Score: 7 (4)	24 (21)
#5 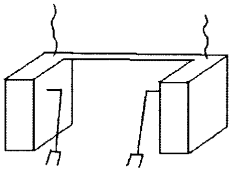	Simpler than #4 but still bulky Score: 5	Relative movement may be small Score: 7	Adjustable BWS Score: 9	Rearing up may be impeded Score: 6	Simple, but attachment to the rat may be difficult Score: 6	33

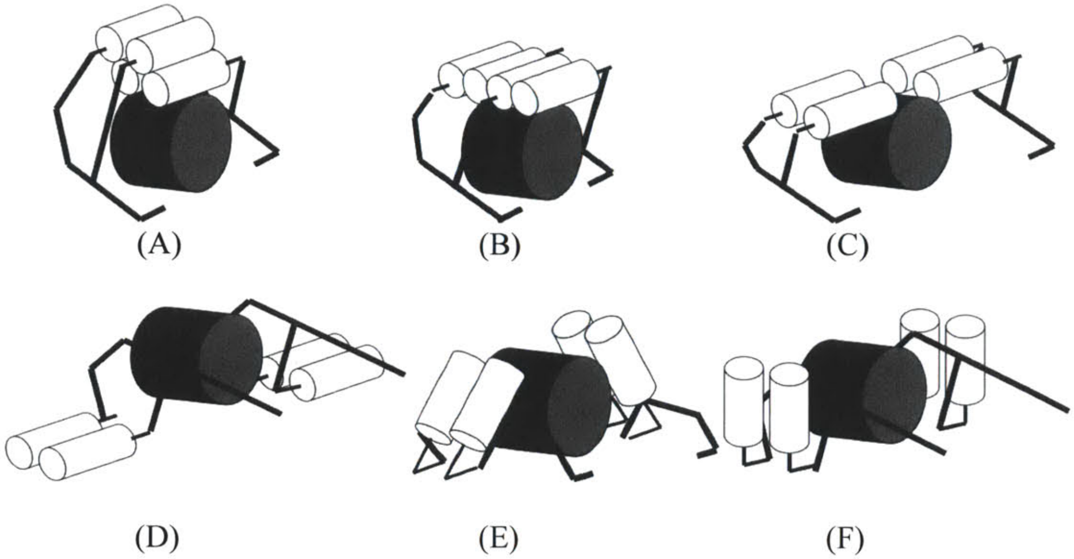

(A) (B) (C)

(D) (E) (F)

Fig. 4-4. Variations of Configuration #2 and #5. The white cylinders represent the motors, black bars depict the linkage mechanism, and the large gray cylinders represent the animal's lower back.

In Fig. 4-4, (A) to (C) are variations of Configuration #2, where (D) to (F) are variations of Configuration #5. (A) and (B) are different from (C) in that the two manipulators are closer to each other. Depending on the length of the motor and the size of the animal, (A) and (B) may be more advantageous than (C), although in case of (A) or (B), the robot arms on either side would be of different dimensions. (D) to (F) are all less favored than (A) to (C), since (D) makes the system unnecessarily wide and (E) and (F) would complicate the transmission mechanism between the motors and the linkages, since the axes of rotation of the motors are not normal to the sagittal plane (as in (A) to (C)).

Because there was no precedent for this device, the design process was iterative, involving many prototypes that were built to understand the relative importance of a large number of inter-related factors. The first prototype (Fig. 4-5) was based on (A), a variation of Configuration #2. The middle part where the motors are placed (hereafter called the 'base' of the Rat Module) as well as the linkages were fabricated in ABS plastic using Rapid Prototyping. Details of the fabrication will be presented in later sections. It became evident that (C) is a better configuration than (A) or (B). The motors were too short for (A) or (B) to accommodate the width of the animal's hindquarters, unless the motor shafts were over-extended. Also, configuration (A) revealed a potential wiring problem, as the flexible connectors to the two bottom-row motors were not readily accessible from above due to the motors on the top row. (see Fig. 4-5(2)). The wires for the two motors in the bottom row had to be accessed either from the front or back of the Rat Module, making the surface of the Rat Module disorganized.

On the other hand, (C) is a viable configuration since the length of two motors together is less than 8 cm, which is slightly wider than the width of the haunches (the muscle groups of the pelvis and femur) of typical rat which is typically less than 7 cm. Also in (C), the connectors can be managed much more neatly. Hence all later versions of Rat Module prototypes assumed configuration (C), which is a variation of configuration #2. One such example is shown in Fig. 4-6.

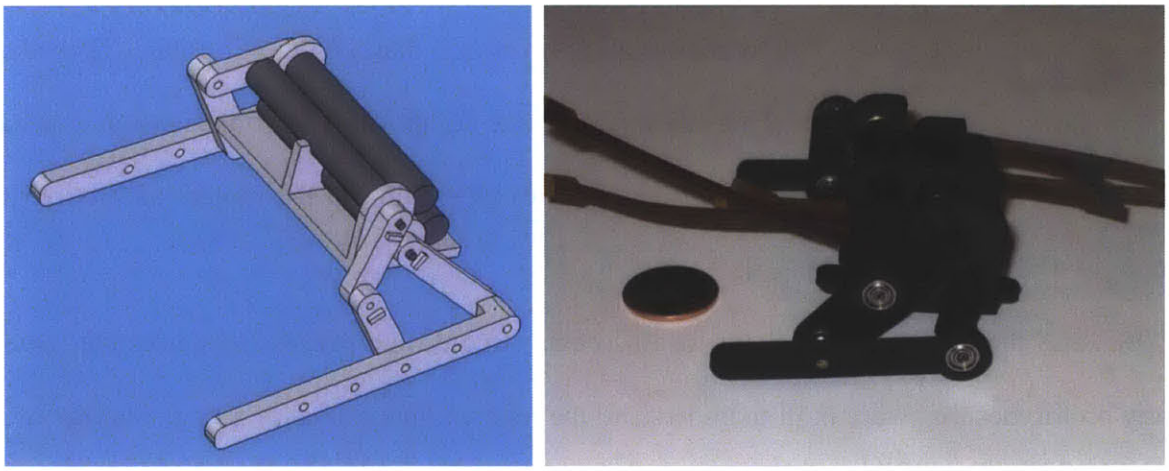

(1) (2)

Fig. 4-5. First prototype with configuration (A) from Fig. 4-4. (1) CAD model. (2) first prototype fabricated in plastic. The flexible connectors to the motors (brown) emerge from both sides of the mechanism.

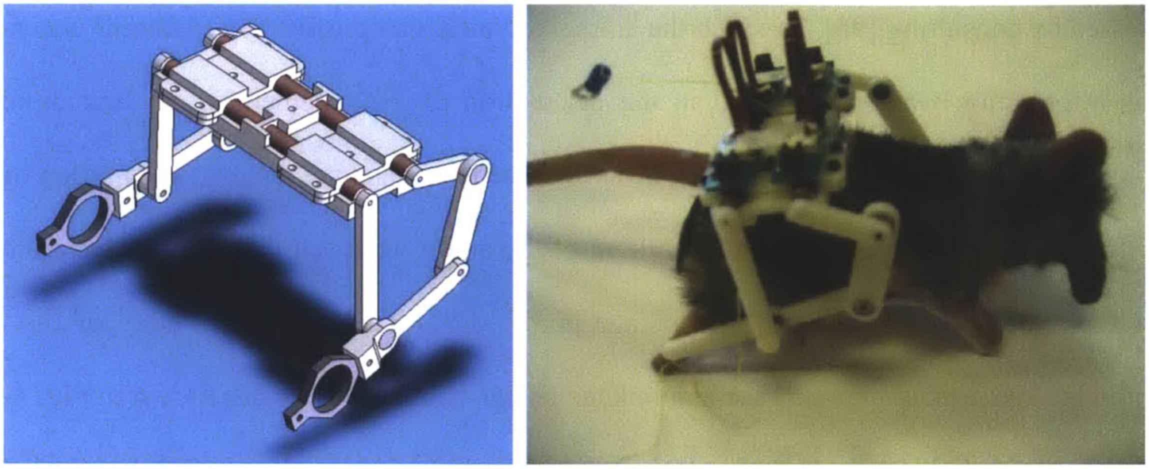

(1) (2)

Fig. 4-6. One of the later prototypes with configuration (C) from Fig. 4-4. (1) A CAD model with the motors depicted as brown cylinders, and (2) an early prototype with motors placed on an actual-size rat doll. Note that the flexible connectors are all facing upwards and are easy to access.

4.2.2 Robotic Arm

Two motors were assigned for each hindlimb to interact with sagittal plane motion of the hip and knee joints. The rotary DOF of the motors were mapped to 2-D Cartesian DOF through a linkage mechanism. In the current design, the mechanism is a 5-bar parallel linkage. It is assumed that the motors are positioned close to and fixed to relative to the pelvic bone. The dimensions of the links were determined considering the following factors.

a) The workspace must cover at least the range of motion of the hindlimb during locomotion
b) The above must be achievable without passing through singularities
c) The links must not impede the animal's movement

Different link dimensions were tested by simulating the reachable end positions of a 5-bar linkage without passing through mechanical singularities (Fig. 4-7). Requirement a) was assessed by consulting [**95**], in which the animal's typical gait profile on a treadmill was reported. This information was incorporated in the calculation to test whether certain link dimensions satisfied requirement a). Requirement c) was achieved by offsetting the plane of motion of the 5-bar linkage from the sagittal plane of motion of the ankle. To reach the ankle of the animal, the last link extended inward from the linkage plane of motion towards the body of the animal (normal to the sagittal plane). The final linkage design and its features are shown in Fig. 4-8. The lengths of each link are presented in Fig. 4-9. Although simulations confirmed that the links will not encounter singularities during anticipated operation, the links were fabricated with mechanical stops to prevent them from reaching the singular positions. Further details of the calculation, which served as the design template for the 5-bar linkage mechanism, are presented in an Appendix.

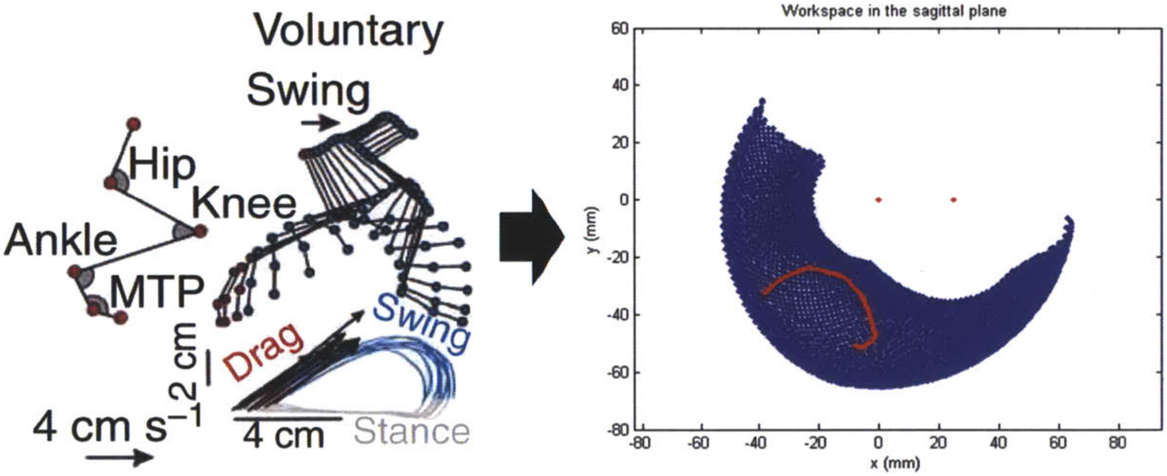

Fig. 4-7. Figure from [**95**] showing the normal gait profile of a rat on a treadmill (left), and a plot from the linkage calculation (right). The two red dots represent the location of the two motor axes, and the blue area denotes the reachable end points of a certain 5-bar linkage configuration (Fig. 4-8 on the right). The red line is the ankle position with respect to the hip joint as derived from [**95**].

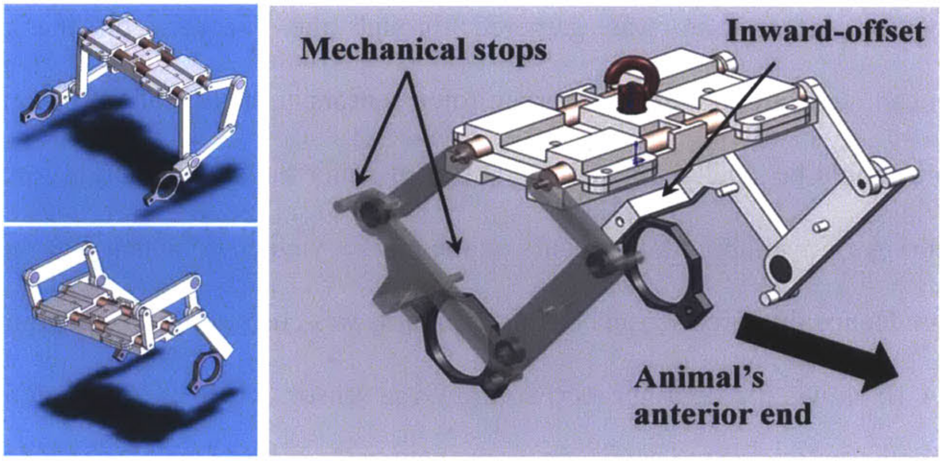
Mechanical stops
Inward-offset
Animal's anterior end

Fig. 4-8. A selection of alternative linkage configurations. The design on the right with grey background is the final design.

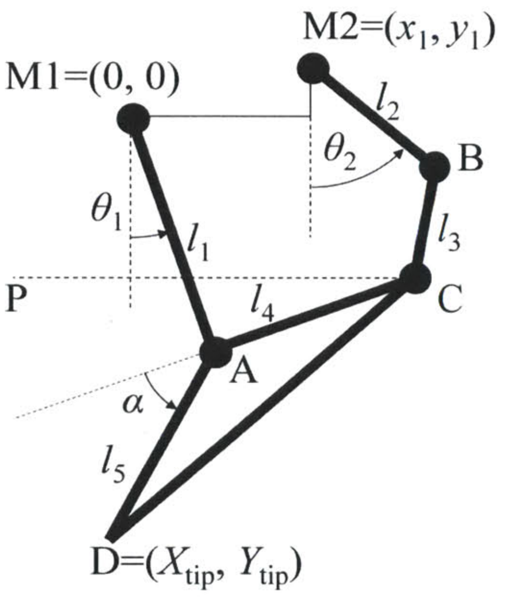
M1=(0, 0)
M2=(x_1, y_1)
l_2
θ_2
B
θ_1
l_1
l_3
P
l_4
C
A
α
l_5
D=(X_{tip}, Y_{tip})

x+ : towards the head
y- : towards the ground

M1 = motor 1
M2 = motor 2
P : parallel to ground
D: end tip
A, B, C: rotary joints

Distance between the motors = 25 mm
$l_1 = 25$ mm
$l_2 = 25$ mm
$l_3 = 40$ mm
$l_4 = 45$ mm
$l_5 = 45$ mm
$\alpha = 155°$

Fig. 4-9. Final linkage dimensions. Triangle DAC forms one rigid link.

4.2.3 Custom Force Sensor

One purpose of the rat module is to measure the dynamics of locomotion as well as to impose various perturbations and/or mechanical assistance to the hindlimbs. For successful control, it is essential to have appropriate sensors to monitor the interaction between the machine and the animal. Position information was gathered through the encoders on the motors. Force information can be acquired with appropriate force sensors at the tips of the robotic arms. These force sensors should be small, compact and able to monitor the 2D interaction forces at the scale of mN. A survey of available force sensors on the market yielded none that met the requirements of the design. Hence the force sensor for this apparatus was custom-designed and manufactured.

Figure 4-10 shows the configuration of the force sensor, which is an octagonal ring design taken from **[96]**. There are four strain gages on the inner surface of the ring, and four on the outer surface of the ring (total of eight). Four strain gages per measurement direction forms a Wheatstone bridge. The voltage difference between the two outputs provides the force measurement. This design allows independent sensing of F_x and F_y while being compact and lightweight. The sensing range was designed to be -3N to 3N for each component. This sensor design was provided to Sensing Systems Corporation which manufactured and calibrated the sensors. See appendix II for more detailed specifications including cross-talk and linearity.

One end of the force sensor was attached to the end of the robotic arm of the Rat Module, as seen in Fig. 4-8. The other end was the force measurement point, which was attached to the ankle of the animal. The sensor was mounted on the robotic arms such that the axial loading force direction (direction of F_2 in Fig. 4-10) was parallel to l_4 in Fig. 4-9. In this way, the angle φ_{PCA} could be used to transform the sensor reading into F_x and F_y in global coordinates. That is,

$$\begin{bmatrix} F_x \\ F_y \end{bmatrix} = \begin{bmatrix} \sin\varphi_{\mathrm{PCA}} & -\cos\varphi_{\mathrm{PCA}} \\ -\cos\varphi_{\mathrm{PCA}} & -\sin\varphi_{\mathrm{PCA}} \end{bmatrix} \begin{bmatrix} F_1 \\ F_2 \end{bmatrix}$$

This calculation was performed in real time when the force information was required for control. In that case, an online filter was used to reduce noise in the signals. For offline measurement, F_1 and F_2 were recorded without filtering and processed subsequently. This allowed less online computation as well as a broad choice of filters.

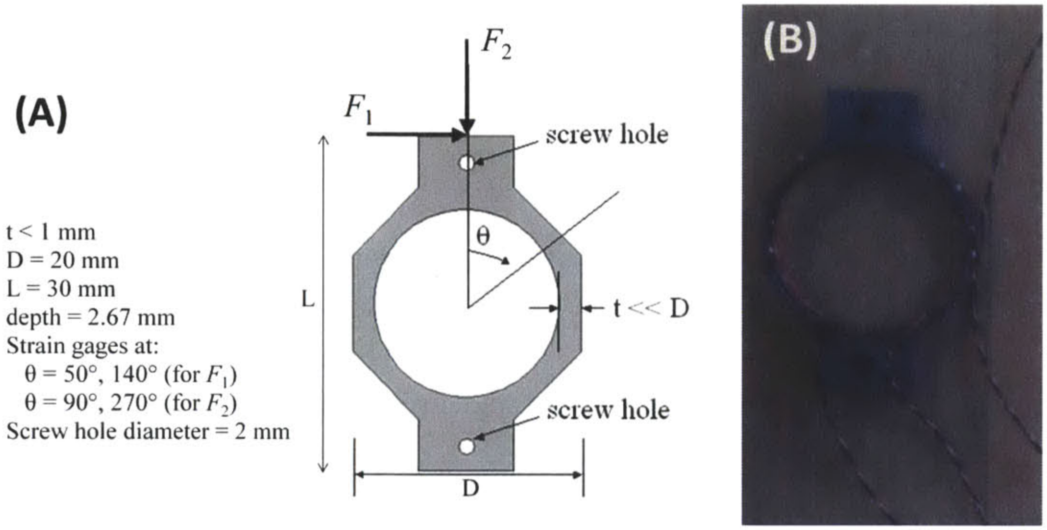
(A)
(B)
F_2
F_1
screw hole
θ
t << D
screw hole
L
D
t < 1 mm
D = 20 mm
L = 30 mm
depth = 2.67 mm
Strain gages at:
θ = 50°, 140° (for F_1)
θ = 90°, 270° (for F_2)
Screw hole diameter = 2 mm

Fig. 4-10. Custom force sensors. (A) configuration and (B) actual photo of one force sensor. The two bundles of wires are for each force measurement direction. The strain gages were placed on the inner surface of the ring, forming two independent Wheatstone bridges.

4.2.4 Base and Cover Design

The “base” of the Rat Module is the main body which houses the four motors. The “cover” is placed on the motors to secure them in position, as well as to allow placement of other parts on top of the cover. The base and cover should be lightweight and compact, while providing structural support to the actuators. The motors were positioned on the base as per the selected design (C) of Fig. 4-4. The distance between the two motors on each side, as determined in Fig. 4-9, was incorporated in the design.

Fig. 4-11 shows a CAD model of the base and cover, and its assembly with the motors. The flat surfaces on the covers are for the miniature PCB boards that serve as the wire junctions (provided by the vendor of the motor). The two holes closest to the tip of the motor shafts are for weight-supporting strings. Multiple weight supporting strings helped keep the Rat Module balanced, while too many strings complicate the design and might physically interfere with the wires for the motor. The bottom of the base included a rectangular groove to reduce the total weight and inertia. The bottom of the base was also contoured to allow better fit to the animal’s lower back.

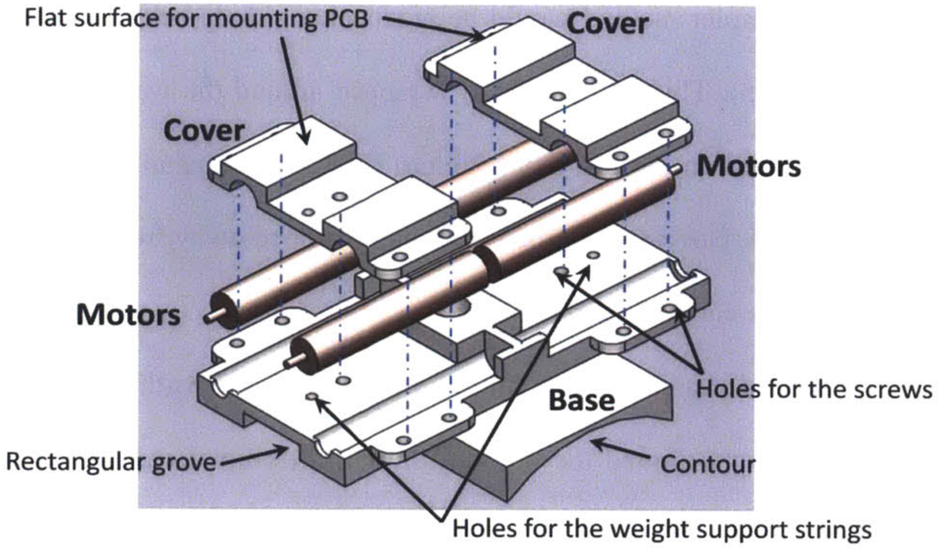
Flat surface for mounting PCB
Cover
Cover
Motors
Motors
Holes for the screws
Base
Rectangular grove
Contour
Holes for the weight support strings

Fig. 4-11. Exploded view of the base, two covers and the four motor assembly.

4.2.5 Biomechanical Coupling

The rat module was coupled to the rat through three mechanical “ports”. One was between the base of the Rat Module and the lower back of the animal (above the pelvic bone), and the other two were between the robotic arms and the animal’s hindlimbs just above the ankle joints. Reliable control of hindlimb motion was facilitated by minimal relative movement between the robot and the animal at these ports.

If the base of the Rat Module had been fixed to the pelvic bone, the locations of the actuators would then have been well-defined relative to the other lower limb segments. A hard mechanical coupling such as using bone pins surgically implanted in the pelvis would eliminate relative movement, but would complicate animal preparation. An alternative option was to use an animal harness and to mount the module on the harness. This yielded simpler, less invasive animal preparation but allowed greater relative movement between the pelvic bone and the actuators.

To test whether the simpler method would be practical, a simple belt-type harness was first investigated (Fig. 4-12, top). This harness easily wrapped around the waist of the animal. The Rat Module was then placed on the belt using Velcro tape. The preparation was simple and the time required was minimal. However, the belt frequently slipped away from the animal towards the tail, thereby making the coupling unreliable.

Another method tested was to use a full-body-length jacket with holes for the limbs. Although the jacket was tight around the body of the rat, the animal crawled out of the jacket very quickly once left alone. This method was abandoned.

An alternative method was to use Elastikon® medical tape instead of the cloth belt (Fig. 4-12, bottom). The tape stayed firmly in place and the animal did not slip out of the tape wrapped around its waist. Velcro tape was placed on top of the Elastikon tape thereby allowing the Rat Module to be attached. This Elastikon attachment was deemed sufficiently secure for the purpose of this research project. Hard coupling methods such as using bone pins were deferred for future work if the current coupling method proves to be problematic.

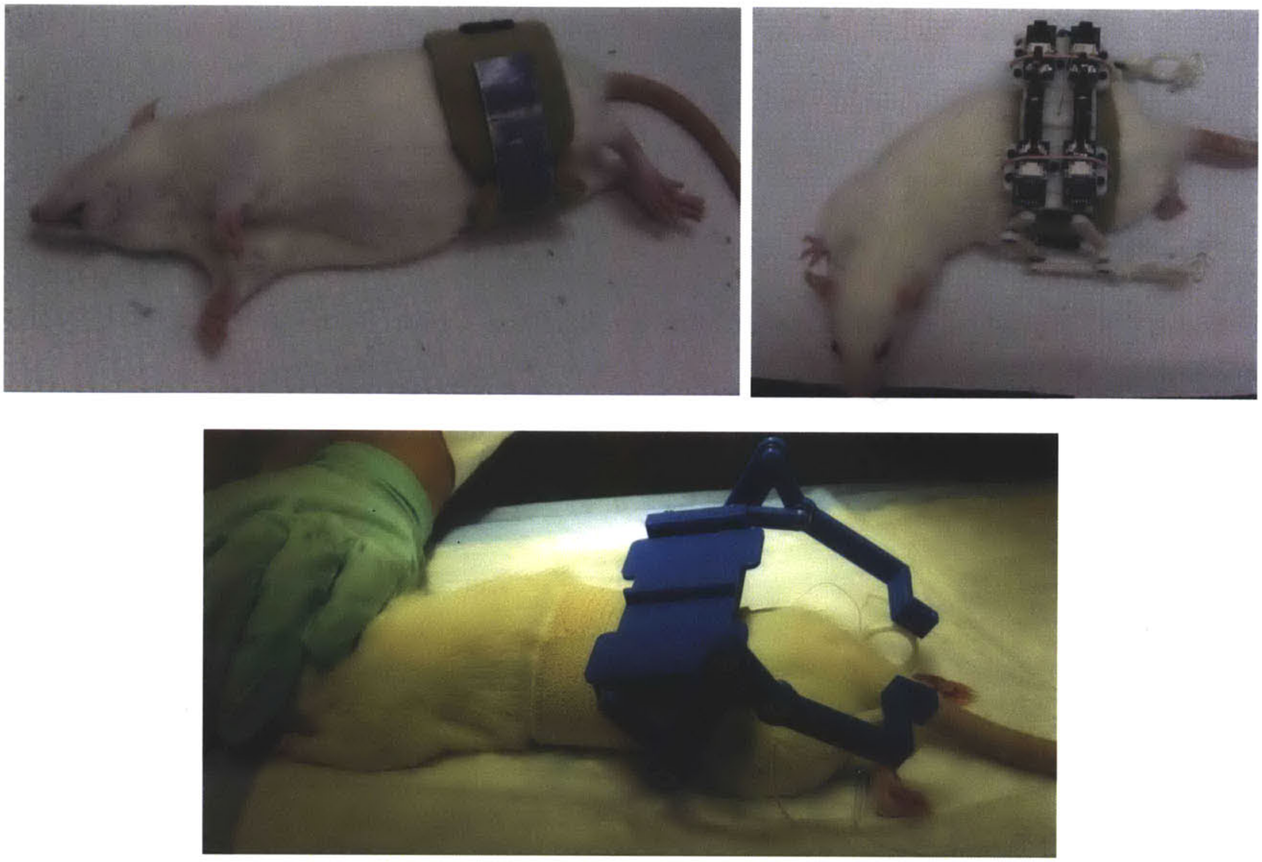

Fig. 4-12. A belt-type harnesses on the animal. (Top-left) the cloth belt was put on the animal while the rat was anesthetized briefly. (Top-right) the rat module was placed on the belt using Velcro tape. This cloth belt easily slipped off the rat's body. (Bottom) the Elastikon® tape around the animal's waist. The tape remained secure on the animal's fur.

Coupling between the robotic arm and the animal's hindlimbs need not be rigid. A known compliance in the coupling to the animal would allow small yet quantifiable movements away from the sagittal plane. Too rigid a coupling might injure the animal or damage the force sensors not only during the attachment procedure but also during experiments.

The present coupling method used a bio-compatible elastic band as shown in Fig. 4-12 (bottom) and Fig. 4-13. The attachment procedure was as follows. A small elastic band (diameter = 2 cm) was made into an '8' shape by placing a plastic bead in the middle of the band. One of the animal's hindlimb ankles was secured into one of the holes in the '8' shape. The hole was then slightly tightened, by holding the bead and pulling the other hole of the '8' shape. This end of the elastic band was secured onto the Rat Module's arm, thereby completing the coupling between the animal's ankle and the arm of the Rat Module.

The feasibility of this coupling method was tested on an anesthetized animal (Fig. 4-12 bottom), and proved to be effective. It allowed the force sensors to be mounted close to the animal's ankle. The linkages followed the motion of the hindlimbs well.

4.3 Fabrication

The parts of the Rat Module (the base, two covers, and four linkage parts per each robotic arm) were fabricated using a Dimension® 3D-printing machine located in the Edgerton Student Shop, or in the Biomimetic Robotics Laboratory. The parts were made of ABS plastic. The parts were printed in such a way that the inside was coarsely filled, to reduce the weight and inertia of each part. The total volume of plastic used to build all parts was less than 2 in^3.

Ball bearings and coiled metal spring pins (both from McMaster-Carr®. See Appendix for more detail) were used to assemble the linkages manually. The motor-gearhead output shafts were press-fit to the appropriate linkage parts. This motor-linkage assembly was then placed on the base part, and the motors secured with the two covers. The covers and the base were then secured by 10 sets of nuts, bolts and washers. Miniature printed circuit boards (PCB) which served as wiring junctions were placed on top of the covers. Finally, the two custom force sensors were mounted at the ends of the two robotic arms. The total time required to assemble all the parts was roughly an hour.

Figure 4-13 shows photographs of the assembled Rat Module resting on top of a plastic block. The base and the two covers are painted in permanent green (oil color). This was done to facilitate vision-controlled BWSS robot movement (See Chapter 3 for more detail).

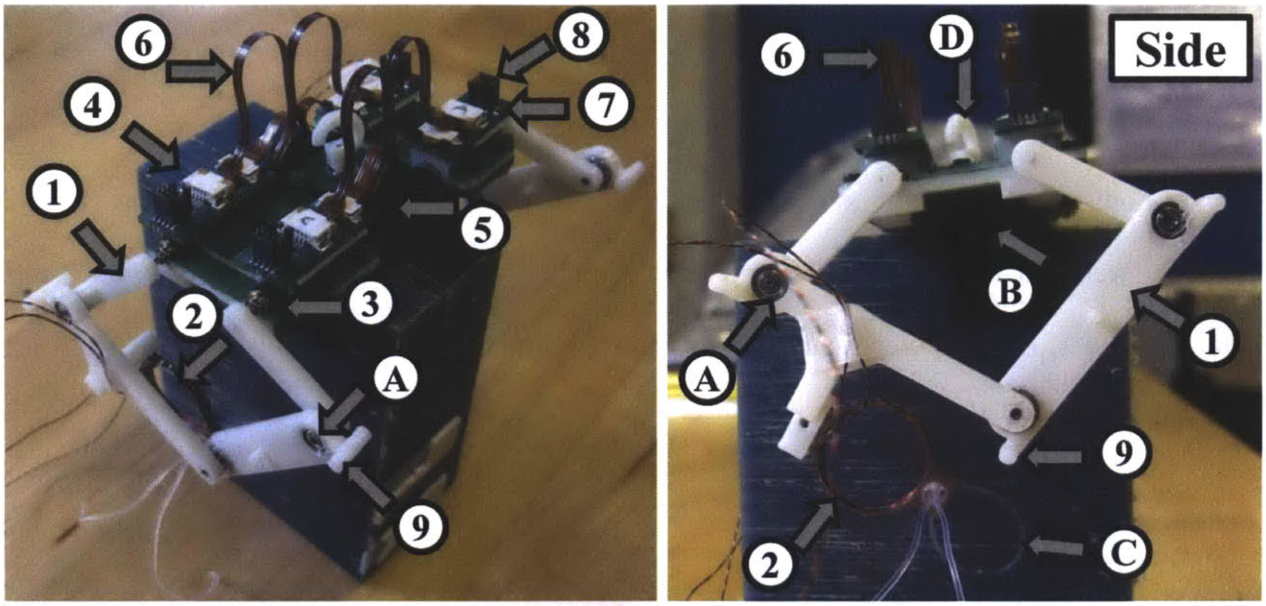

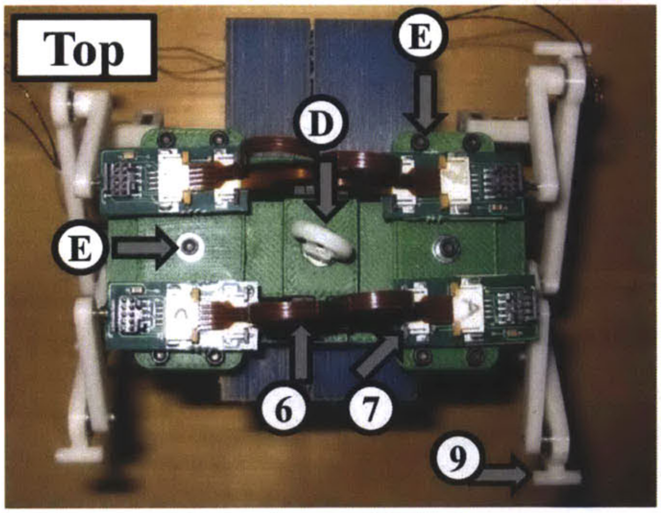

1. Linkages built in ABS plastic
2. Custom 2D force sensor
3. Gearhead
4. The motors are under the PCB boards
5. Optical encoder for each motor
6. Flat wire from the motors and encoders
7. PCB board with wiring terminals
8. Wiring junction for motors and encoders
9. Mechanical stops to avoid mechanism singularity

A. Rotary bearings and coil-spring pins are used to connect the linkages
B. Velcro attachment for biomechanical coupling at the lower back of the animal
C. Elastic strings for biomechanical coupling at the ankles of the animal
D. Plastic hook for BWSS (see Chapter 3)
E. Screws, washers and nuts keep the two covers on the base

Fig. 4-13. Photo of the Rat Module placed on a plastic block. Features of this device are enumerated and explained in the table.

4.4 Supporting Hardware

All sensor signals were collected at 1000 Hz and processed on a master computer running real-time Linux. Motor commands were issued through the motor servo amplifiers (Copley Controls, Accelnet) which were wired to the Rat Module. Limp and flexible wires were used between the BWSS and the Rat Module.

Fig 4-14 shows the apparatus setup used for the experiment. To facilitate transport between laboratories, the supporting systems, including the controller board, power supply, controller box for the body-weight support system, desktop PC (master computer) and the laptop (BWSS control), were put on a low-profile utility cart. The body-weight support system was fixed to a corner to cover as much workspace on the floor as possible. Further details of the BWSS are provided in Chapter 3.

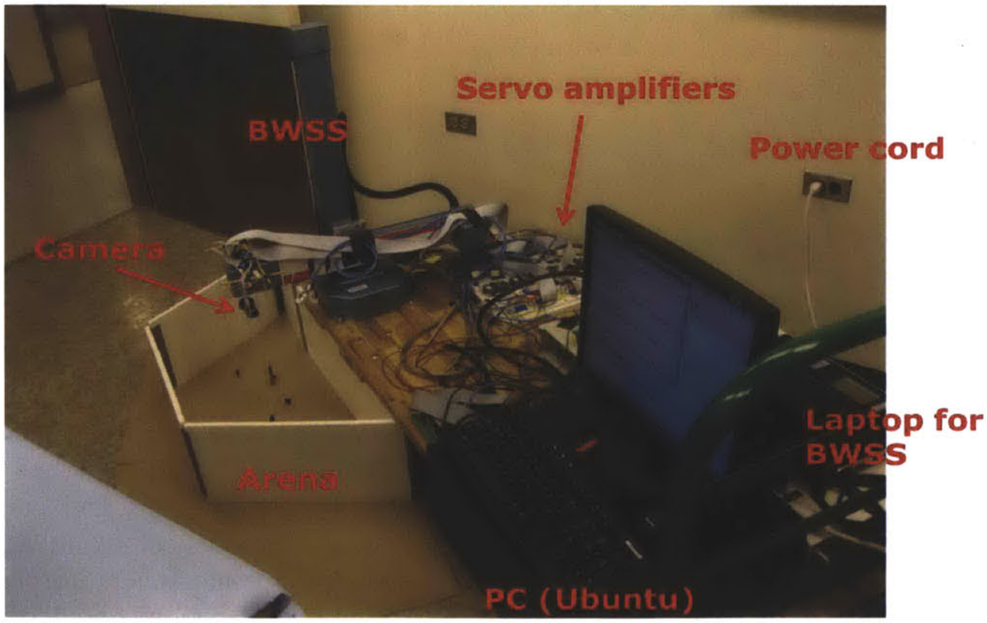

Fig. 4-14. Supporting hardware items were fixed onto the utility cart. The cart could easily be transported between labs.

4.5 Summary and Discussion

The final specification of the Rat Module can be summarized as follows.

Rat Module Specification

- For rat hind-quarters
- 4 DOF total (2 DOF on each side)
- Actuator: Maxon EC6 with gearhead
- Power output : 1.2 W x 4
- Average maximum pushing force at the tip of the robot arms at the 'home' position* : 1.3 N on each side
- Average maximum resisting force at the tip of the robot arms at the 'home' position* : 2.0 N on each side
- Encoders on each motor shaft (400 counts per turn)
- 2-D force sensors on each side
- Non-invasive attachment to the animal
- Body: ABS plastic
- Total weight = 75 grams

* 'Home' position: $\theta_1 = -45^\circ$ and $\theta_2 = 45^\circ$.

The unique features of the Rat Module are:

- It is for overground experiments. It allows 2D movement of the rat in an open area.
- It allows a wider repertoire of natural movements than other existing equipment capable of forceful interaction with rodents.

- It is lightweight and compact.

The average maximum force output was measured to be 2.0 N on each side. With both sides acting together, this would be able to support 400 grams of weight. Since the weight of the typical adult female Sprague-Dawley rats is around 250 grams and the Rat Module itself weighs 75 grams, the Rat Module has the potential to support its own weight and all of the animal's weight. Also, it was confirmed that the motors met the force requirement presented in section 4.1.2.

The maximum pushing force of the robot arm was smaller than the maximum resisting force measured by the force sensor. This was due to static friction in the motor/gearhead shafts, substantially reducing back-drivability (see chapter 6). More back-drivable actuators that meet the requirements are recommended should they become available in the future.

In this exoskeletal design with minimal components onboard, the actuators were by far the most critical determinants of the final configuration. At the time of the design of the Rat Module, little choice of actuators was available. Future prototypes with more advanced actuators should revisit this chapter and redesign the Rat Module around the new actuator of choice.

Since other supporting equipment was placed away from the animal and the Rat Module to allow maximal freedom of natural movement, spanning the long distance between the motors/sensors onboard the Rat Module and the supporting equipment was non-trivial. Further detail is presented in the next chapter.

Chapter 5

Body-Weight Support System

5.1 Motivation

The design principle guiding this project was to develop equipment useful for locomotion studies in rodents. To achieve that goal, the apparatus should minimally encumber the animal's natural movement. The Rat Module described in the previous section was designed to meet this specification. An important feature of the Rat Module was its light weight (~75 grams). Nonetheless, the weight of the rat module may be sufficient to encumber the animal, especially in certain preparations where the animals are partially disabled. Hence it was necessary to provide a means to remove the weight exerted on the animal by the Rat Module. The same feature may allow partial weight support for the animal.

To provide vertical weight support while the animal is freely moving about in the 'arena' (Fig. 3-6), the weight support was conceived to be a crane-like robot, with a workspace that covered the 2-D area of the arena. A weight-bearing tensile element (a string) attached between the Rat Module and the end-point of the arm of the crane-like robot, was to be maintained vertical at all times. If the robot succeeded in keeping the weight support vertical, the position of the robot end-point would be identical to the position of the animal in the arena. Thus logging the time history of the robot's movement provided the 2-D movement trajectory of the animal.

A secondary use of the weight-supporting robot is as a conduit for wiring. The Rat Module was deliberately designed to contain only the minimum necessary components onboard. All other essential components may be located outside of the arena. The communication between the

Rat Module and these other components was made through wires that run along the arm of the Body-Weight Support System (BWSS) robot.

5.2 Body-Weight Support System (BWSS)

The BWSS robot should meet the following requirements:

R1: Minimally interfere with the rat's motion

R2: Minimal bulk to facilitate easy relocation

R3: Follow the motion of the rat in the rat arena

R4: Have a robust structure to support the Rat Module

5.2.1 Configuration

The body-weight support system was the most bulky sub-system to be placed within (or near) the rat arena. The configuration of the BWSS greatly influences the above mentioned requirements, R1 to R4.

Referring to Table 5.1, possible BWSS designs may be located within (A1) or outside (A2) the arena. Also, they may be largely rotational (B1) or translational (B2). Combinations of A's and B's result in roughly four design configurations. Each configuration was evaluated using the requirements R1 to R4 on the scale of 1 to 5, where 5 denoted strongly meeting the requirements (Table 5.1). Overall scores were compared to select the most desirable configuration.

Table 5.1
Possible BWSS configurations

	A1+B1: crane type 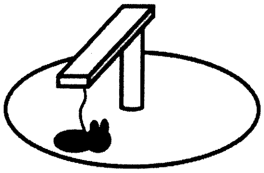	A1+B2: frame type 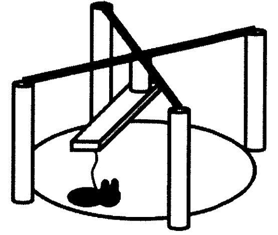	A2+B2: rail type #1 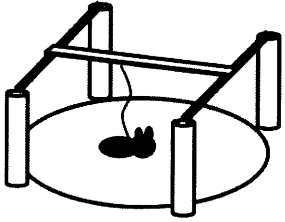	A2+B1: rail type #2 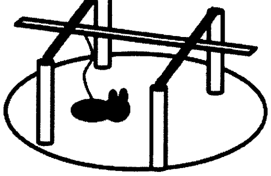
R1	The center pole may interfere with the rat's movement. However, the footprint of the pole may be small. (4/5 pt)	There is nothing in the way of the animal's movement within the arena. (5/5 pt)	There is nothing in the way of the animal's movement within the arena. (5/5 pt)	The four pillars inside the arena may impede the animal's movement along the edge of the arena. (3/5 pt)
R2	This design is the least bulky and by far the simplest. Easy access to the animal from every direction. (5/5 pt)	At least three pillars and a cross-bridge make this configuration bulky. Pillars occlude access to the animal. (2/5 pt)	At least four pillars and three cross-bridges make this configuration bulky. Pillars occlude access to the animal. (2/5 pt)	Similar to the rail type design #1. The distance between the pillars is shorter and occludes access to the animal even further. (1/5 pt)
R3	Animal's movement trajectory may pass close to the singular position of the robot (center of the arena). (3/5 pt)	Animal's movement trajectory may pass close to the singular position of the robot (center of the arena). (3/5 pt)	The robot can follow the animal's movement within the arena (5/5 pt)	Animal's movement near the supporting pillars may be harder to follow accurately (3/5 pt)
R4	Supported by a single pillar. May require a large. (3/5 pt)	Supported by at least three pillars. (5/5 pt)	Supported by at least three pillars. (5/5 pt)	Supported by at least three pillars. (5/5 pt)
R5	Robotic systems of this configuration are readily available (5/5 pt)	Not readily available but parts can be obtained and assembled (3/5 pt)	Not readily available but parts can be obtained and assembled (3/5 pt)	Not readily available but parts can be obtained and assembled (3/5 pt)
Total Score	20/25	18/25	20/25	15/25

The crane type design and the rail type #1 design received the highest scores of 20/25. Between the two designs, the crane type design was first pursued because

1) It was the only design that scored 3 or higher in all requirements. Designs with serious deficiencies in meeting certain requirements were considered undesirable.

2) A commercial robot of this form was readily available for testing.

A wide variety of robotic arms were considered, where robots in cylindrical format were preferred, since the workspace of the robot was expected to be cylindrical as well.

5.2.2 The R19 Robot Arm

A commercially-available robot from ST-Robotics (strobotics.com) appeared to meet the above requirements. ST-Robotics manufactures a series of desktop-sized robot for tasks such as laboratory sample handing. The R19 robot is a cylindrical format robot with the following specification:

Drives:	Hybrid rare earth micro-stepped stepping motors, incremental encoder feedback
Reach:	max 549mm, min 149mm
Lift stroke:	501mm, mounting flange minimum 91mm above bench
Speed:	Standard: Waist 180 deg/sec. Lift 500mm/sec, extend 500 mm/sec. Turbo: Waist 180 deg/sec, Lift 750mm/sec, extend 750 mm/sec.
Resolution:	Standard: 0.075mm, Turbo: 0.15mm
Payload:	2Kg at flange.
Repeatability:	+/-0.1mm
Weight	14.5Kg/33lbs (robot only)

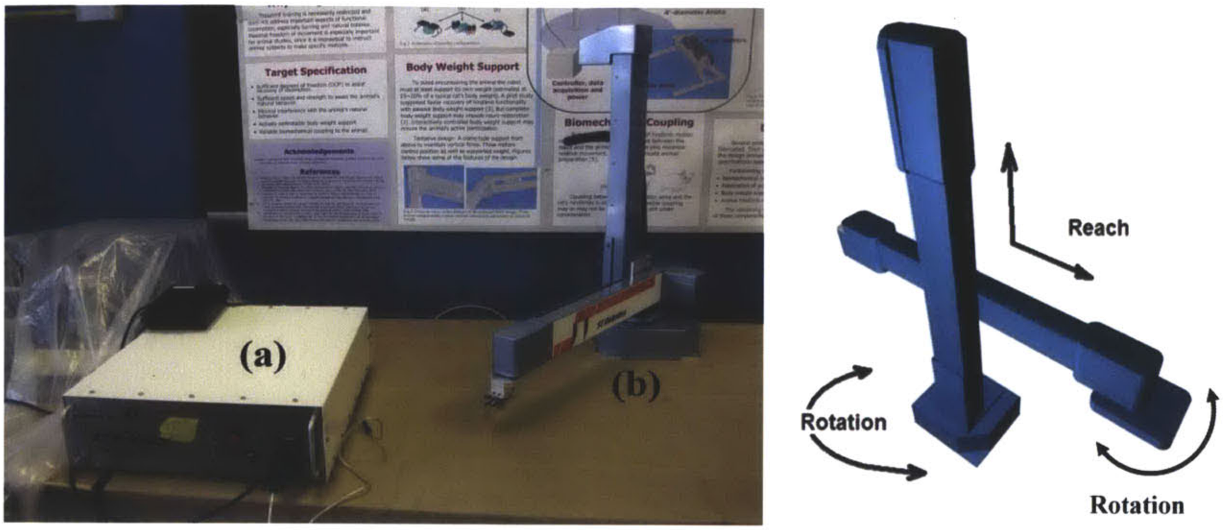

Fig. 5-1. R19 robot from ST-Robotics. Left: photo of the robot (a) and the controller box (b). Right: actuated degrees of freedom.

The specification allowed the robot arm to cover an annulus with outer diameter 1.1 meters and inner diameter 30 cm. Operating in standard mode, it was fast enough to follow an animal moving across a diameter of the arena in two seconds. While at maximum speed a rat may be able to run faster than this, it is unlikely that such locomotion will occur unless the animal feels highly threatened. This would not be conducive to well-controlled studies of normal locomotion. Subject to this minor limitation, the R19 robot met requirements 1 to 5 stated in the previous section.

However, the R19 robot proved to have some significant limitations not evident from its specifications.

1) The stepping motors were highly non back-drivable. Impedance control could not be applied to this robot without adding a force sensor at the end-effector and use it in a high-

bandwidth feedback control loop. Position control was the only option provided by the accompanying software.

2) The robot could only be controlled with its own software, which implemented position control loops no faster than 3.3 Hz. The velocity profile, when moving from one position to another, was fixed in the code as a trapezoid. Only the acceleration, deceleration and maximum speed could be modified. The range of the 'speed factor' was 100-32000 and the range of the 'acceleration factor' was 10-5000, where even the manufacturer was unable to provide these numbers in units such as m/s or m/s^2. (However, the maximum speeds of each joint were provided.)

3) Interfacing the robot to the main computer was difficult. The robot could only be run using software compatible with Windows® machines (whereas the Rat Module was controlled on a Linux machine). Moreover, communication to this robot could only be made using Analog-to-Digital (A/D) or Digital-to-Analog (D/A) terminals on the robot controller box. For example, all information from other modules could only be transferred to the R19 robot through the D/A terminal of the Linux machine and then the A/D terminal of the R19 controller box. The data was transferred as an analog voltage, subject to noise, ground conditions and the resolution of the A/D and D/A conversion.

Although these were significant drawbacks, the R19 robot still met requirements 1 to 5 stated in the previous section. The drawbacks were technical implementation difficulties rather than fundamental flaws that would disqualify the R19 robot as a candidate BWSS.

5.4 Vision Feedback

5.4.1 Why Use Vision Feedback?

The primary role of the BWSS was to provide vertical weight support at all times, as the animal moved freely in the arena. It was thus important to know where the animal was within the 2-D surface, so that the BWSS could reposition itself to provide vertical weight support. Accurate position information with sufficiently high sampling rate was required to monitor the rat's motion. Three possible choices of sensors were considered.

1) A video camera installed to view the arena vertically from above.
   - Pros: direct measurement of position (compared with accelerometers). Easier handing of the sensor (camera).
   - Cons: vision processing algorithm may be affected by ambient light. Sampling rate may be limited. Camera may be bulky.
2) Miniature accelerometers on the Rat Module.
   - Pros: very small, thus can be attached directly on the Rat Module. High sampling rate possible.
   - Cons: Sensor is prone to damage (because it is near the animal). Needs double integration to get position data - a biased acceleration would yield a linearly diverging velocity and a quadratically diverging position. May increase the number of wires connected to the Rat Module.
3) Use force sensors (with a compliant medium. See Fig. 5-2)
   - Pros: force data is useful to have. May be used later to implement a force control loop to manipulate lateral forces exerted by the BWSS on the animal.

- Cons: The robot is likely to be much closer to the animal than in the other two options above. The robot is mechanically coupled to the animal in this setup, potentially compromising safety of the animal.

While the advantages of using accelerometers were significant, having to integrate twice to get position was perceived to be a critical difficulty. Using a force sensor with the highly non-back-drivable R19 robot was deemed unlikely to be satisfactory. The maximum control loop bandwidth of the R19 robot, 3.3 Hz, would not yield sufficiently low mechanical impedance to avoid encumbering the animal. To compensate, a highly compliant medium with a well-characterized compliance both in compression/tension and in shear would be required but it was not obvious how to identify such a material.

In comparison, a video system was substantially more practical. A video system was already in use in another machine under development in the laboratory such that the technology was readily available. The ability to measure and record the rat's position directly was an additional advantage. Vision-based position monitoring was selected for the BWSS based on the R19 robot.

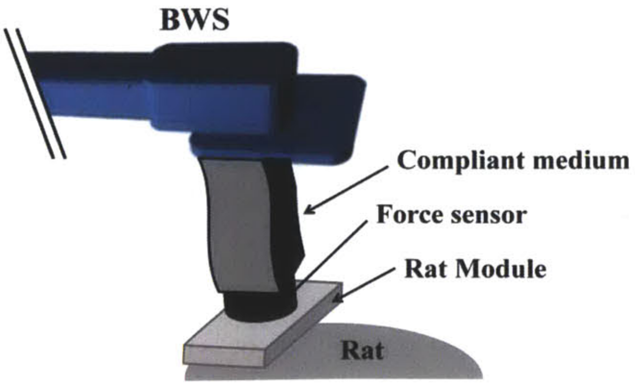

Fig. 5-2. Illustration of the idea of using a force sensor to measure the position error between the BWSS and the animal. The force sensor measures the shear force in a compliant medium, whose compliance is presumed known.

5.4.2 Image Processing

The image capturing device must satisfy the requirements below:

1) Sampling rate greater than the maximum bandwidth of the position control loop (3.3 Hz) is necessary. Typical video cameras have at least 24 frames-per-second (fps) and thus easily satisfy this requirement.

2) Must have sufficient resolution – for video processing, the minimum number of pixels per meter was tentatively set to 500, corresponding to one pixel per 2x2 mm^2.

The video camera used was Logitech® Quickcam Pro 9000. The native frame rate of this camera was 30 Hz (>> 3.3 Hz) and the highest resolution at this frame rate was 320 pixels by 240 pixels at a fixed 60° viewing angle. At a measured maximum height of the R19 robot (50 cm), this resolution translated to 551 pixels per meter.

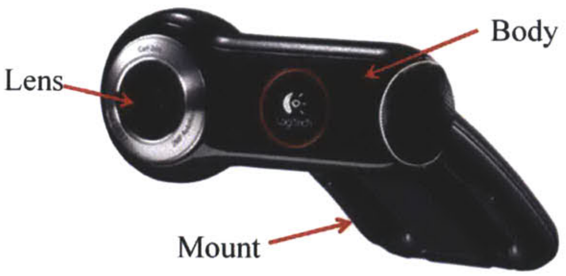

Fig. 5-3. Video camera used in the BWSS (Logitech Quickcam Pro 9000).

The image-processing software for the camera was run in Linux, where the general controller for the Rat Module was also implemented. Details of the controller software and the Linux machine are presented in a later section; here, it is sufficient to mention that the code ran in parallel with the code that modulated the Rat Module and provided information about the Rat Module's position in real time. The software then logged this information in a file, while also sending this information to the ADC ports of the BWSS controller through the DCA ports of the Linux machine.

The camera recognized the position of the Rat Module using a simple color filter. The Rat Module was painted in natural green. The video camera then detected the green pixels, thereby recognizing the position of the Rat Module alone. More specifically,

1. At every 1/30 seconds (30 fps), the current camera view was captured.
2. Green pixels were marked as follows.
    a. For each pixel, calculate brightness = Mean(Red, Green, Blue).
    b. For every pixel brighter than 30, check if Red/Green < 0.8
    c. For every pixel that satisfied b, check if Blue/Green < 0.8
    d. If a pixel satisfied c, the pixel was marked as 'green'.

3. For each marked pixel, investigate the neighboring 8 pixels. If more than 4 out of the 8 pixels were also marked, then the current pixel was a 'true-green' pixel.
4. After all pixels have been investigated, find the center location for all 'true-green' pixels, where $x_{center} = \text{Mean}(x_{true\_green\_pixels})$ and $y_{center} = \text{Mean}(y_{true\_green\_pixels})$. This is the location of the Rat Module in the view of the camera.
5. Send this information to the controller that modulates the motors on the Rat Module.

In short, the filter identified pixels that were 'greener than red' and 'greener than blue'. The Rat Module was painted in green rather than blue, red or yellow, because green is the color most rarely seen in mammals such as rats or in the laboratory environment in which animal experiments are anticipated. Red is the color of the animal's eyes and also of human hands (which may be seen by the camera). Blue is also occasionally seen on human hands near the skin above blood vessels, or on Latex laboratory gloves. Yellow is common in the skin of the animal and also human hands, as well as on recycled paper pads that are commonly used in animal laboratories. The current image processing algorithm was tested in real laboratory settings and is strongly recommended for any future versions of the apparatus.

Harsh conditions were simulated to address the performance of the image processing algorithm. Such conditions include: rats moving quickly, wires partially blocking the view, or a slanted Rat Module. Figure 5-4 shows examples of processed images in these conditions. The 'true-green' pixels were marked bright yellow for clarity. The software successfully detected the Rat Module in all simulated conditions. The calculated center of Rat Module may differ from the actual center of Rat Module. Nonetheless, these conditions occurred rarely and even when they did, the estimated center of Rat Module was within a 1-cm radius circle centered at the actual center of Rat Module. For example, the distances between the calculated and actual centers of the Rat Module in Fig. 5-4 (b), (c) and (d) were approximately 10 mm, 7 mm, and 5 mm, respectively.

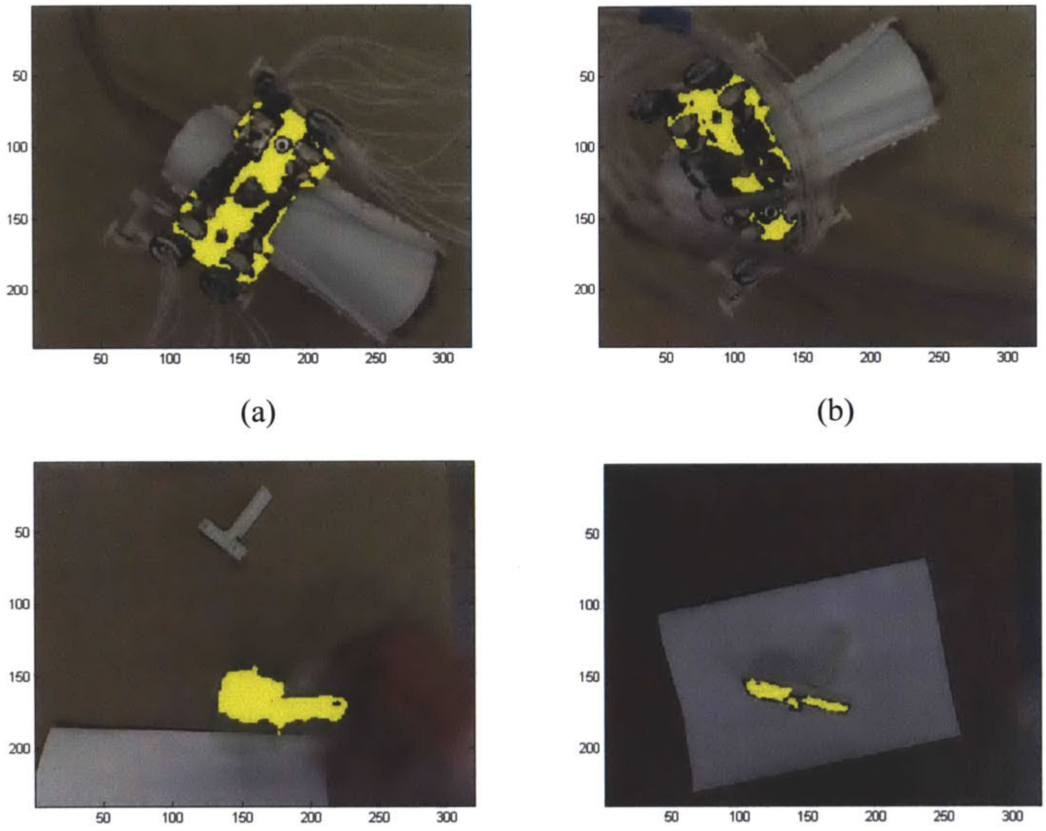

(a) (b)

(c) (d)

Fig. 5-4. Examples of processed images acquired from the video camera. The yellow pixels are those detected as 'true green' using the algorithm presented above. All pictures are 320 pixels by 240 pixels. (a) Rat Module on a rat doll. This is a typical view from the camera. (b) through (d) are cases when the video system may work less efficiently. (b) In rare cases, the wires may be tangled and partially block the view of the Rat Module. (c) The rat may be moving quickly, blurring the image. (d) The animal may rear up such that the Rat Module is slanted relative to the image plane.

5.4.3 Camera Attachment

The video camera was attached to the R19 robot at the wrist degree of freedom. A mount was fabricated to attach the camera to the R19 robot (Fig. 5-5). The mount was designed to ensure that the rotational axis of the wrist DOF of the BWSS robot aligned with the center of the camera lens. In this way, rotation of the wrist did not change the camera position with respect to the end-point of the manipulator arm as recognized by the robot controller. That is, the wrist of the robot determined the orientation of the camera view with respect to the robot frame.

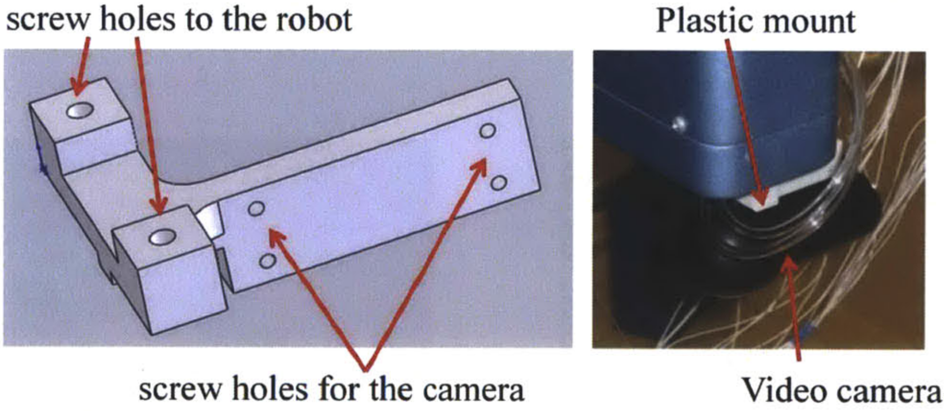

Fig. 5-5. Camera mount for coupling the video camera to the R19 robot. Left: CAD drawing of the mount. Right: Attachment to R19.

5.5 Weight Bearing

The camera was approximately 20 cm above the top surface of the Rat Module to ensure a sufficiently large viewing area. The weight supporting cords were also of this length. The weight supporting cord was composed of two parts: 1) 15 cm of fishing line and 2) a 5-cm-long tension springs (Fig. 5.6). The stiffness of the tension spring was 45 N/m. Thus 1 cm of elongation increased the vertical support by 45 grams. By lifting or lowering the BWSS arm, the length of the support (and because of the spring, the supported weight) could be adjusted.

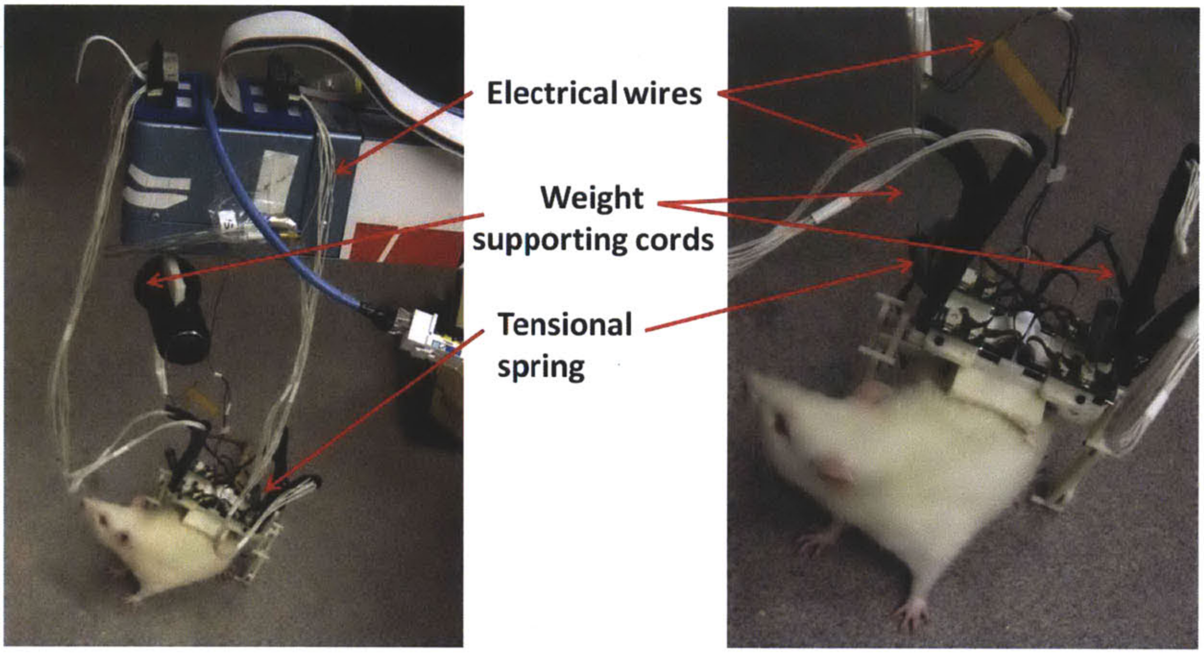
Electrical wires
Weight supporting cords
Tensional spring

Fig. 5-6. Weight supporting cord and tension spring attached to the BWSS and the Rat Module.

5.6 Wiring

A total of 56 electric wires connected to the Rat Module – 10 for each motor (3 for each motor winding, 3 for Hall effect sensors, 1 for voltage input, 1 for ground, 2 for encoder signals A/B) and 8 for each force sensor. Additionally, a USB cable connected to the video camera. All of these wires were carried by the BWSS robot as shown in Fig. 5-7.

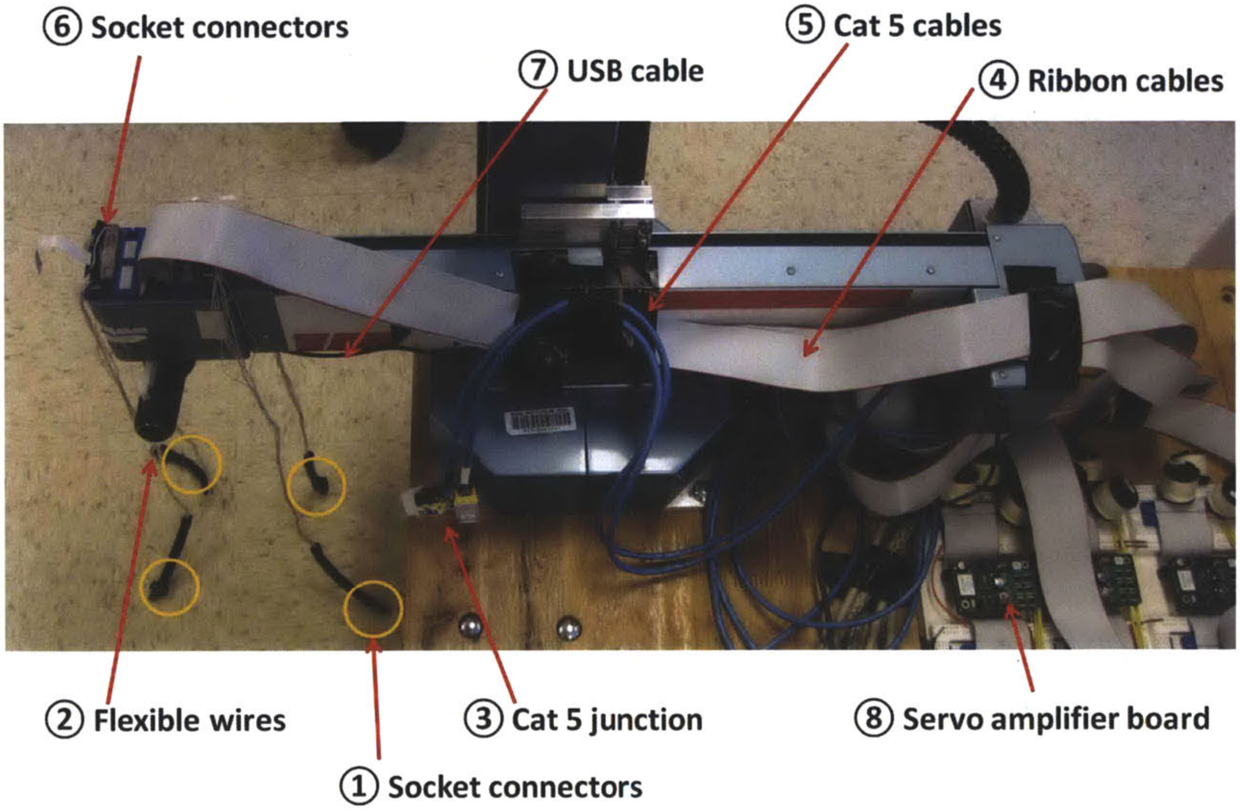
⑥ Socket connectors
⑦ USB cable
⑤ Cat 5 cables
④ Ribbon cables
② Flexible wires
③ Cat 5 junction
⑧ Servo amplifier board
① Socket connectors

Fig. 5-7. Wire connections. See text for explanations.

Between the motors on the Rat Module (not shown) and the electronics providing signals to the motors, such as the servo amplifier ⑧, a total of 40 wires originated from the socket connectors ① shown inside the orange circles, which continued through the flexible wires ② and the wiring arms ③, and were transferred to ribbon cables ④ (which were substantially less compliant) through the socket connectors ⑥. The ribbon cables ④ eventually terminated on the servo amplifier board ⑧.

The two force sensors on the Rat Module had 8 wires each, 4 for each DOF (2 for power and 2 for measurement). The signals to and from the force sensors traveled through the Category-5 (Cat 5) cable ⑤, twisted pair cables typically used in computer networks, and Cat 5 junctions ④. These cables eventually terminated on the I/O junction board for the controller computer.

The video camera on the BWSS was connected to the controller computer through an extended USB cable ⑦.

The integrity of this wiring was tested and verified in all relevant conditions, including when the R19 robot traveled between its extreme positions.

Ensuring proper connection between a large number of terminals complicated the overall implementation. Note that the wireless design originally envisioned does not have this problem. Designs requiring little to no wire connections may later become feasible when the technology barriers such as lag in wireless transmission or energy density of batteries are resolved.

5.7 Performance

The ability of the R19 robot to follow a rat's motion with vision feedback was evaluated with an animal equipped with a Rat Module. (Details of the experiment are presented in a later section.) The rat arena was reduced in size from the originally conceived full circle into a trapezoid (Fig. 5-8). The reduced area was nevertheless sufficient to validate the design.

Throughout the experiment, visual observation confirmed that the weight supporting cord remained substantially vertical. Tracking of the Rat Module's position that was consistent with observation was also demonstrated. Figure 5-9 shows the history of the rat's overground movement, as tracked by the R19 robot. The yellow trapezoid depicts the area in which the rat was free to move. The data recording started first, before the BWSS was turned on. At this point, the data acquisition board (DAQ) on the controller computer read zero voltage, corresponding to the (0, 0) position. When the body-weight support system was turned on, the robot immediately tracked and located itself above the current location of the animal. In this particular experiment, the animal was recovering from anesthesia near the center of the trapezoid and spent some time there (point A in Fig. 5-9). When the animal awoke, it decided to move towards the y+ direction for about 20 mm then stayed there until it recovered further (point B). Then, the animal turned left to eventually place itself in a corner (point C)—a typical behavior of rats exposed to an unfamiliar environment.

This measurement agreed well with visual observation of the rat's overground behavior. The resolution was less than 2 mm (expected: 1.25 mm) but this experiment demonstrated that the body-weight support system was capable of tracking and recording the animal's 2-D movement in the rat arena with acceptable resolution.

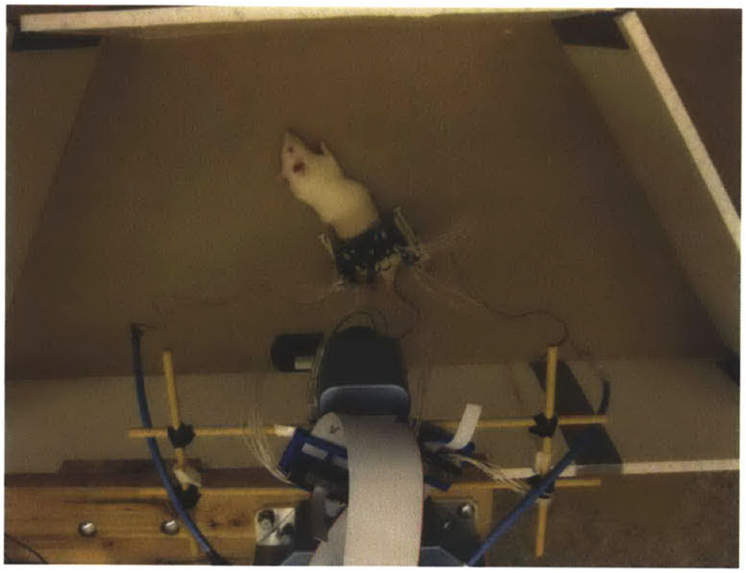

Fig. 5-8. Experiment setup viewed from above. The body-weight support system was mounted on a low-profile wooden cart. The animal, initially anesthetized, was placed in the trapezoidal rat arena.

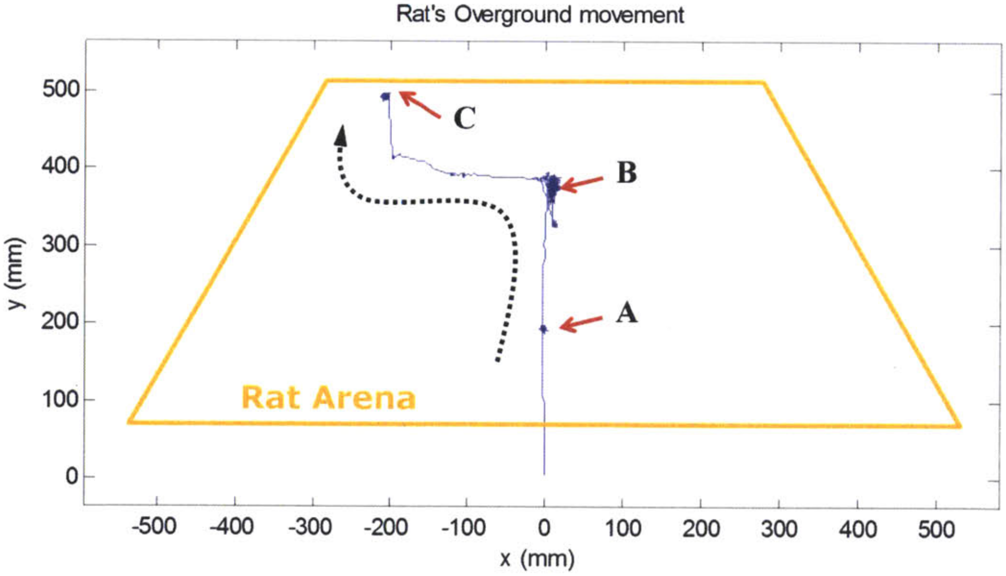

Fig. 5-9. Data from an experiment showing the animal's movement in the rat arena. See text for details.

5.8 Discussion

Weight bearing plays a significant role in rehabilitation research. In some cases, the subject is physically challenged and needs external support. However, the degree to which the weight support is provided may also affect the outcome of rehabilitation [**97**], suggesting that determining a helpful amount of weight support is an interesting research topic in its own right. Another important aspect of providing weight support is that it may influence the amount of loading on the foot of the animal. As reviewed in chapter 2, loading related afferent signals significantly affect motor behavior. Varying the degree of weight support at different stages of the step cycle may affect locomotor patterns. In some machines, sophisticated active BWSS have been designed and implemented [**40**][**87**]. Ultimately, the body-weight support system designed for this project is also expected to be capable of controlled weight bearing. Implementation of this feature is left for future research.

The tracking ability of the body-weight support system is potentially more important to minimize interference with the rat's natural overground movement. To provide vertical weight support at all times, the BWSS must be able to constantly monitor the position of the animal inside the rat arena and reposition itself accordingly in a short time. This requires appropriate sensing and actuation. Vision feedback from a conventional Web Cam appeared to be adequate.

The major limitations of the BWSS system implemented derived primarily from the R19 robot. The robot's programming language allowed a maximum control bandwidth of only 3.3 Hz. The robot was non-back drivable and it did not provide digital communication to and from other devices. Future implementations should consider developing a custom BWSS system in place of the R19 robot.

Chapter 6

Simple and Robust Method to Manage Uncertainties with Discrete-State Control

The Maxon EC6 motors were the only suitable choice of actuators available at the time of development. Gear reduction was necessary to amplify the torque output. The compact packaging of this geared motor is advantageous in applications requiring compact and light actuators. However, as will be shown, the predominance of static friction and stiction made control of the motor shaft a non-trivial task. Moreover, the large, non-linear friction of the gearhead compromised back-drivability of the linkages on the Rat Module. As lowering output impedance was one of the crucial requirements, improving back-drivability through feedback control was necessary. Conventional PID control was applied to modulate the motor shaft or to improve back-drivability of the motor, only to achieve partial success.

In order to address this issue, a simple Discrete-State Control (hereafter referred as DSC) was developed. It took advantage of low-cost, high-speed computation and sensing to achieve desired performance. DSC was used to substantially improve position control of the motor shaft as well as the back-drivability of the linkages on the Rat Module.

6.1 Difficulties due to the Current Selection of the Motor

6.1.1 Position Control in the Presence of Large Static Friction

Figure 6-1 depicts a system consisting of a miniature brushless DC motor (Maxon EC6) with a planetary gearhead. The open-loop response of this system to a quasi-static ramp input (from zero to maximum control input in 10 seconds) is shown in Fig. 6-2. The 3-stage miniature gearhead caused stiction and static friction whose magnitude was as large as 45% of the maximum available control effort. Worse yet, whereas a permanent magnet DC motor should respond with a steady angular velocity in response to a steady voltage input, once it began to move, the motor velocity was extremely sensitive to voltage. The velocity quickly ramped up from zero to maximum in a narrow region of control input. Furthermore, the input required to overcome static friction varied from trial to trial with large variability (Fig. 6-2). In short, the velocity response of the motor to the quasi-static input was highly non-linear and highly variable. The compact packaging of the motor and the gearhead allowed no room for any 'mechanical' remedy (such as the use of low-friction bearings) for these undesired behaviors. It seemed evident that formulating a mathematical model to describe this behavior would be inordinately challenging; it might even be impossible, especially if reliable parameter values were required. Consequently, it was unclear whether any friction-compensation technique that relied on a mathematical description of system behavior could successfully be applied to control the position of this system.

6.1.1.1 Using PID-Control

PID control is one of the most widely used control schemes. It is simple yet yields reasonably good performance in many applications. Thus it was a natural choice to first apply a PID controller to the system described above.

Figure 6-3 shows an exemplary result of PID-control at a 2 kHz sampling rate, attempting to modulate the position of the motor shaft to follow a sinusoidal input at 0.5 Hz. Even for this low-frequency commanded trajectory, and using very high controller gains (the largest that did not saturate the motor command) substantial position tracking error was observed, especially at low velocities. Furthermore, the error was not repeatable from cycle to cycle, indicating that performance was even poorer than shown in this Figure. Alternative controller gains yielded no observable improvement of the response.

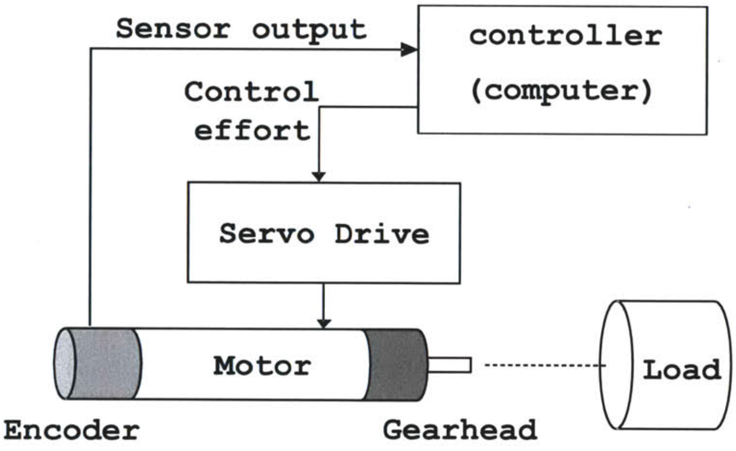

Fig. 6-1. Schematic of the system used. A miniature brushless DC motor (Maxon EC6, diameter 6 mm) was connected to a load through a planetary gearhead (57:1 reduction). An encoder was mounted on the motor shaft. The current into the motor was determined by a trans-conductance servo-amplifier (Copley Controls, Accelnet), which was driven by a control signal from a computer, in which different control schemes were programmed and tested.

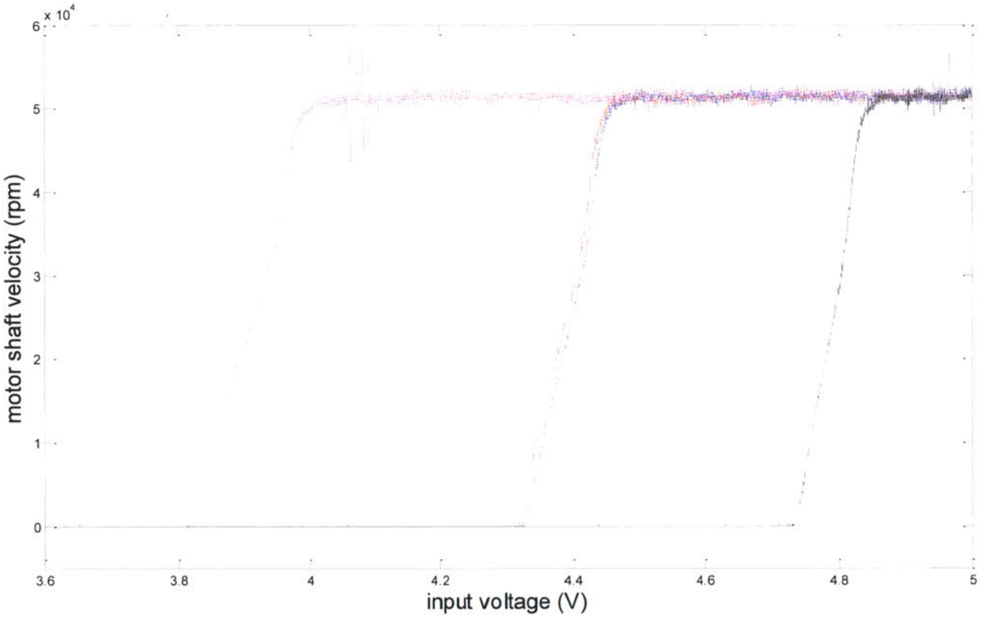

Fig. 6-2. Open-loop velocity responses of the system in Fig. 1 to a quasi-static ramp input. The input rose from 0 V to 10 V over 10 seconds. The velocity responses from four different trials are shown. The voltage at which the system first responded with non-zero velocity was different from trial to trial (by as much as 10% of the maximum control effort of 10 V). Once moving, the system reached its maximum velocity of 51,000 rpm after less than a 0.2 V increment of the input.

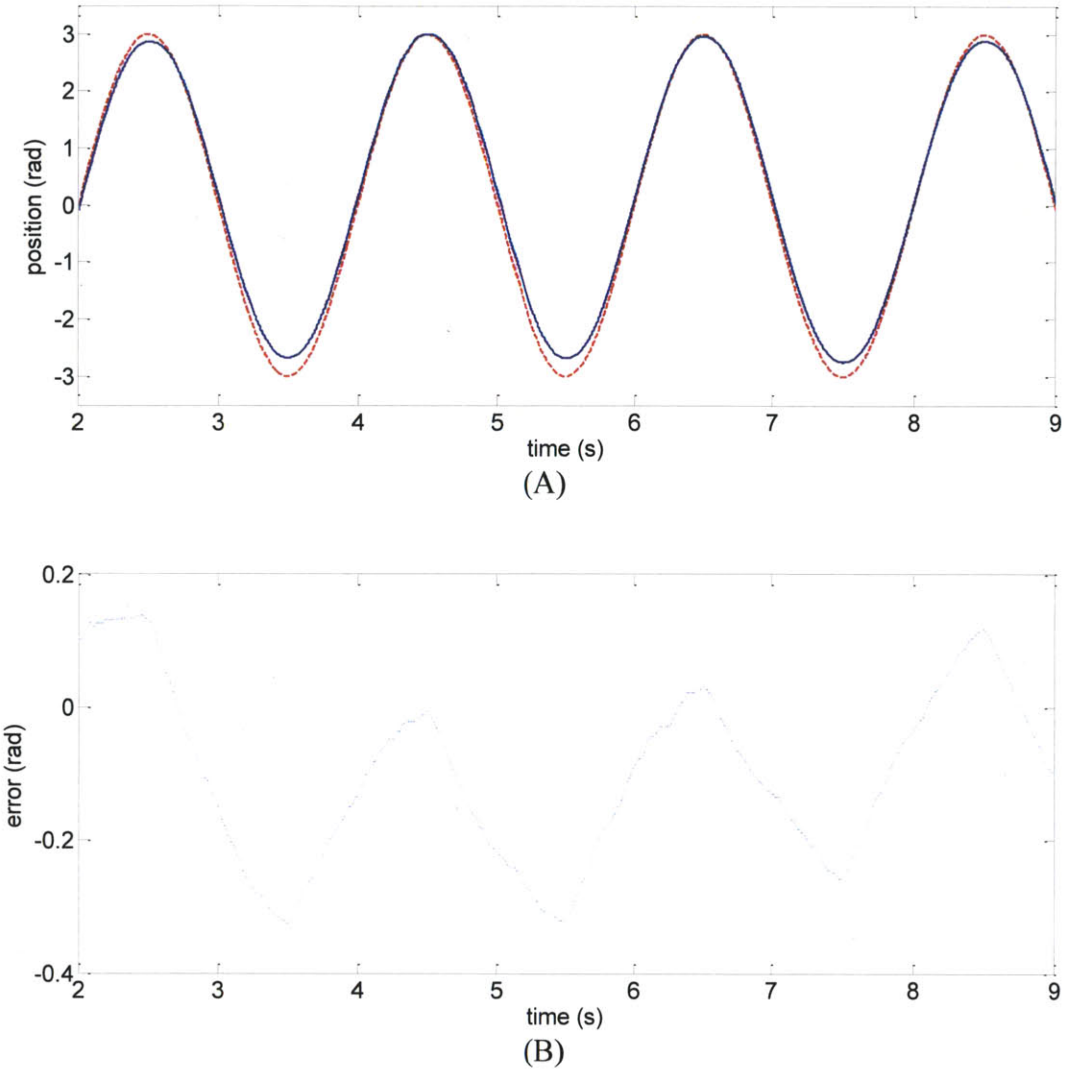

Fig. 6-3. Behavior of the plant of Fig. 6-1 when driven by a PID controller to modulate the position of the motor shaft. Plotted are the gear-reduced, expected positions and error of the shaft outside of the gearhead, assuming no backlash. (A) Position tracking. The system response (blue) deviated from the commanded trajectory (red). (B) Time history of position tracking error. The error was largest at low velocities and varied substantially from cycle to cycle.

6.1.2 Improving Back-Drivability

Fig 6-4 shows the 2-DOF, 5-bar linkage system using the Maxon EC6 motor/gearhead. The large friction of the gearhead compromised back-drivability as shown in Fig. 6-6, top row. The force sensor at the tip of the manipulator read up to 1.3 N of force required to back-drive the system. This was a substantial fraction of the maximum effort of the motors, which generated 2.0 N of resisting force on average at the tip of the manipulator (chapter 4).

In addition to the challenge posed by the highly non-linear static friction of the actuators, the analog voltage signals from the custom-designed force sensor suffered non-negligible high frequency noise even after filtering. Furthermore, the DC bias of the force sensor signal tended to drift slowly. The bias measured on one occasion differed from measurements made on another occasion.

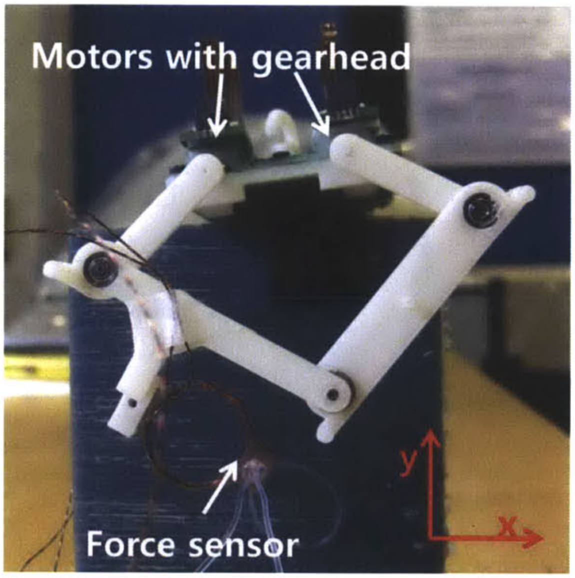

Fig. 6-4. The 2-DOF manipulator using two motors described in section 4-1. A 2D force sensor measured the x and y interaction forces at the tip.

With non-zero output impedance, the interaction force at the tip of the manipulator (point A in Fig. 6-5) was non-zero as the user attempted to back-drive the system. To improve back-drivability, the command was to achieve zero interaction force. Therefore, the interaction force measured by the sensor was the error.

Assuming low friction in the joints and negligible inertia of the links, the error can be represented in terms of equivalent motor torques using the Jacobian (*J* in Fig. 6-5). These torque values were the individual 'errors' for each motor controller. Note that because the force sensor was noisy, the computed torque values were also corrupted by noise.

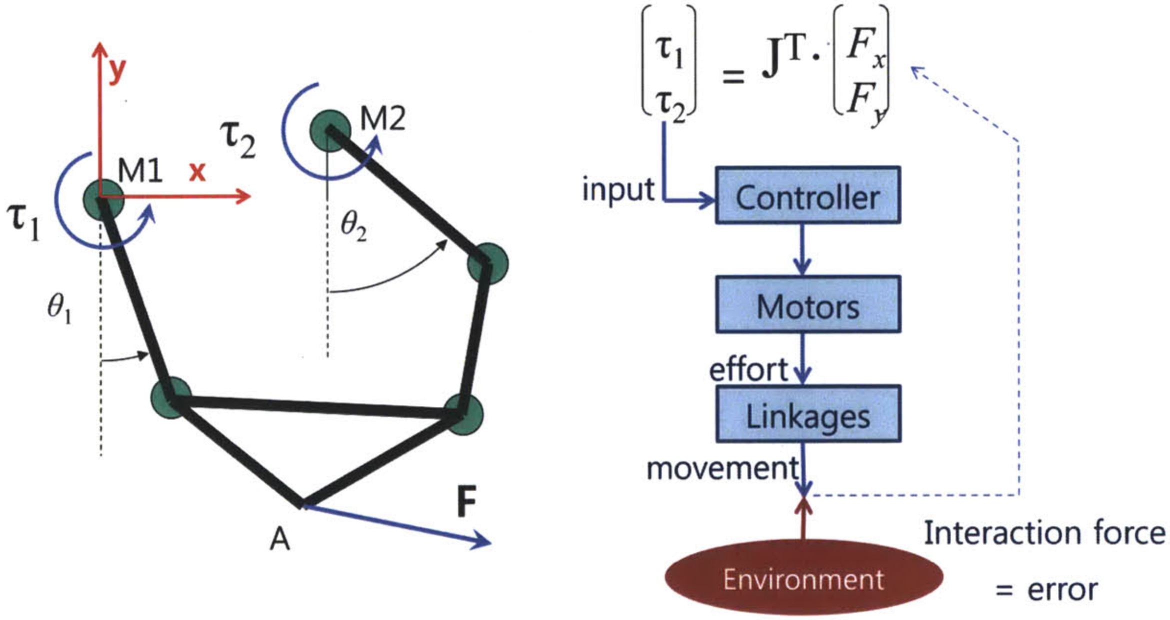
y
M1
x
τ_1
τ_2
M2
θ_1
θ_2
A
F
$\begin{pmatrix}\tau_1\\ \tau_2\end{pmatrix} = J^T \cdot \begin{pmatrix}F_x\\ F_y\end{pmatrix}$
input
Controller
Motors
effort
Linkages
movement
Environment
Interaction force
= error

Fig. 6-5. (Left) Kinematic model of the system in Fig. 6-4. M1 and M2 are the two motors with poor back-drivability, and A is the point of interaction which is the tip of the force sensor in Fig. 6-4. (Right) The force feedback scheme used in this study (right).

6.1.2.1 PI force feedback control

As mentioned in the earlier example, PID control is widely used and is a reasonable first choice for most applications. In this specific case, the computed torque vector was the input to the PID controller.

However, because the signal from the force sensor included high frequency noise, having a derivative gain may amplify noise. High integral gain may also be disadvantageous in the presence of a non-zero DC bias of the force signal. Considering these aspects, one may utilize a PI controller where the integral gain is relatively small. In fact, [**98**] have successfully used an approximately-PI controller (a low-frequency lag compensator) to enhance back-drivability of a 1-DOF manipulator with significant friction.

The bottom row of Fig. 6-6 shows the performance of a PI controller with manually tuned gains. The end point trajectory is smoother than when no controller is used. The overall magnitude of the interaction force is also lower. Defining (mean damping) = (mean force)/(mean velocity) to be a measure of output impedance, mean damping was reduced from 6.66 Ns/m in the open-loop case (measured at 10~20 sec interval) to 1.34 Ns/m with PI control (measured at 5~20 sec interval). However there are occasional and highly unpredictable peaks of interaction force, which could exceed 0.5 N.

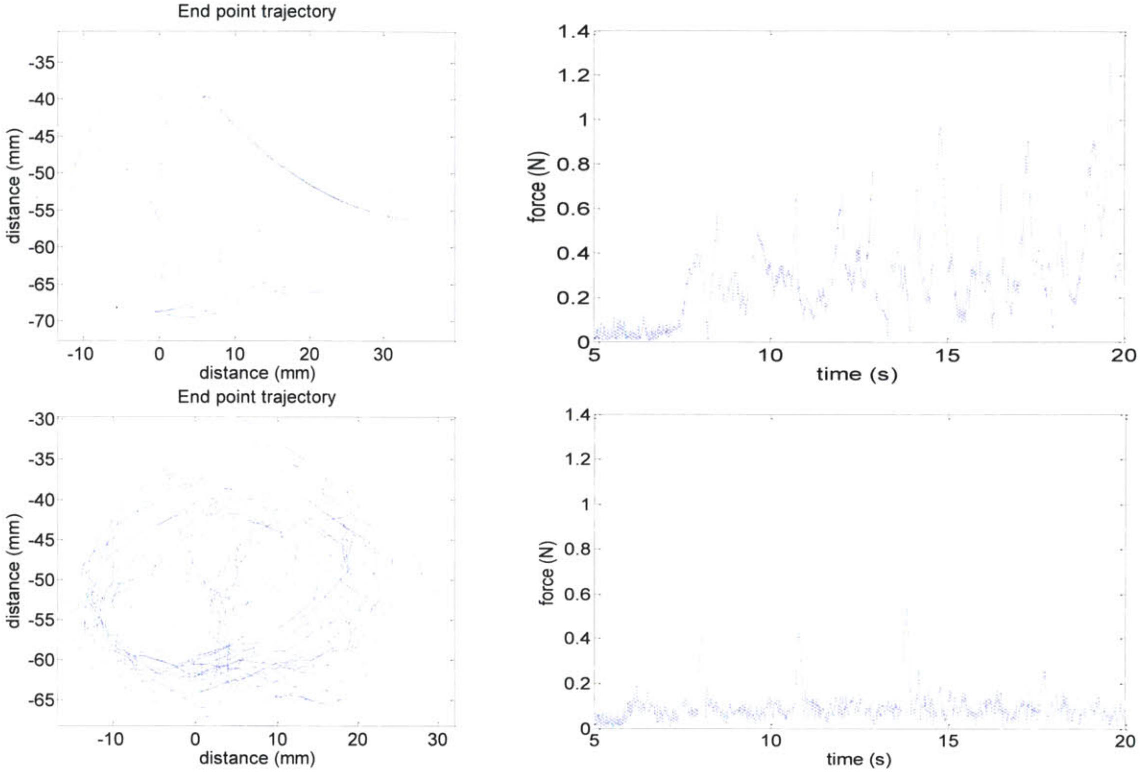

Fig. 6-6. Trajectories and interaction forces while manually back-driving the system in Fig. 6-4. Top row: Open-loop measurement with no controller. The trajectory consisted almost entirely of arcs, characteristic of only one motor back-driven at a time due to significant static friction of the other motor. The peak interaction force was in excess of 1.3 N. Bottom row: Force feedback using a PI controller. The back-drivability is enhanced, although interaction force could occasionally exceed 0.5 N.

6.2 Using Discrete-State Control

In order to address these issues, a novel control scheme was developed, Discrete-State Control, the performance of which is presented in this section. It will be shown that DSC outperforms PID in the two examples shown in the previous section.

6.2.1 The DSC-Scheme

In pseudo-code, DSC is written as

```
(for each time step)
e = $x_c$ - x
IF (e > M), u = +V
Else if (e < - M), u = -V
Else, u = 0
```

where x_c is the reference (command) input, x is the actual value, e is the measured error in the current time step, M is the margin or threshold for the error, and V is a fixed, positive value, and u is the output from the controller. In short, the DSC scheme pushes the system with either $u = +V$ or $u = -V$ in order to reduce the error, unless the error is small enough (then $u = 0$). The time history of u resembles a series of square pulses of varying width. Remarkably, this extremely simplified control scheme with minimal knowledge of the system was robust against uncertainties, as will be shown in the next sections.

An implicit assumption was that the sampling rate was sufficiently fast. The DSC scheme decides the value of u for the next time step solely based on the information given in this time step only, with no estimation of how the system may respond to this u. Thus it may be necessary for the controller to make as frequent decisions as possible in order to quickly react to changes the system response, especially when little information about the system is provided. Also, the sampling frequency determines the minimum width of the square pulse, which then determines the minimum size of impulse provided to the system (minimum impulse = V/f where f is the sampling frequency). The higher the sampling frequency, the finer the control that may be achieved. The effect of this assumption on the performance of DSC remains largely unexplored.

6.2.2 Using DSC to Modulate Position

In contrast to PID control, DSC successfully controlled the position of the motor shaft in the presence of highly variable static friction (section 6.1.1). Figure 6-7 shows the position command and the system response using DSC, with $V = 5$V, $M = 0.0125$ rad, at 2 kHz. In fact, panel A of this figure shows two curves (corresponding to the commanded and actual position) but they are so similar that the latter obscures the former. This is a substantial improvement over the PID controller performance shown in Fig. 6-3. The position error remains small even in the low-velocity region. In addition, the highly non-linear and non-repeatable nature of the physical system is much less evident. With the same sensor resolution, the same sampling frequency, and arguably a simpler control algorithm, DSC out-performed the best PID controller—its maximum tracking error was about six times smaller. The root-mean-squared (RMS) was reduced from 0.16 radians with PID to 0.02 radians with DSC (a factor of 8 improvement).

Note that in this example, the large static friction worked to dissipate energy in the system. This gave the system the property that 'pushing to oppose error reduces error', an important feature of a 1st order system.

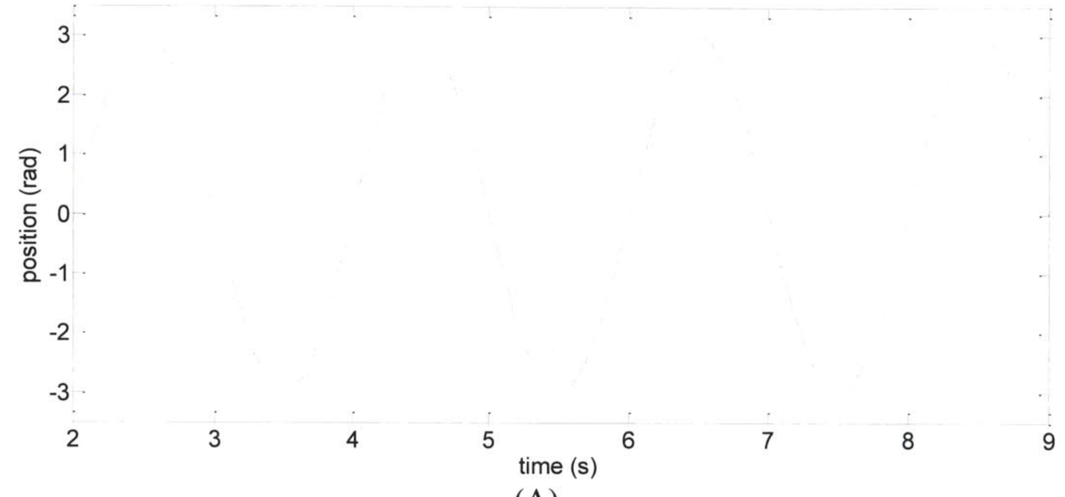

(A)

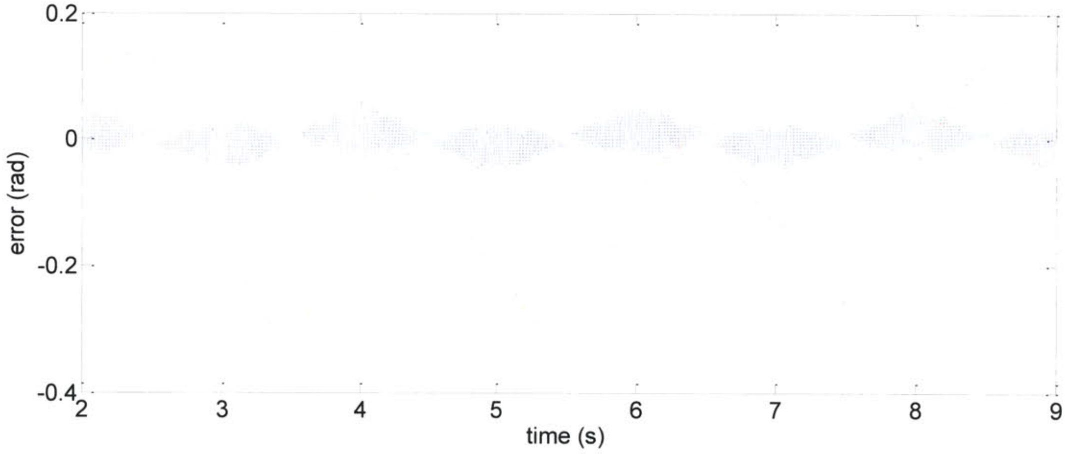

(B)

Fig. 6-7. Response of the system of Fig. 6-1 to DSC with $V = 5$ V, $M = 0.0125$ rad. Plotted are the gear-reduced, expected positions and error of the shaft outside of the gearhead, assuming no backlash. (A) Position tracking. The commanded input (red) and the response (blue) of the plant in Fig. 6-1 to a DS-controller. The two curves are on top of each other. (B) Time history of error (blue), a substantial improvement over the performance with PID control (red).

6.2.3 Using DSC to Improve Back-Drivability

At first glance, the extremely simple DSC control scheme may seem unlikely to work in this case. However, note that the physical system exhibits a 1st-order-like behavior: in order to reduce the error—the non-zero interaction force—the motors may simply push towards the direction of interaction force. It is speculated that this property is what enables DSC to work in this example.

Figure 6-8 shows the manually back-driven end-point trajectory and the corresponding force magnitude plot using force feedback with DSC. The interaction force is substantially reduced, and the trajectory is smoother than the no-controller case in Fig 6-6. DSC also outperforms the PI controller in reducing the peak interaction force. During the 15 seconds of manual manipulation, peak interaction force with DSC was less than 0.2 N whereas with PI controller, peak force of 0.5 N was observed. Mean damping as defined in section 6.1.2.1 was 1.19 Ns/m which is lower than the mean damping with PI control (1.34 Ns/m).

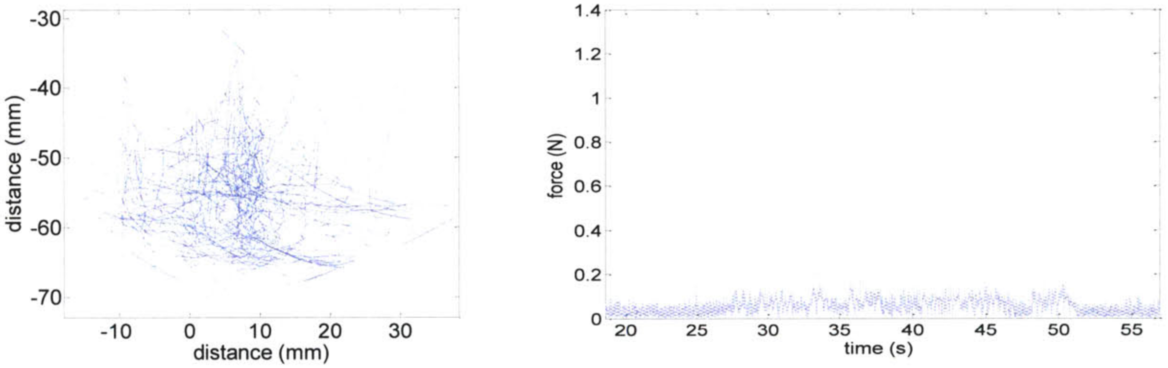

Fig. 6-8. Force feedback using DSC. Back-drivability is enhanced with a peak interaction force substantially less than 0.2 N.

6.2.4 Another Example - Torque Modulation with a Series Damper

Discrete-State Control defined in the previous section attempts to reduce the error in the system by pushing hard in the direction that is expected to reduce the error. Not all systems may be compatible with such a property. However, strictly proper 1st order systems present this property and may work well with DSC. The motor-gearhead in the Rat Module may not be a 1st order system. Nonetheless, static friction is such a dominant feature of its behavior that the friction element may work to quickly dissipate high frequency dynamic responses. As a consequence, the system may behave as though its dynamics were predominantly 1st order. This may be why DSC worked well in the examples above, by taking advantage of the dominant dissipative element in the system.

To further investigate this possibility, a DC motor apparatus with a damping element in series was examined. Figure 6-9 shows a system with a motor, gearhead, rotary damper and torque sensor all in series. The goal was to modulate the torque magnitude measured by the sensor.

With the rotary damper in series, it was reasonable to assume that a positive voltage into the motor would result in a positive torque reading, where as a negative input would produce a negative output. In other words, the presence of the damper made the mechanical part of the system approximate a mass-damper system with 1st order dynamics. Further assuming that the motor shaft velocity was approximately proportional to the input voltage, the whole electromechanical system was then reduced to approximate 1st order dynamics.

Taking advantage of this useful feature, a DSC scheme demonstrated modulation of torque as shown in Fig. 6-10. Running at a modest sampling frequency of 200 Hz, the controller with noisy input was able to track the desired torque trajectory ($V = 10$ V, $M = 0.01$ V). In contrast, DSC did not work very well when the damper was removed. A similar contrast was observed when the sampling frequency was increased to 2 KHz, highlighting the importance of the damper in this example. This is not surprising however; without the damper, the task would be to modulate torque against a very stiff environment with a very stiff actuator with gear stages – a difficult control problem. One cannot stabilize force control with high gains in this situation [**99**].

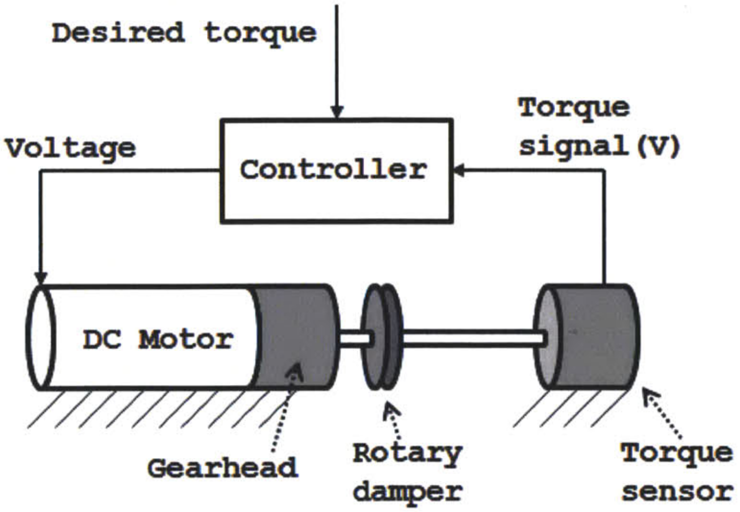
Desired torque
Voltage
Controller
Torque
signal (V)
DC Motor
Gearhead
Rotary
damper
Torque
sensor

Fig. 6-9. The DC motor with gearhead is connected in series with a rotary damper. The right side of the damper is the torque sensor. The torque reading is determined by the velocity of the motor shaft.

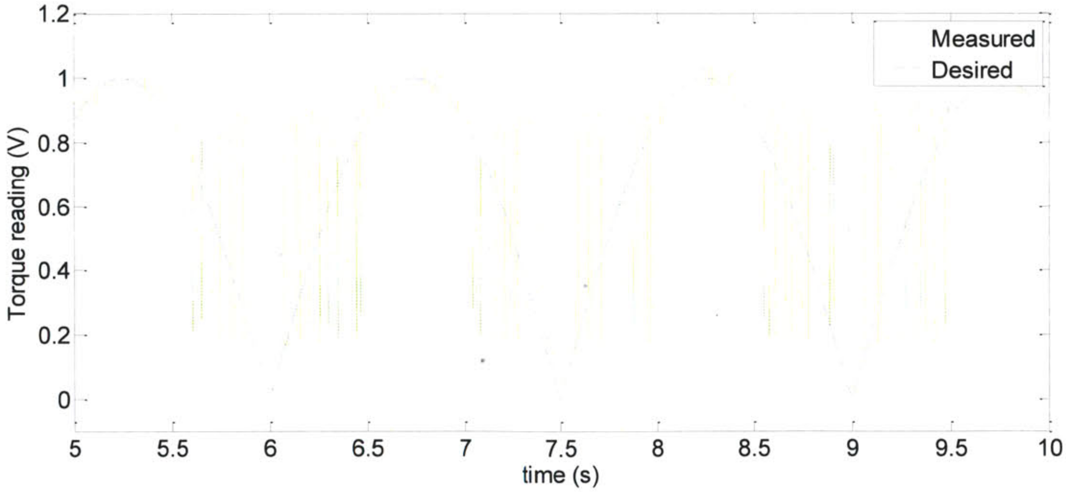

(A)

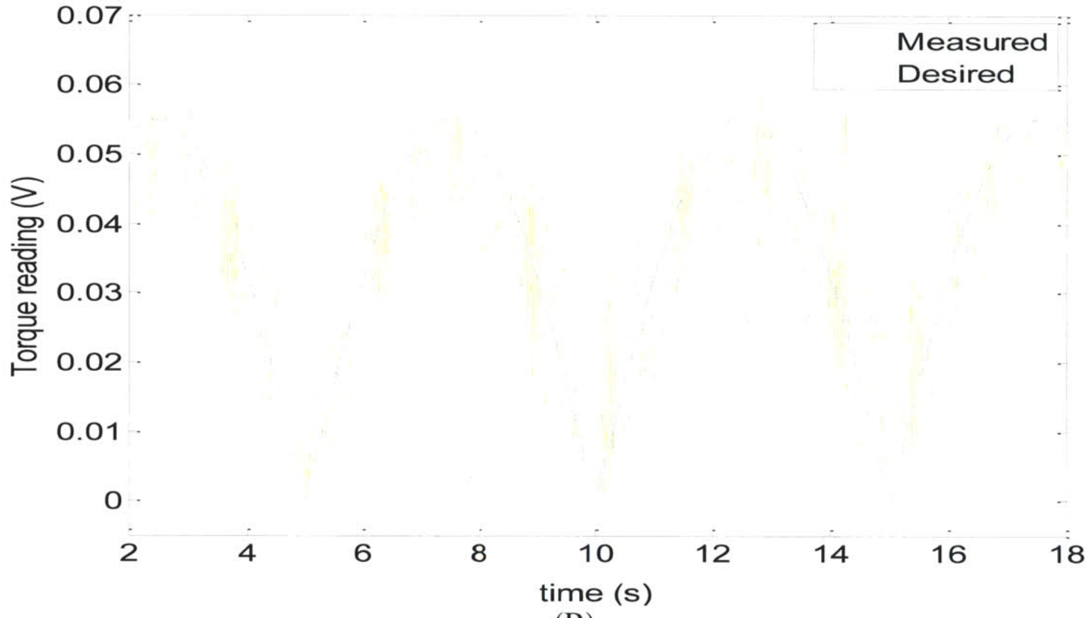

(B)

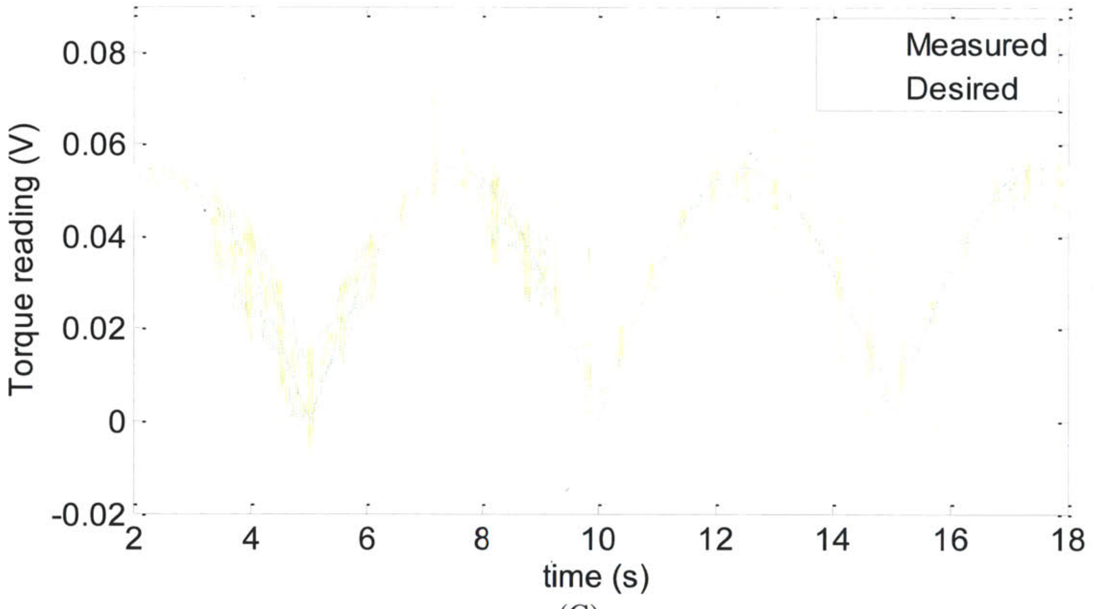

(C)

Fig. 6-10. Torque modulation with DSC. (A) Without the damper in series and in 2 kHz sampling rate. (B) Damper is in series and with 200 Hz sampling rate. RMS error was 0.007 V. (C) Damper in series and with 2 kHz sampling rate. RMS error was 0.005 V. In all cases, $V = 10$ V, $M = 0.01$ V.

6.3 Formulation of Discrete-state control

6.3.1 Formulation

Let $x = F(u)$ denote the system dynamics, where F is a dynamic operator, u is the input to the system F, and x is the resulting output. To modulate the output $x(t)$ to follow the given, desired time history $x_c(t)$, we set up a controller G with what we know about F, which determines the input $u(t)$ to the system based on the information given ($x(t)$, $x_c(t)$). More information on F warrants better design of G (Fig. 6-11).

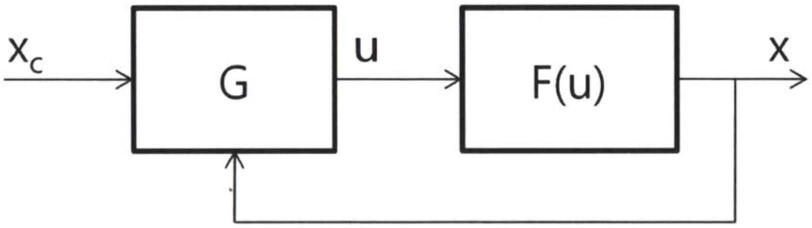

Fig. 6-11. System $F(u)$ modulated by the controller G.

However in reality, uncertainties and noise complicate the design of G. First of all, our knowledge on F is never complete. For example, a linear model of the system cannot adequately represent non-linear static friction. Simple, lower-order models of the system offer useful insights about the system's general behavior, but do not incorporate the higher-order dynamics that may emerge in some situations. Secondly, the inputs and outputs from the controller G may be corrupted by noise (due to digital-to-analog conversion, sensor resolution, etc). Aggressive controllers may respond to noise, causing undesired system behavior. A classic example is the effect of high derivative gain feedback in the presence high frequency noise.

Going back to Fig. 6-11, we may simply address the uncertainties and noise as follows. 1)

Address the possible uncertainties in F by simply assuming that the system F behaves like a strictly proper 1st-order system. More specifically, we assume that a sufficiently large positive value of the input u will increase the value of x in the following time step, while a sufficiently large negative u will decrease x. Under this assumption, G will now decide to output one of three values: zero, a fixed, positive value, or a fixed, negative value. G is then capable of increasing, decreasing or possibly maintaining the value of x in the next time step. 2) Prevent G from over-reacting to small apparent errors that may be due to noise, by setting up a margin for the value of error that G may respond to. As a result of 1) and 2), the new controller G may only output preset, discrete values according to the current, discrete state of the error. This controller is thus named a Discrete-State Controller. DSC can be written as

$$\mathrm{u(t) = V \cdot D(e)} \tag{a}$$

where D(e) is defined in Fig. 6-12. In this thesis, the region $-\mathrm{M} \leq \mathrm{e} \leq \mathrm{M}$ is sometimes referred as a 'don't-care-region', in which the controller simply is 'off'.

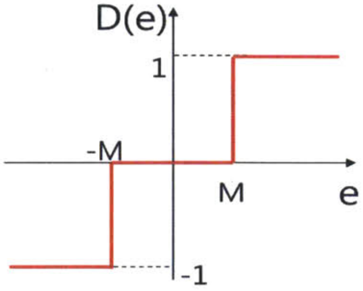

Fig. 6-12. Function D(e) used in (a).

6.3.2 Heuristic Method to Select the Parameters

When using the widely popular PID control, selecting the right gains is important to achieve desired performance. While there are tuning criteria in the literature based on assumptions about the system [**100**][**101**], many of them are heuristic rules (e.g. the Ziegler–Nichols tuning method). While heuristic methods lack mathematical rigor, they were often derived from physical insight about how the controller works and therefore offer useful recommendations.

A heuristic method can be developed for DSC as well, based on the observations from the physical examples presented in this chapter. There are three parameters to tune in DSC. They are: 1) fixed, positive 'effort', V, 2) threshold or 'margin of error' M, and 3) sampling interval, L. This section reports a heuristic method of choosing V and M where L is assumed to be known.

6.3.2.1 Choosing V

Based on the assumption that $F(u)$ behaves like a 1st order system, it is clear that the steepest slope of the step response, S, occurs at time = 0 (Fig. 6-13). Then, the largest change in x that can occur in one time step is

$$\Delta x_{\mathrm{max}} = V \cdot S \cdot L \tag{1}$$

This value is then compared with the largest possible change in the input in one time step, denoted $\Delta x_{\mathrm{C\_max}}$. In order to have a strong-enough controller that can follow the commanded input, it is necessary to have $\Delta x_{\mathrm{max}} > \Delta x_{\mathrm{C\_max}}$. That is,

$$V > \frac{\Delta x_{\mathrm{C\_max}}}{SL}$$

Specifically, we assign

$$V_{\mathrm{crit}} = \Delta x_{\mathrm{C\_max}}/SL \tag{2}$$

to be the critical value of V, below which the controller is simply not strong enough or fast enough to follow the given command. Any V that satisfies $V \geq V_{\mathrm{crit}}$ is a good candidate. Note that $\Delta x_{\mathrm{C\_max}}$ is not entirely unknown when designing the control scheme (the user often has the information on what $x_c(t)$ is going to look like), S is obtainable by running a simple step response test on the system, and L is chosen as needed thus V_{crit} is not difficult to estimate.

Another concern is to avoid the range of values of V, for which the system response is not exactly known or uncertain. For example, heavy static friction in the system may prevent the system from moving at low V. If the user knows these regions of uncertainties in the system, it is advantageous to choose large enough value of V that ensures operation of the system beyond these regions.

In summary, when choosing V, it is suggested that

$$\mathrm{V} \geq \mathrm{V}_{\mathrm{crit}} \text{ and } \mathrm{V} > (\textit{region of uncertainty in the system}) \tag{3}$$

Note, however, that higher V is not necessarily always desired. Too high V may induce undesired system behavior as will be explained in the next section.

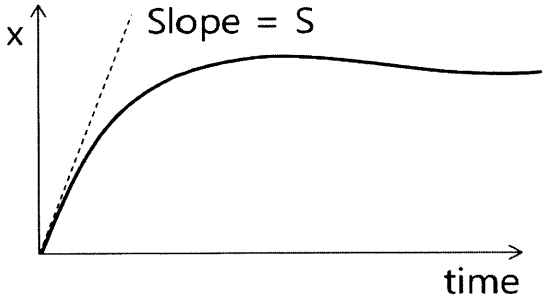

Fig. 6-13. Step response of a system and the maximum slope S.

6.3.2.2 Choosing M

As M is the margin of error below which the controller will not respond (outputs zero), M can be regarded as the parameter that directly affects the performance of the controller in terms of RMS-error. For this reason, it is advantageous to have as low M as possible. However, the following must also be considered:

1) M should be large enough to exceed any expected noise or disturbance, $M >$ (noise level).

2) M should be large enough to suppress undesired 'bouncing' from occurring (Fig. 6-14). That is, given the value of V, S and L, we want

$$2M > \Delta x_{max} = V \cdot S \cdot L \qquad (4)$$

Otherwise, if $\Delta x > 2M$, the controller output u may bounce between $+V$ and $-V$. As a result, x(t) may also bounce around the command input $x_c(t)$. This phenomenon, illustrated in Fig. 6-14, resembles the 'chattering' in sliding control [**102**]. To prevent this from happening at all times, (4) must be satisfied. We thus define the critical margin as a function of V as follows:

$$M_{crit}(V) = V \cdot S \cdot L/2 \qquad (5)$$

Note that (5) defines the relationship between all three parameters, V, M and L. Then, given V, we choose

$$M \geq M_{crit} \qquad (6)$$

In summary, smaller M is usually desirable as long as it satisfies the following:

$$M \geq M_{crit} \text{ and } M > \text{(noise level)} \qquad (7)$$

From (4-7), a higher value of V results in a higher M. For the smallest possible M, V must be as small as possible ($V = V_{crit}$). In cases where higher V is desired for a faster system response, the value of M must be adjusted according to (6).

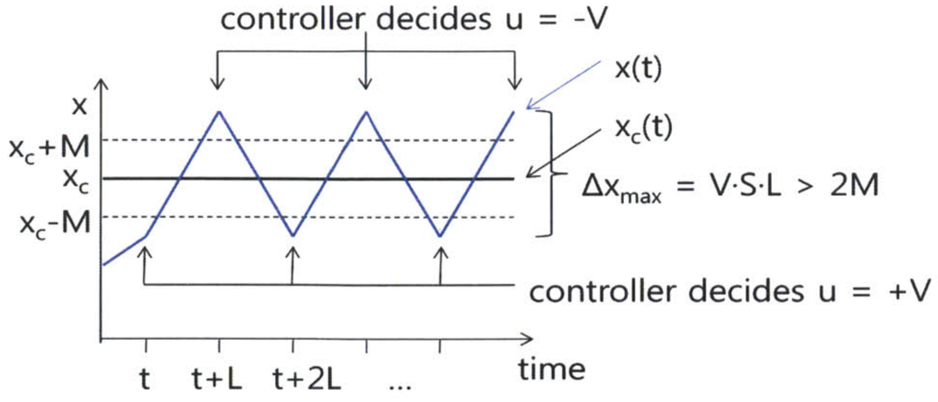
controller decides u = -V
x(t)
x
x_c+M
x_c
x_c-M
$x_c(t)$
$\Delta x_{max} = V \cdot S \cdot L > 2M$
controller decides u = +V
t
t+L
t+2L
...
time

Fig. 6-14. An example where undesired bouncing of *x* can occur.

6.3.3 Simulation Examples

To illustrate the effect of the parameters *V* and *M* and the effectiveness of the heuristic method to choose them according to (3) and (7), a few simulation examples of low-order, linear, time-invariant systems are presented in this section.

Consider a simple 1st order system, $F = 10/(s+10)$, with $x_c = \sin(2\pi t)$ and 1 kHz sampling rate ($L = 0.001$ s). Finding the maximum slope *S* from the step response of *F*, we can find that $V_{crit} = 0.6315$.

This system was modulated by DSC with different values of *V* and *M* (Table 6.1). The performance of the controller was assessed in terms of RMS error. As seen in Table 6.1, smaller *M* or *V* does not necessarily result in lower RMS error. Combinations of *V* and *M* that satisfy (3) and (7) result in much smaller RMS error, especially near $M = M_{crit}$.

Another example is $F = 24/(s^2 + 10s + 24)$, which is a 2nd order system with two real poles. As a result its step response exhibits 1st-order-like behavior in general. However, since the initial slope is zero for 2nd order systems, the value of *S* is taken as the maximum slope at $t = (0, 1]$ s instead at $t = 0$.

Given the same command and L as in the previous example, we can find $V_{\text{crit}} = 3.5343$. Table 6.2 shows the RMS error when this system is driven by a DSC controller with different values of V and M. Similar to the previous example, it is necessary to satisfy (3) and (7) to achieve low RMS error.

In summary, the simulation work suggests that abiding by (3) and (7) is necessary and useful. A good combination of V and M was able to achieve 0.8% RMS error in the second example.

Table 6.1
DSC performance on $F = 10/(s+10)$,
$L = 0.001$ s and $x_c = \sin(2\pi t)$

RMS Error	V = 0.3	0.6	1	2	5	10
M = 0.002	**0.4923**	**0.2748**	**0.0536**	**0.0218**	**0.0494**	**0.0998**
0.005	**0.4926**	**0.2754**	**0.0533**	**0.0207**	**0.0479**	**0.0990**
0.01	**0.4931**	**0.2759**	**0.0535**	**0.0101**	**0.0469**	**0.0969**
0.02	**0.4938**	**0.2771**	**0.0563**	**0.0188**	**0.0447**	**0.0920**
0.05	**0.4964**	**0.2816**	**0.0712**	**0.0469**	**0.0373**	**0.0279**

$M > M_{crit}$

$V > V_{crit}$

Table 6.2
DSC performance on $F = 24/(s^2 + 10s + 24)$,
$L = 0.001$ s and $x_c = \sin(2\pi t)$
Performance evaluated after 5% settling time (0.6 sec)

RMS Error	V = 2	3	4	5	7	10	20
M = 0.002	**0.4061**	**0.0095**	**0.0189**	**0.0255**	**High**	**-**	**-**
0.005	**0.4019**	**0.0088**	**0.0081**	**0.0120**	**0.0176**	**High**	**-**
0.01	**0.4010**	**0.0127**	**0.0107**	**0.0097**	**0.0131**	**0.0223**	**High**
0.02	**0.4015**	**0.0231**	**0.0196**	**0.0180**	**0.0155**	**0.0143**	**0.0423**
0.05	**0.4065**	**0.0588**	**0.0499**	**0.0453**	**0.0396**	**0.0357**	**0.0272**

$M > M_{crit}$

$V > V_{crit}$

6.4 Discussion

Many conventional methods have been proposed to minimize the influence of uncertainties and noise. For example, attempts to compensate for static friction have been proposed **[103][104][105]**. Sliding Control assumes the uncertainty in the system to be bounded, and re-formulates a higher-order control problem to be first order in s **[102]**. Time-delay control uses the system response from the previous time step to estimate unknown dynamics and unexpected disturbances in the current time step **[106]**. Kalman filtering techniques keep updating the model of the system at each time step, thereby adapting to transient changes of the system as well as to unmodeled (uncertain) system behavior. Combinations of control strategies can be used to address application-specific uncertainties in the system, as in **[107]**, where time-delay estimation was used in conjunction with ideal velocity feedback to overcome soft and hard non-linearities in a 2-DOF SCARA-type robot. It should be noted however, that using such methods often require significant modeling and computational effort.

In contrast, one may choose to drastically reduce modeling and computational effort as long as robustness to uncertainty is not significantly compromised. In fact, simple feedback control schemes with little knowledge of system dynamics can be impressively successful in specific applications. One example is temperature regulation in a refrigerator. The controller is indifferent to the complex dynamic behavior of the cooling system, which includes highly non-linear subsystems such as a compressor, evaporator, etc., variations in the composition and distribution of objects in the refrigerator, or the response of internal temperature to disturbances such as opening and closing the door. Yet the simple strategy of turning the cooling system on or off as needed is enough to successfully regulate temperature in the refrigerator. This extremely simplified control scheme is good enough for its application. The success of discrete-state control is reminiscent of such examples.

6.4.1 System order and DSC

An assumption made in the formulation of DSC is that the system under consideration exhibits the property that ‘pushing to oppose the error reduces the error’. Whereas applying this simple strategy may destabilize a system with high-order dynamics, it is quite effective for a system with 1st order dynamics.

Nonetheless, we find that a system with approximately 1st order dynamics is not a strict requirement for DSC to work. DSC showed reasonable performance in a simulation of a 2nd order system with no zeroes, even with very light damping of $\zeta < 0.1$ (Table 6.3, Fig. 6-15). The simulation result suggests that DSC may work even on practical 2nd order systems with high overshoot.

Furthermore, when a real-valued zero at -10 is added to the lightly damped 2nd order system, the DSC performance is greatly improved even well before the 5% settling time (Fig. 6-16, $V=V_{\mathrm{crit}}$, $M=M_{\mathrm{crit}}$). Compared to the system in Fig. 6-15, the addition of zero reduces the RMS error by as much as 95%. This is presumably due to the fact that the zero enhances the system response rate at $t = 0$. In other words, the zero in this case makes the 2nd order system behave similar to a 1st order system. This result suggests that DSC may work well in a wider range of application whose relative degree is low. An example is shown in Fig. 6-17.

Note that for higher order systems, the maximum slope in the step response may not occur at $t = 0$. In these examples, S is measured as the maximum slope during the first ‘oscillation’ in the step response (roughly one cycle of the natural frequency).

Table 6.3
DSC with 2^{nd} order systems.
$F = \omega_0^2/(s^2 + 2\zeta\omega_0 s + \omega_0^2)$ where $\omega_0^2 = 50$
Command = $1 \cdot \sin(2\pi \cdot t)$, Frequency = 1 kHz

ζ	0.966	0.707	0.259	0.087
Least RMS error (after 5% settling time)	0.0084	0.0083	0.0125	0.0462
V/V_{crit}	1	1	1	1
M/M_{crit}	2	2	4	2

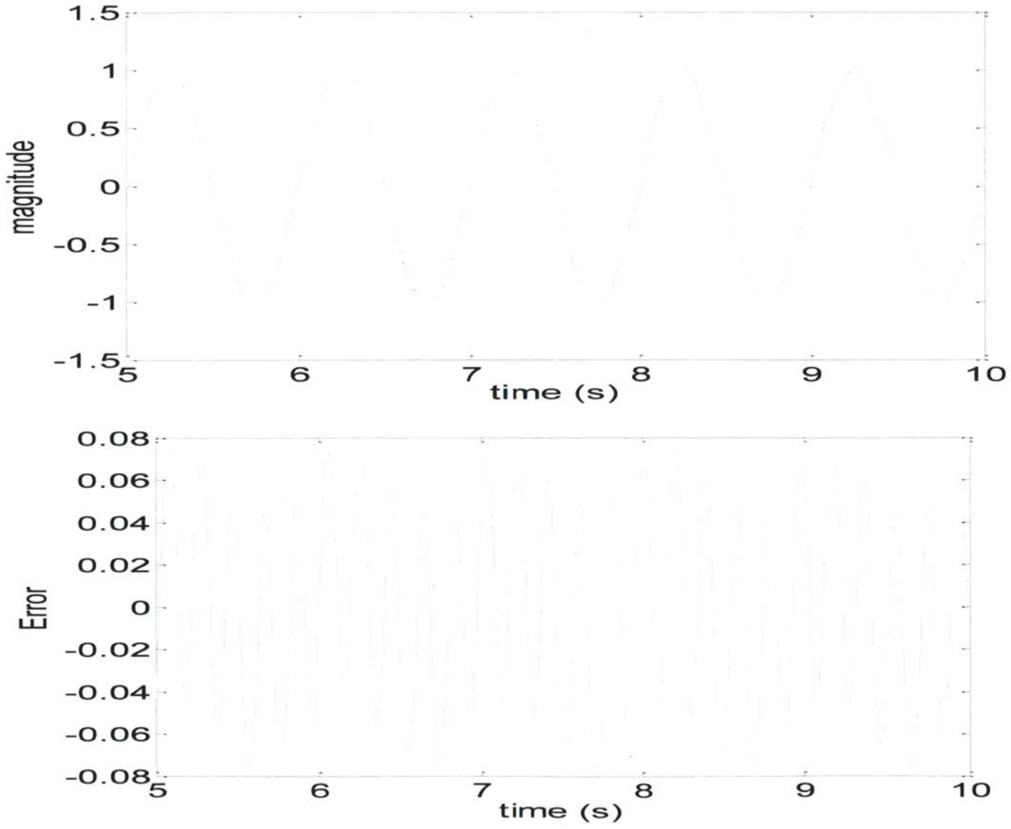

Fig. 6-15. DSC on a lightly damped 2^{nd} order system (ζ = 0.087 in Table 6.3). Top: Command (red) versus the response with DSC control (blue) after 5% settling time (5 sec). Bottom: error. RMS value over this time window is less than 5% of the amplitude of the sine input.

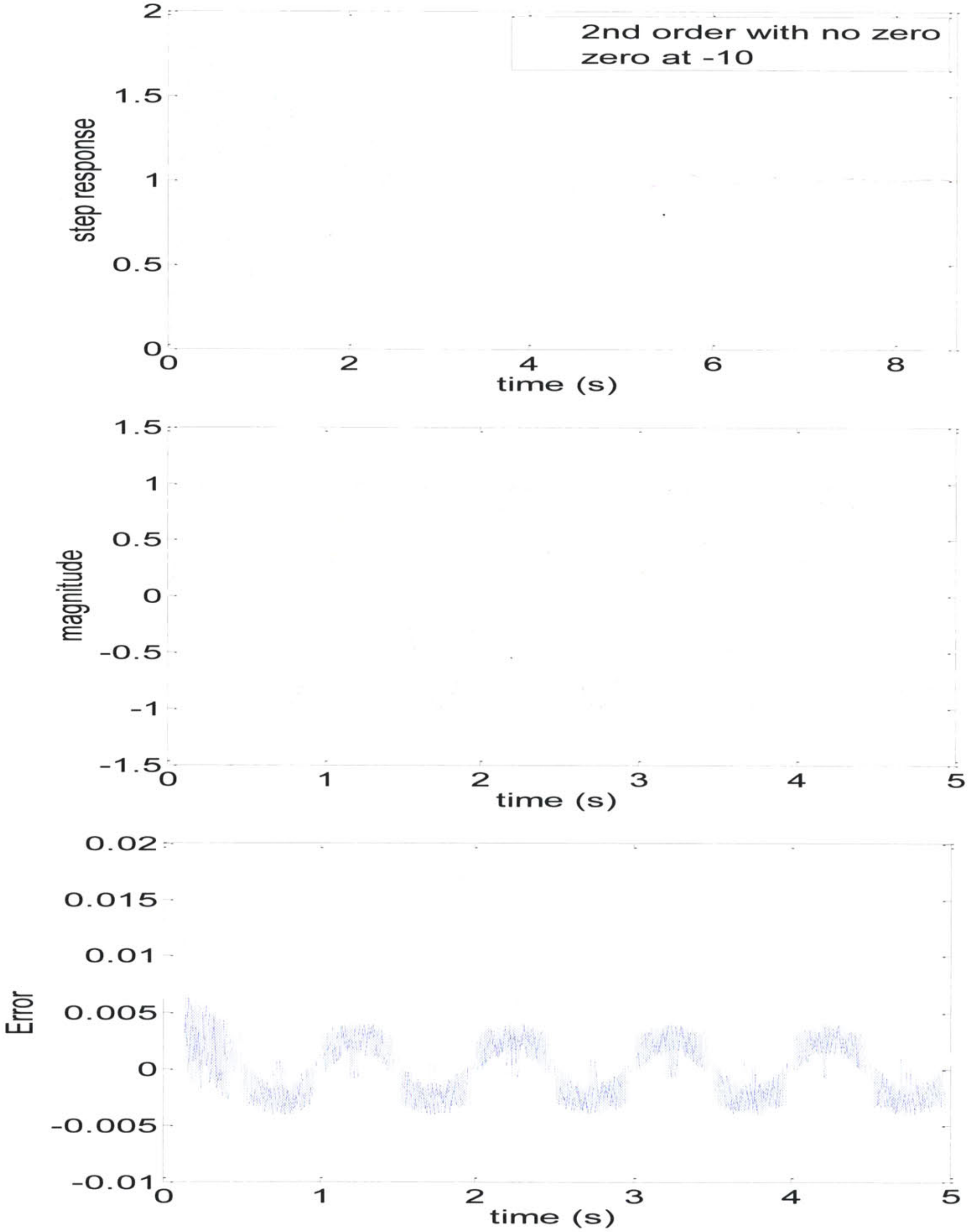

Fig. 6-16. DSC on a system in Fig. 6-15 with an added zero at -10. Despite the similarity in the step response, DSC performs much better when a zero is added. Top: Adding a zero at -10 does not drastically improve the system response to a step input. Middle: DSC performs well. Command (red) and response (blue) are indistinguishable. Bottom: error. RMS value after transient response (before t = 1s) is 0.23% of the amplitude of the sine input, an improvement of more than 95% over the no-zero case in Fig. 6-15.

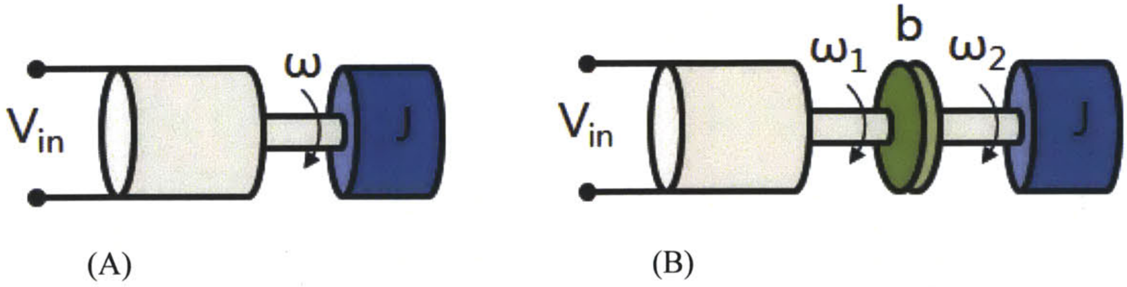

Fig. 6-17. (A) A motor-load system can usually be modeled as a 2nd order system with no zero for $F = \omega/V_{in}$. (B) A damper in series with the load introduces a zero to the transfer function of $F = \omega_1/V_{in}$.

6.4.2 Comparison with Sliding Mode Control (SMC)

DSC and SMC share several interesting similarities. First of all, similar to DSC, taking advantage of first-order error dynamics is the essence of how sliding control works [**102**]. In SMC, the problem of keeping the tracking error of an n-th order system is simplified to a 1st order tracking problem in s (a scalar value). Secondly, because the dynamics of s are 1st order, the control effort u(t) changes sign at the 'sliding surface' ($s = 0$). To reduce the often unstable rapid, undesired switching of u(t) near $s = 0$, one may setup a 'boundary layer' inside which the control law is linear in s. Choosing the size of this 'boundary layer' in SMC is analogous to setting up the error margins in DSC.

To further investigate what insight SMC might provide into the operation of DSC, we assume a 1st order, single-input single-output system $\dot{x} = f + bu$, where f and b are system parameters that are not exactly known. Although f is not known, we let $\hat{f}$ be an estimate of f where the estimation error is bounded. That is, for some known positive value ζ, we have $|f - \hat{f}| \leq \zeta$.

Using the standard SMC formulation, we find

$$u(t) = (\dot{x}_c - \hat{f})/b + q \cdot \mathrm{sign}(x - x_c) \quad (8)$$

where q is a scalar, and x_c is the command (desired) trajectory of x. Note that in the 1st order case, $s = x_c - x = -e$. In order for (9) to satisfy the 'sliding condition', which is

$$\frac{1}{2}\frac{d}{dt}s^2 \leq -\eta|s|$$

where η is a positive value. The value of q that satisfies the above condition is

$$q \geq (\zeta + \eta)/b$$

We then incorporate a boundary layer of width 2Φ to reduce chattering (Fig. 6-18). A commonly used method is to replace the signum function in (8) with a saturation function (Fig. 6-18). In DSC, we use a more discrete alternative, $D(x - x_c)$, illustrated in Fig. 6-18. Then, (8) becomes

$$u(t) = (\dot{x}_c - \hat{f})/b + q \cdot D(e) \qquad (9)$$

Now if we put $V = q$ and $M = \Phi$, the second term of (9) becomes (a), which is the DSC scheme. Note that a very high q makes (9) dominated by the second term. In short, DSC may be regarded as a simpler version of SMC for 1st order systems. The 'don't-care-region' ($-M \leq e \leq M$) is a crude version of 'boundary layer' of SMC (although the method to tune Φ in SMC is different from choosing M based on V in DSC), while V, just like q, must be selected sufficiently high to encompass the region of uncertainty in the system.

However, unlike SMC, the error dynamics apparently does not have to be linear and first order for DSC to work. In addition, DSC does not require a mathematical model to formulate first-order error dynamics as in SMC. On the other hand, this is also a limitation of DSC. Unlike SMC, there exist no mathematical proofs of stability or robustness at this point.

It is interesting to note that in some cases, setting up a boundary layer in the controller design is rendered pointless by often un-modeled static friction. For example, in the position control case in section 6.1.1, the sliding surface $s = 0$ corresponds to a tracking position error of zero.

Suppose we had implemented SMC to resolve the problem and used the saturation function in Fig. 6-18 within the boundary layer. The controller action *u* may then be small when e < Φ. In the presence of high static friction, the small *u* may not be enough to overcome the static friction and push the system towards reducing the error. In the end, the controller is silent when the error is small, as if *D*(*e*) is used instead of the saturation function. In this hypothetical example, static friction serves as a boundary layer in hardware that works like the don't-care-region in DSC.

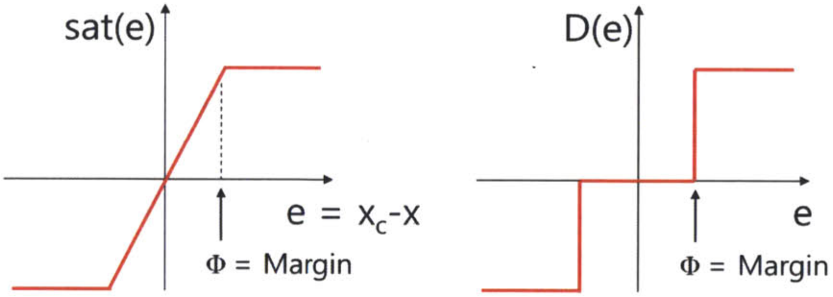

Fig. 6-18. Left: The saturation function often used in SMC. Right: DSC may be considered to use an alternative function with more aggressive suppression of control action within the boundary layer.

6.4.3 Other remarks

The simplicity and robustness of DSC is reminiscent of digital circuitry and digital communication. The simple, binary nature of digital signals is responsible for the robustness of digital data transmission. Combined with high-speed computation and sampling it provides reliable signal reconstruction. In the case of DSC, the discrete nature of the control effort in response to error confers robustness in the presence of uncertainties, while high-speed sampling appears to be an important requirement to ensure the success of DSC.

Aside from the fact that DSC succeeded where other schemes did not, it has a few notable advantages over other controllers. First, the DSC scheme is simple. Implementing it requires only a few lines of computer code. It is so computationally cheap that implementation of DSC on a simple logic board may be feasible. Secondly, despite (or perhaps because of) its simplicity, DSC can be robust. As demonstrated in this chapter, DSC succeeded in the presence of uncertain and highly nonlinear system behavior that rendered other comparably-simple methods ineffective.

Stiction and/or static friction is extremely common in mechanical transmission systems, especially low-cost actuators, and often compromises their ability to control position. DSC may be packaged with existing low-cost actuators and sensors to provide a precisely controllable position without substantially increasing cost.

Note that it is common for physical systems to exhibit significant energy dissipation, e.g. due to friction or resistance. While one goal of DSC was to manage the undesirable consequences of friction, dissipative elements may in fact contribute to better performance with DSC, as seen in the torque-modulation example.

Moreover, dissipative elements may reduce detrimental effects of the high-frequency impacts caused by DSC. For example, in the position-modulation example in section 4.4.1, the discrete nature of DSC may excite unwanted resonance in the transmission system between motor and output. On the other hand, because DSC is discrete and outputs zero (i.e., does nothing to the system) when the error in position is sufficiently small, static friction in the transmission system may then act to remove energy from any excited resonant modes.

Impedance control may also be implemented with DSC, provided that the system exhibits 1st-order like behavior. In essence, controlling impedance is to control the interaction force/torque based on the error in kinematics such as position or velocity. The desired value of interaction force may be modulated by DSC similar to the example shown in section 6.2.4.

6.5 Conclusion

Discrete-State Control is a simple and robust scheme that manages uncertainties and noise without an explicit mathematical model. It can be used to control position or force, or to reduce output impedance in systems with hard non-linearities such as heavy static friction. Moreover, DSC outperforms the common alternative (PID control) in the examples presented in this paper. When the system under consideration exhibits 1st-order-like behavior (pushing to oppose the error acts to reduce the error), DSC can be a simple and robust alternative to conventional methods such as PID control. In short, DSC may be a reasonable first candidate controller to implement, especially in applications that require quick, low-cost solutions.

At present DSC offers no guarantee of stability or robustness, or prediction of the consequences of changing sampling rate, sensor resolution, or using 'shaped' or filtered error signals. Analytical investigation seems warranted to address these shortcomings and gain deeper insights about the advantages and limitations of DSC.

Chapter 7

Validation Experiments with Rodents: Part I

7.1 Motivation

The goal of this thesis was to develop an apparatus which minimally impeded overground locomotion with the ability to provide interaction. In the previous chapters, the design and implementation of the apparatus were presented. To improve back-drivability, a novel control scheme was developed. Questions still remain as to whether the current design met the requirement stated in chapter 3.

Conducting animal experiments was an important step in the design and evaluation of the system. First of all, this 'road test' provided assessment of several assumptions and decisions made during the design and implementation of the apparatus, thereby providing insights about how the current design might best be updated and modified. Secondly, data collected from the experiment was used to identify and address questions about the apparatus that were not evident during the design process. The data was also used to highlight features of this apparatus and compare it with other available machines.

Assessments of these aspects of the apparatus will demonstrate how the apparatus performed in action with a real animal to prove the effectiveness of the system and suggest its potential uses (see chapter 8: validation experiment part II).

7.1.1 Questions Addressed in the Experiments

A. Coupling strategy

Interfacing with the animal through robust coupling is important. In chapter 4, simple coupling strategies such as using Elastikon® tape or elastic string were tested on an anesthetized animal. Whether the couplings would remain secure and robust on a sober animal remained to be seen.

B. Kinematic constraint

In the design of the Rat Module, a decision was made to allow only 2-DOF movement of the ankle. Although some frontal plane motion was still possible due to compliance of the ankle couplings, the effect of this kinematic constraint required further evaluation.

C. Apparatus Functions

The sensors and actuators onboard the Rat Module as well as on the body-weight support system were sufficiently tested during the design process. Nonetheless, possible improvements of the sensor location, resolution, or post processing of the signals might be identified through a live animal experiment.

D. Animal Anxiety

As stated in chapter 3, rats may be intimidated by the experiment and may perform poorly. Observation and data collection while the animal was not anxious would allow better assessment of the animal's locomotion. Experiments with live animals were required to identify and remove possible sources of anxiety.

The DSC scheme developed in chapter 6 substantially improved the back-drivability of the apparatus. However, the interaction force was not completely eliminated. The animal's reaction to this control scheme required further assessment.

7.2 Methods

To address the questions identified in the previous section, three sets of live animal experiments were conducted which are presented below. As learned from a survey of the literature, Sprague-Dawley rats are one of the most commonly used rodent strains in locomotion studies [**95**][**87**], especially females since they are more tolerant of changes to their environment. When fully mature (> 8 weeks), females are 15 to 18 cm in body length excluding the tail, and 200 to 400 grams in body weight. The specific rat used in these experiments was a female rat, 400 grams in weight.

All animal experiments were conducted in the animal housing facility. The Division of Comparative Medicine (DCM) at MIT runs a number of animal housing facilities, among which the E25 facility houses rodents. This facility was temporarily moved to building E17/18 for renovations. All experimental procedures were detailed in the document, Hogan 1010-094-13, which was reviewed and approved by MIT's Committee on Animal Care (CAC).

7.2.1 Experiments Using a 'Mockup'

This experiment used a 'mockup', a passive version of the Rat Module. The mockup did not contain any motors or sensors and hence did not require power. The mockup was identical to the

Rat Module in overall size, linkage dimensions and sagittal plane workspace, but was lighter in weight (33 grams) and required no wire attachments.

The mockup shared many features with the active Rat Module. Firstly, the method to interface the mockup to the animal was identical to the method used for the Rat Module. This allowed addressing the performance of the couplings without risking damaging actuators and sensors on the Rat Module. Secondly, the mockup allowed an assessment of the effect of the kinematic constraint imposed by the Rat Module. This was possible due to the extremely low output impedance of the 5-bar linkage. All joints, including the two axes on the base where the motors would be for the active Rat Module, were made of low-friction rotary bearings. The inertia of the linkages is also practically negligible (less than 5 grams) as the reflected inertia of the motors (armature inertia times the square of the gear ratio, estimated to be 16 $g{\cdot}cm^2$) was absent. Hence, applying the mockup to the animal was, in essence, adding a sagittal plane kinematic constraint to the ankle. The mockup thus served as a platform to test the effect of the kinematic constraints on the animal's locomotion.

The mockup also enabled assessing the animal's anxiety during the experiment. For example, the procedure of applying the mockup might agitate the animal. Also, the sensation of a bulky, solid structure surrounding the lower half of the body might induce anxiety.

In this experiment, a 1-D arena shown in Fig. 7-1 was used. The narrow corridor in the middle encouraged the animal to walk in a straight line. The transparent wall allowed video recording (30 Hz, 1.5 mm per pixel) and also served as a reference to assess step length.

The experiment sessions took place at a fixed time of the day for seven consecutive days, in the same environment. The mockup was applied to the animal in the following order: 1) Waist coupling was applied. 2) Mockup was attached to the waist coupling through Velcro® attachment. 3) The ankles of the animal were coupled to the linkages of the mockup. 4) The animal was placed inside the 1-D arena.

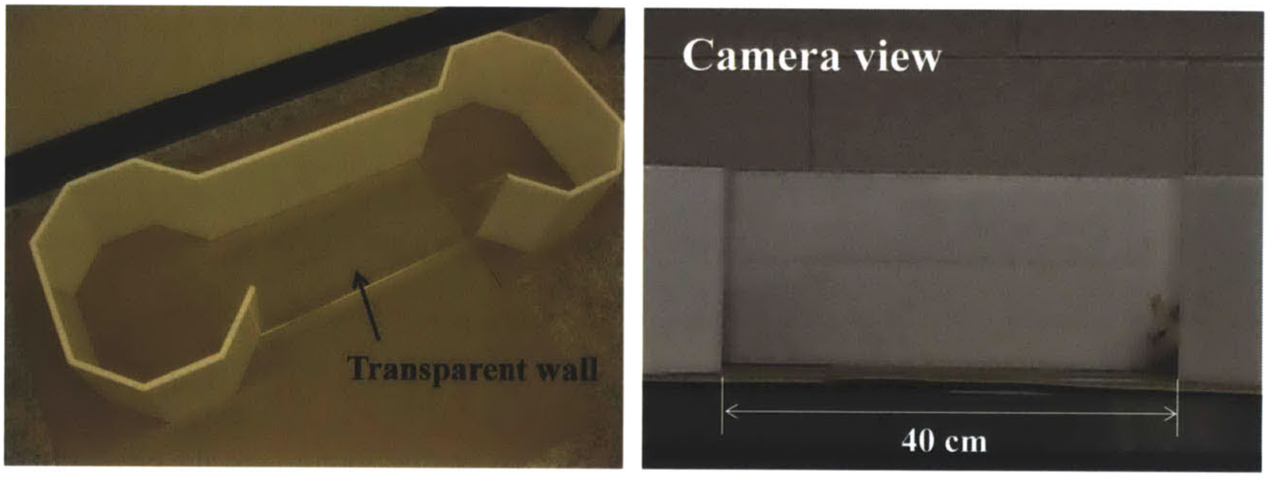

Fig. 7-1. 1D-arena used in the experiment.

7.2.2 Powered Device on an Anesthetized Animal

To evaluate apparatus function without damaging the prototype, an anesthetized rat was used to reduce the risk of possible 'failure scenarios' (e.g. the animal might attempt to damage and disconnect the wires between the Rat Module and the body-weight support system). All sensors and actuators on the Rat Module and the body-weight support system were powered. All motors were commanded to zero current, and hence back-drivability of the motors was higher than when the motor terminals were short-circuited. However, the substantial friction of the gearhead was still present. The discrete-state control developed in chapter 6 was not implemented in this experiment. A 2-D trapezoidal arena shown in Fig. 5-8 was used in this experiment. This experiment was done in a single day.

The experiment was conducted in the following order. 1) The animal was anesthetized using inhalant anesthesia (1~4% isoflurane). 2) The Rat Module was attached to the animal. 3) The animal was placed inside the 2-D arena. 4) The Rat Module was connected to the supporting hardware. 5) All sensors and actuators were powered up. Data collection began.

7.2.3 Rat Module with Force Feedback

A sober animal's reaction to the overall experimental apparatus was addressed. In addition, the force feedback scheme used in this experiment was the DSC force feedback described in Chapter 6. The active body-weight support system was not tested in this experiment, as its performance had previously been evaluated sufficiently. However, the body-weight support system was still used to support the weight of the rat module as well as to serve as a conduit for wiring. The weight support given by the system was estimated to be around 80 grams (which is slightly higher than the weight of the Rat Module).

The experiment was performed using the 1D-arena of Fig. 7-1. As mentioned earlier, the purpose of the 1D-arena was to enable evaluation of the apparatus, by allowing video-based comparison of locomotion in different animal preparations.

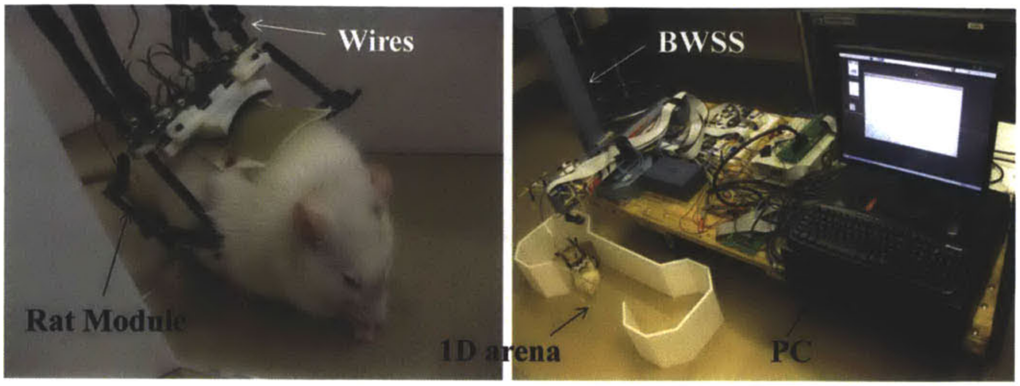

Fig. 7-2. Experiment setup.

The experiments were conducted at the same hour of day for 9 consecutive days, in the designated procedure room. The experiment procedure was as follows. 1) Waist coupling was applied. 2) Rat Module was attached to the waist coupling through Velcro® attachment. 3) The ankles of the animal were coupled to the robotic arms of the Rat Module. 4) The animal was placed inside the 1-D arena. 5) The Rat Module was connected to the supporting hardware. 6) A force feedback scheme was applied to the Rat Module. Data collection began. 7) Voluntary movements were observed.

Videos were recorded for steps 6 and 7. Due to a malfunctioning force sensor on the left side of the Rat Module, force data were collected only on the right side where force feedback control was implemented. Position data from the encoders were recorded from all four motors.

7.2.4 Addressing Anxiety of the Animal

Throughout the experiments, signs of animal anxiety were identified and logged. Temporal indications included:

- Excessive grooming

- Squeaking
- Reluctance to move (ex. exploring the area while only moving the fontal half of the body)
- Excessive urination
- Folded-back ears
- Aggressive behavior (ex. biting attachments)

Signs of continued stress and anxiety, which were checked before the start of experiments on each day, included:

- Abnormal loss of hair (in patches)
- Changes in the color of the facial hair
- Excessive loss of weight

The above list of anxiety signs was created after consulting experts in rodent experiments (Dr. Matthew Wilson and Dr. Allison Hayward).

7.3 Results

7.3.1 Coupling Strategy

The coupling methods presented in chapter 4 remained secure and robust in all experiments. Attachment of the mockup or the Rat Module required less than 3 minutes, and detachment required less than 1 minute. Overall, the coupling strategy was successful.

7.3.2 Kinematic Constraint

The kinematic constraint imposed by the mockup did not induce any apparent abnormality to the animal's behavior. Figure 7-3 lists the major examples of voluntary movement observed in this experiment (either with mockup or with Rat Module). Despite the kinematic constraint, the animal's movements did not appear to differ from those observed in a free animal.

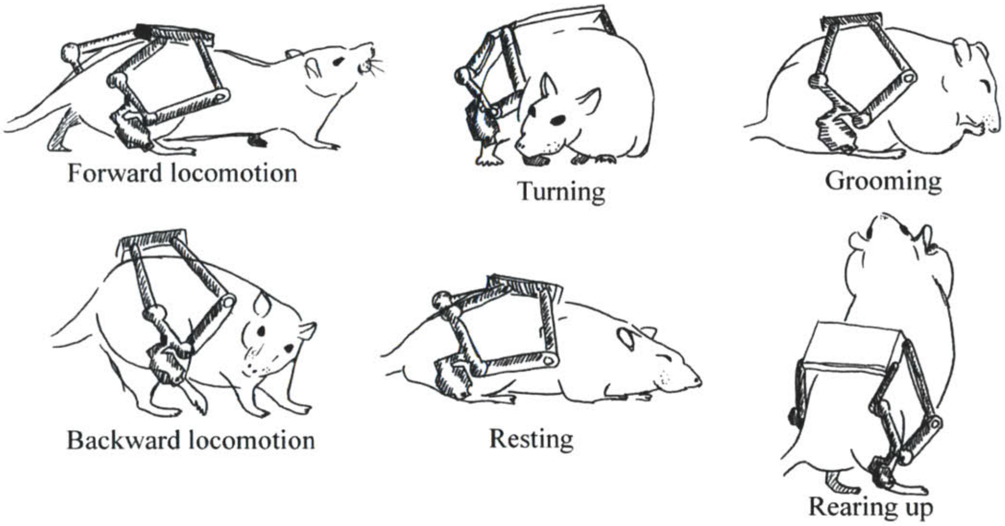
Forward locomotion
Turning
Grooming
Backward locomotion
Resting
Rearing up

Fig. 7-3. Collection of movements commonly observed in this experiment.

7.3.3 Apparatus Function

All sensors (four encoders, two 2-axis force sensors, video camera on the BWSS) worked properly and recorded meaningful data, except for when a force sensor was broken in the experiment with powered Rat Module (section 7.2.3). An estimate of the x-y movement of the ankles relative to the coordinate frame of the Rat Module base was successfully reconstructed from the encoder data. The force sensors provided data consistent with the motion data acquired from the encoders. (However, appropriate filtering was required.) The video camera functioned correctly within the control loop of the BWSS.

A. Trajectory of the ankle

The encoder readings were used to reconstruct the x-y movement of the animal's ankle with respect to the base of the Rat Module (Fig. 7-4). The blue dots in Fig. 7-4 are the locations of the end-point of the 5-bar linkage, with respect to different positions of the motor shaft. The ankle trajectories are plotted on top of these dots.

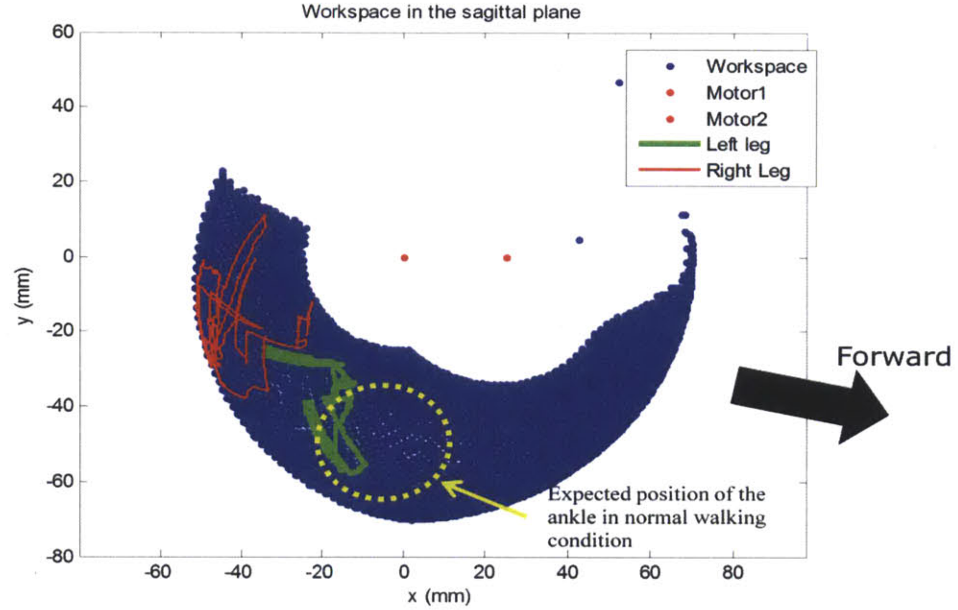

Fig. 7-4. Trajectory of the left and right leg ankles plotted over the entire workspace of the 5-bar linkages. The yellow dotted circle represents the area in which the ankle position would be expected in normal (sober) conditions.

B. Interaction Force

Fig. 7-5 shows the magnitude of the raw force measured on the left hindlimb. The force reading is noisy and contains what may be a DC bias. Further assessment of the force data is presented in the discussion (section 7.4).

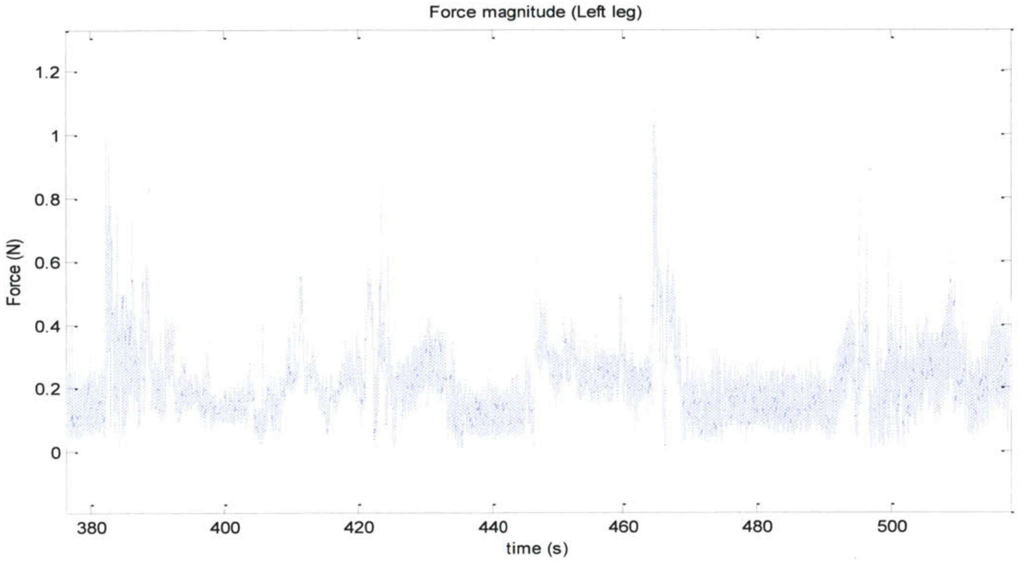

Fig. 7-5. Magnitude of the force measured at the left hindlimb ankle.

C. Tracking Overground Movement

The body-weight support system successfully achieved its two main objectives: 1) follow the animal's overground movement inside the arena, and 2) acquire a time-history of the animal's position in the arena. Detailed assessment was made in chapter 5.

7.3.4 Animal Anxiety

A. Experiments with the Mockup

For the first few days of the experiment, the animal showed signs of anxiety such as reluctance to move inside the 1D-arena or excessive urination. There were occasional squeaks from the animal during the coupling attachment procedure. Nonetheless, the animal seemed indifferent to the couplings themselves. The animal practically paid no attention to the attachments starting from the first day and throughout the duration of the experiment.

After 3 days, the animal became more active inside the 1D-arena and showed much less evidence of anxiety. Attaching a dummy weight (to simulate the sensation of the inertia of the Rat Module) had no observable effect. However, the animal was sensitive to the noise generated when the dummy weight hit the wall of the 1D-arena.

On the 7th day, the animal was comfortable inside the 1D-arena with the mockup attached. Occasional collision of the mockup with the wall did not bother the animal. The animal actively examined the corners of the arena, occasionally attempting to climb over the wall to explore outside. Overall, the animal behaved as if there was no mockup attached to it. The kinematic constraint imposed by the Rat Module did not induce anxiety.

At the end of the experiment, it was concluded that the animal was now sufficiently exposed to the experimental apparatus such that it no longer showed anxiety.

B. Experiments with the Rat Module

As in the previous experiments, it took several days for the animal to become accustomed to the change in its environment, including having the bulky hardware cart close to the 1D-arena or the BWSS robot above the animal. For example, the animal occasionally reacted to the Rat Module (e.g. biting the linkages) in the earlier days of the experiment. However, after this period, the animal showed no significant signs of anxiety and made voluntary movements. Applying force feedback did not induce anxiety.

7.4 Discussion

7.4.1 Anxiety was Reduced through Training

The animal showed multiple signs of anxiety during the first three days of a new experiment protocol in the experiment with a mockup as well as in the experiment with an active Rat Module. The occurrence of the indications of anxiety was drastically reduced in the following three days. By the 7th day of the experiment, the animal showed no apparent signs of anxiety or continued stress. Specifically, we identified that the following would not induce anxiety in a suitably trained animal: 1) the act of attaching the mockup or the Rat Module, 2) the couplings and the sensations from them, 3) additional weight on its lower back, 4) the kinematic constraint imposed by the mockup or the Rat Module, and 5) being inside the 1D-arena. The animal's movement appeared normal and unconstrained. Thus it was concluded that the anxiety of the animal to a new experiment setup could be reduced or even completely removed by multiple days of training. Sufficient exposure of the animal to the experiment setup is essential.

7.4.2 Coupling Strategy and Kinematic Constraint

As reported in section 7.3, the coupling strategy used in this thesis was robust and secure. The Elastikon® tape and Velcro® attachment for the waist coupling as well as the elastic string for the ankle coupling survived the duration of the experiment each day. The kinematic constraint imposed by the mockup or the Rat Module did not prevent the animal from exhibiting what appeared to be normal, voluntary overground movements (Fig. 7-3).

To address this question quantitatively, videos of the animal walking in a corridor of the 1D-arena with the mockup attached were analyzed. Features of forward locomotion such as stride length and stride duration were compared between the animal with couplings only (elastic strings around ankles and elastic tape around the waist) and the animal with mockup (Fig. 7-6). The animal with mockup was trained in the setup for several days before collecting data.

The mockup condition yielded no statistical difference between both stride length and stride duration compared to the animal with couplings only, suggesting that the effect of the kinematic constraint imposed by the mockup was minimal, at least for forward locomotion. We thus concluded that the sagittal plane constraint allowed natural forward locomotion of the animal (verified by the stride length/duration data), and other normal behaviors (as evidenced by Fig. 7-3 and a number of video clips taken during the experiment).

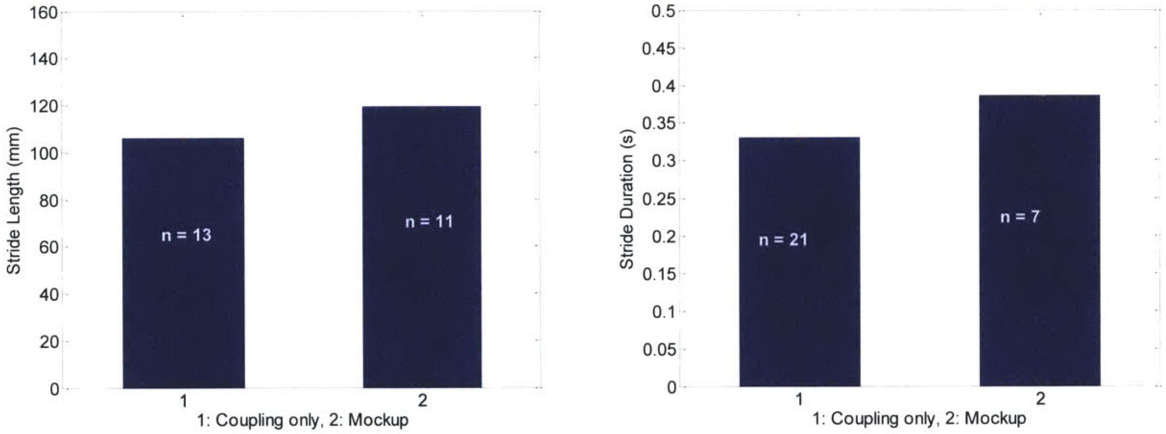

Fig. 7-6. Stride length (left) and stride duration (right) compared between 1: an animal with coupling attachments only, and 2: identical animal trained in mockup.

7.4.3 Apparatus Function

A. Data collected by the Encoders

The two trajectories for the left and right legs in Fig. 7-4 show arcs and sharp corners. These are evident signs that only one motor shaft turned (resulting in arcs). In short, the recorded trajectories did not represent 'normal' movements of the animal. However, this was not surprising as the animal was not in a normal condition (i.e., it was under the influence Isoflurane).

Since the animal was under the influence of anesthesia and was mostly lying flat on the ground, the positions of the ankles of the two hindlimbs showed negative values in x. However, even in that posture, the animal occasionally showed intentional overground movements as captured by the encoders. In Fig. 7-7, the force vectors are 'stamped' on the ankle trajectory at every 100 ms. Regions inside the red-dotted circles are where the ankle was the majority of the time. All trajectories outside these regions occurred when the animal attempted movement. Overall, the encoder data correctly represented the actual behavior of the animal under the influence of anesthesia.

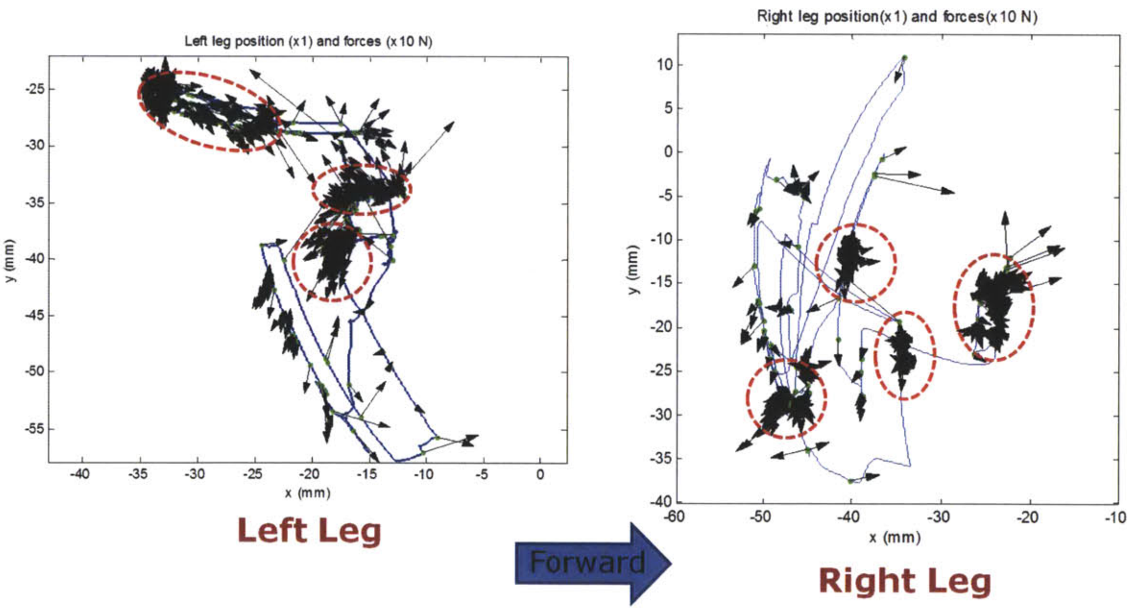

Fig. 7-7. Recorded force vectors are plotted on top of the trajectories of the ankles shown in Fig 7-4. The vectors are plotted at 100 ms intervals. Force vector of length 1 (mm) represents the force magnitude of 0.1 N. Regions inside the red-dotted circle are where the ankles were for most of the duration of the experiment.

B. The Force Sensors

During the experiment with the anesthetized rat, the motors on the Rat Module were commanded to zero current, thus were not active during the whole experiment. Hence all forces were generated purely by the animal back-driving the linkage system. For example, high force means intention of movement but low back-drivability in that specific configuration, whereas low force may occur in configurations with high back-drivability and/or when the animal has no intention to move.

Fig. 7-5 shows the magnitude of the raw force measured on the left hindlimb. First of all, the force reading is noisy and contains what appears to be a DC bias. The noise level is as high as 0.2 N (about 20 gram-force), which is unacceptably large, almost 10% of the animal's body weight (250 g). Appropriate filtering was required to improve the quality of the force data.

Secondly, one can observe peak forces of nearly 1 N (about 100 gram-force) occurring in a number of instances. Even after considering the high noise level and DC bias, these peaks show that the Rat Module has high intrinsic output impedance.

Lastly, although the sensors were noisy, the force data itself appeared plausible as seen in Fig. 7-7. When the animal intended no movement (inside the red-dotted circle), the corresponding force reading was small. On the contrary, higher forces were often seen outside of these regions. This suggested that the force sensor was working properly except for noise and a possible bias.

In summary, the force sensor may benefit from a prior characterization of its bias as well as filtering out high frequency noise.

7.4.4 Other Remarks

A question not sufficiently addressed in these experiments was "is the Rat Module back-drivable"? The lower bound of "sufficient back-drivability" was established by the mockup, where no motors or gearheads introduced static friction while the inertia or friction of the mechanism joints was negligible. As the mockup allowed natural movement, we can conclude that the back-drivability of the mockup was 'sufficiently low'. We had also learned that since a highly back-drivable mockup allowed natural movement, a back-drivable Rat Module would also allow natural movement. See chapter 8 for more assessment of this topic.

Another important aspect of the act of conducting animal experiment is for the engineers to become familiar with the challenges involved in working with live animals. Researchers with prior experience in the experiment procedure drastically decreased the hardware preparation time and handled the animals better. Experienced researchers may also contribute to decreasing animal anxiety.

Chapter 8

Validation Experiments with Rodents: Part II

The results from the experiments presented in the previous chapter suggested that the current design allowed addressing the main question: whether the exoskeletal design with force feedback allowed natural movement. Unlike other experimental apparatus which substantially restrains the animal's movement, the apparatus designed here was intended to allow maximal freedom of movement while permitting physical interaction. A live animal experiment was conducted to address the performance of the design. Specifically, how much natural overground locomotion did the equipment allow?

8.1 Experiment Setup

Self-paced forward locomotion under three conditions was compared: 1) Unconstrained animal, 2) Animal with the mockup, 3) Animal with the fully active Rat Module. The active Rat Module condition was further divided into the last three days of the experiment. The 'unconstrained' measurement was conducted first, followed by 3 days of measurement with the mockup and a subsequent 5 days of measurement with the active Rat Module. On each day the experiment lasted 30 minutes including preparation time. A healthy female Sprague-Dawley rat (8+ weeks, body weight 250 grams) was used in this study.

Several additional considerations influenced the design of this apparatus evaluation experiment. Firstly, the motors and gearheads used in the Rat Module exhibited significant static friction which compromised back-drivability. Without compensation, the force required to back-drive the manipulators was known from previous experiments to be as high as 1.3 N. A novel force feedback controller compensated for the friction and reduced the peak interaction force by as much as a factor of eight as shown in Fig. 8-1. The experiment with the active Rat Module was conducted with this force feedback implemented, which was termed 'low-impedance mode'.

When the active Rat Module was used, passive weight support was provided through compliant elongation springs between the Rat Module and the end effector of the BWSS. While the exact amount of supported weight was not recorded, weight support was verified by observing that the springs were constantly in tension.

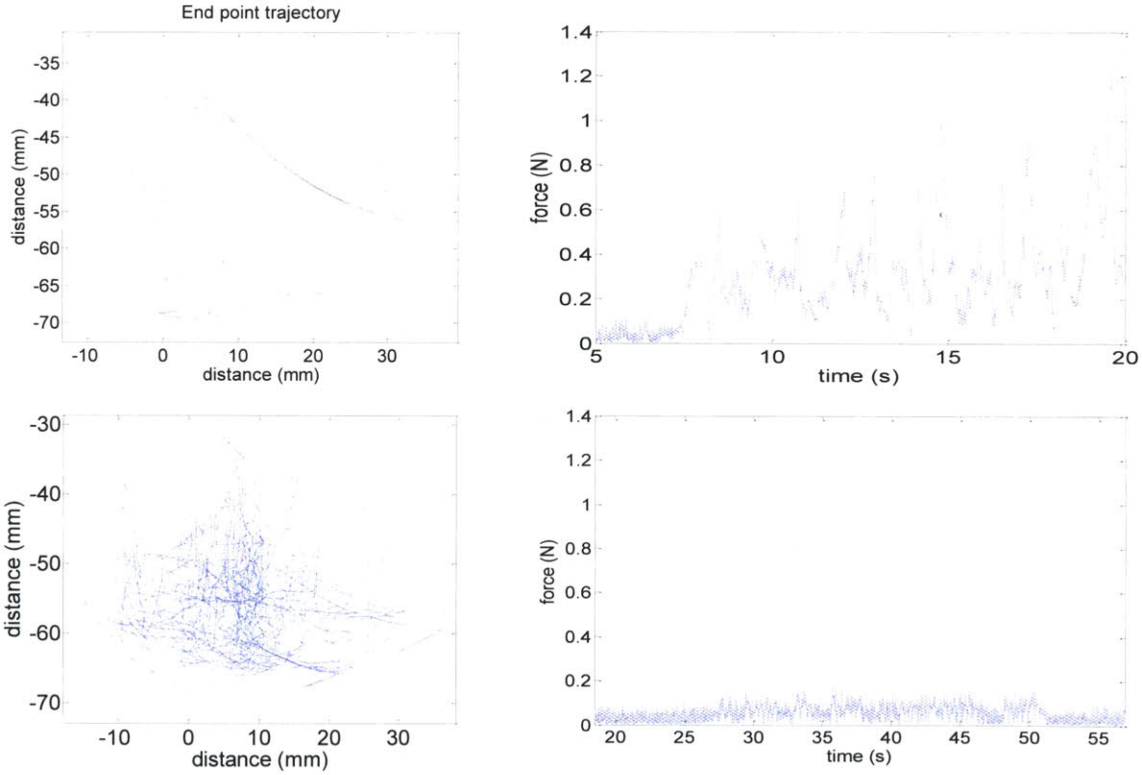

Fig. 8-1. Addressing back-drivability of the Rat Module (these figures were presented in chapter 6.) Trajectories and interaction forces while manually back-driving the right side of the Rat Module. Top row: Open-loop measurement with no controller. The trajectory consists of arcs, characteristic of only one motor back-driven at a time due to significant static friction on the other motor. The peak interaction force is over 1.3 N. Bottom row: with force feedback. Back-drivability is enhanced with peak interaction force of 0.2 N.

8.1.1 Encouraging Forward Locomotion

In other experimental apparati such as [87][108], the animal is heavily constrained and voluntary locomotion is minimal. For example, the frontal half of the animal is restrained and the animal is forced to react to a moving treadmill belt even when that is not what it desires to do. An advantage of this arrangement is that the allowed set of behaviors is small and thus more easily predicted. A disadvantage is that any observations may not apply to normal behavior. In contrast, the equipment presented in this thesis was designed to allow maximal freedom of voluntary movement. As a result, the animal wearing this equipment is unlikely to perform consistently repeatable movements conducive to straightforward analysis.

To address this problem, a relatively dark 'hallway' was introduced as illustrated in Fig. 8-2. It is known that rats prefer narrow openings or corners with reduced ambient light. The purpose of the 'hallway' was to encourage the animal to perform straight-line forward locomotion which could be recorded and analyzed. First, the animal was placed in the open area. Then the 'hallway' was pushed towards the animal with the opening facing the animal. The rat then chose to walk into the dark corridor and find a food reward at the closed end. The self-paced forward locomotion during this period was recorded on video (30 Hz, 1.5 mm per pixel, Fig. 8-3). After the reward was consumed, the rat was manually removed from the hallway and placed in the open arena to prepare for the next observation. The number of repetitions of this procedure required for the animal to understand the protocol was minimal—less than 5 minutes of training were required. Using this protocol was especially beneficial when using the active Rat Module.

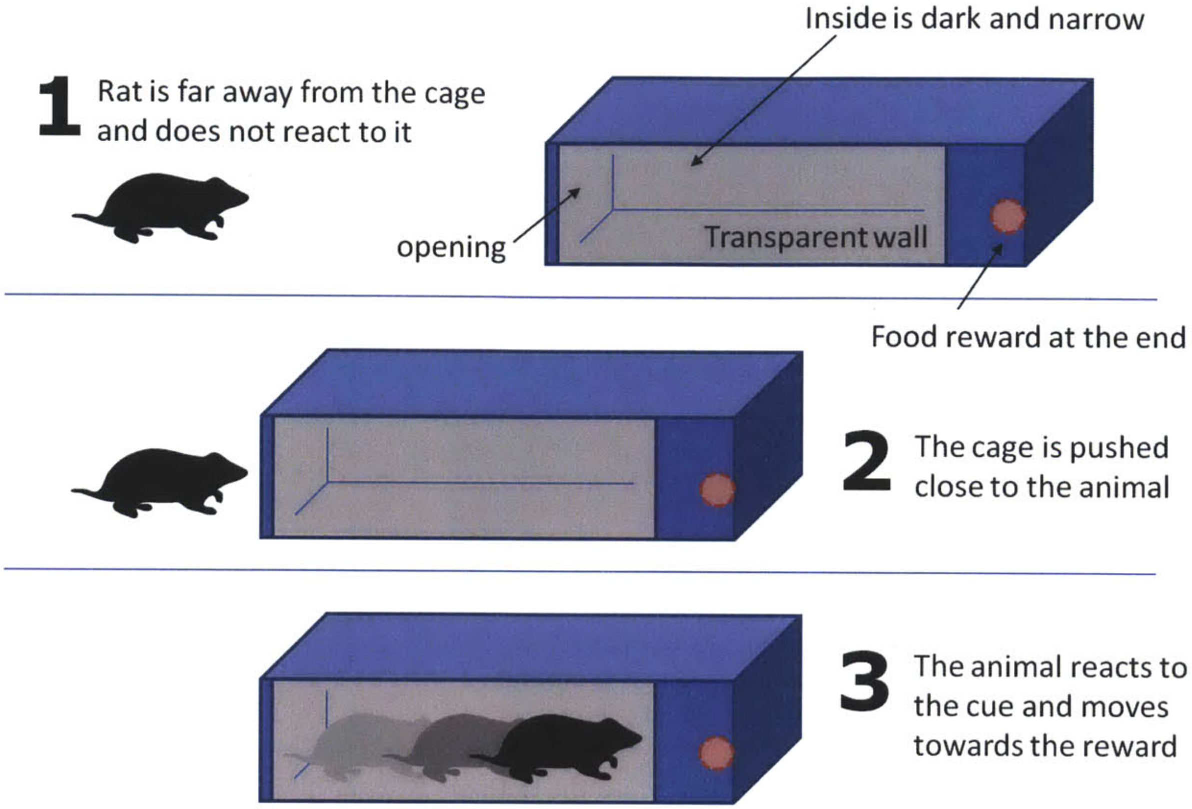
Inside is dark and narrow
1 Rat is far away from the cage and does not react to it
opening
Transparent wall
Food reward at the end
2 The cage is pushed close to the animal
3 The animal reacts to the cue and moves towards the reward

Fig. 8-2. The animal was trained to respond to and walk through the dark 'hallway'. A side wall was transparent to allow video recording of the locomotion.

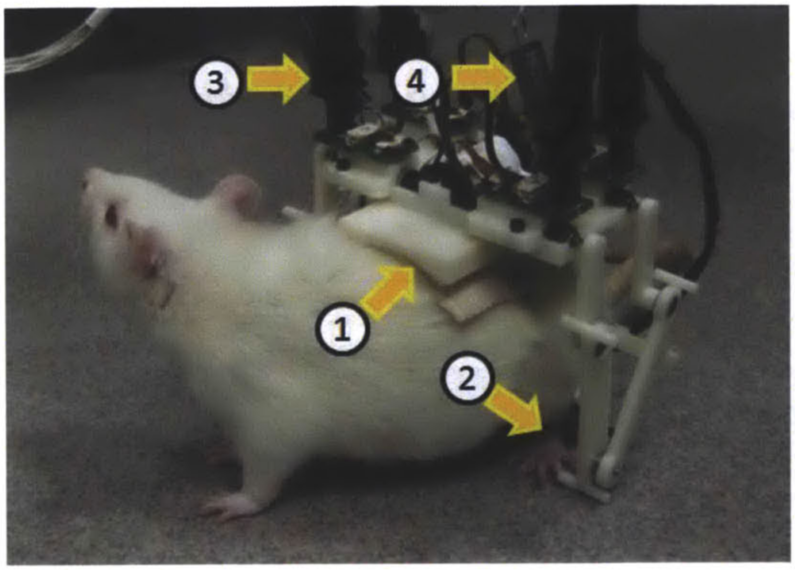

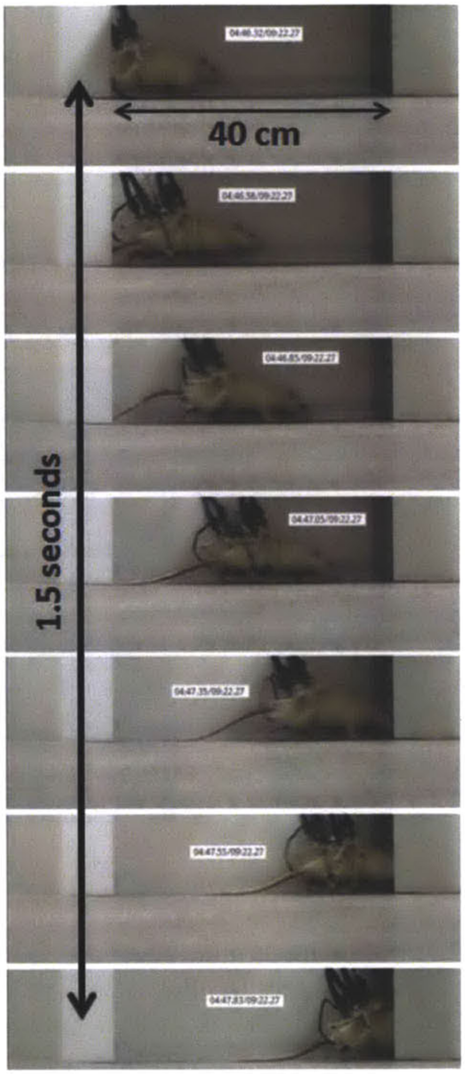
40 cm
1.5 seconds
04:46.32/09:22.27
04:46.58/09:22.27
04:46.85/09:22.27
04:47.05/09:22.27
04:47.35/09:22.27
04:47.55/09:22.27
04:47.83/09:22.27

Fig. 8-3. Snapshots from a live animal experiment. Top: The Rat Module mounted on the animal. 1-Waist coupling. 2-Ankle coupling. 3-Wires for the sensors and actuators. 4-Compliant elongation springs for partial weight support. Right: snapshots from the video recorded while the animal performed self-paced, forward locomotion.

8.2 Results

8.2.1 Observed Movements

A variety of natural voluntary movements were observed throughout the experiment. Forward locomotion was most often observed, as this movement was encouraged by using the 'hallway' (Fig. 8-2). Other movements were also observed, include turning, rearing up, grooming, and backward locomotion. Note that turning and rearing up against the side walls required deviation from 1-D motion. In general, the animal appeared to move as freely in the mockup or active robot as when it was unconstrained.

8.2.2 Stride Length

Limb position information was determined from the video frames. The stride lengths measured are shown in Table 8.1 and Fig. 8-4. The normality of the datasets for each condition was addressed with a Jarque-Bera test (null hypothesis: the dataset comes from a normal distribution), where the distributions did not significantly differ from a Gaussian distribution ($p > 0.05$). Pairwise comparisons using two-sample T-tests between the unconstrained dataset and mockup/Rat Module cases revealed $p > 0.05$ for all pairs, suggesting that the stride lengths in the mockup condition or in the active Rat Module condition did not significantly differ from the unconstrained normal case.

8.2.3 Stride Duration

Timing information was also determined from the video frames with a resolution of 0.033 s. Measured stride durations are shown in Table 8.2. Unlike the stride length data, the unconstrained animal's stride duration was significantly shorter than when the mockup was attached and for the first two days when the active Rat Module was attached ($p << 0.05$). However, data collected on the third day with the active Rat Module attached showed no statistically significant difference from the unconstrained condition. Figure 8-5 shows evidence that the animal adapted its stride duration to the kinematic constraint but did not adapt its stride length, as shown in Fig. 8-4. This trend is also seen in Fig. 8-5 where the peaks of the histograms of stride durations recorded during the three days when the constraint was attached (mockup or active Rat Module) apparently shifted towards the peak of the histogram recorded in the unconstrained case.

8.2.4 Swing Duration per Stride Duration (Duty Cycle)

The ratio of swing duration per stride duration remained approximately constant across all conditions, as seen in Fig. 8-6. No statistical difference between any pair of data sets was found. Pairwise t-tests all resulted in $p > 0.1$.

Table 8.1
Stride Length

	Stride Length [mm]		Jarque-Bera test (p)	Significance (p) vs. Unconstrained condition
	Mean ±STD	Number of samples		
Unconstrained	119.5 ±18.1	12	> 0.50	N/A
Mockup	128.9 ±21.7	16	0.27	0.23
Robot-Day1	132.5 ±16.3	10	0.39	0.09
Robot-Day2	128.7 ±17.0	20	> 0.50	0.16
Robot-Day3	129.8 ±16.3	14	0.30	0.14

Table 8.2
Stride Duration

	Stride Duration [s]		Jarque-Bera test (p)	Significance (p) vs. Unconstrained condition
	Mean ±STD	Number of samples		
Unconstrained	0.42 ±0.072	12	> 0.50	N/A
Mockup	0.66 ±0.067	11	0.44	0.00
Robot-Day1	0.57 ±0.041	9	0.12	0.00
Robot-Day2	0.52 ±0.065	18	0.32	0.00
Robot-Day3	0.46 ±0.069	14	0.30	0.16

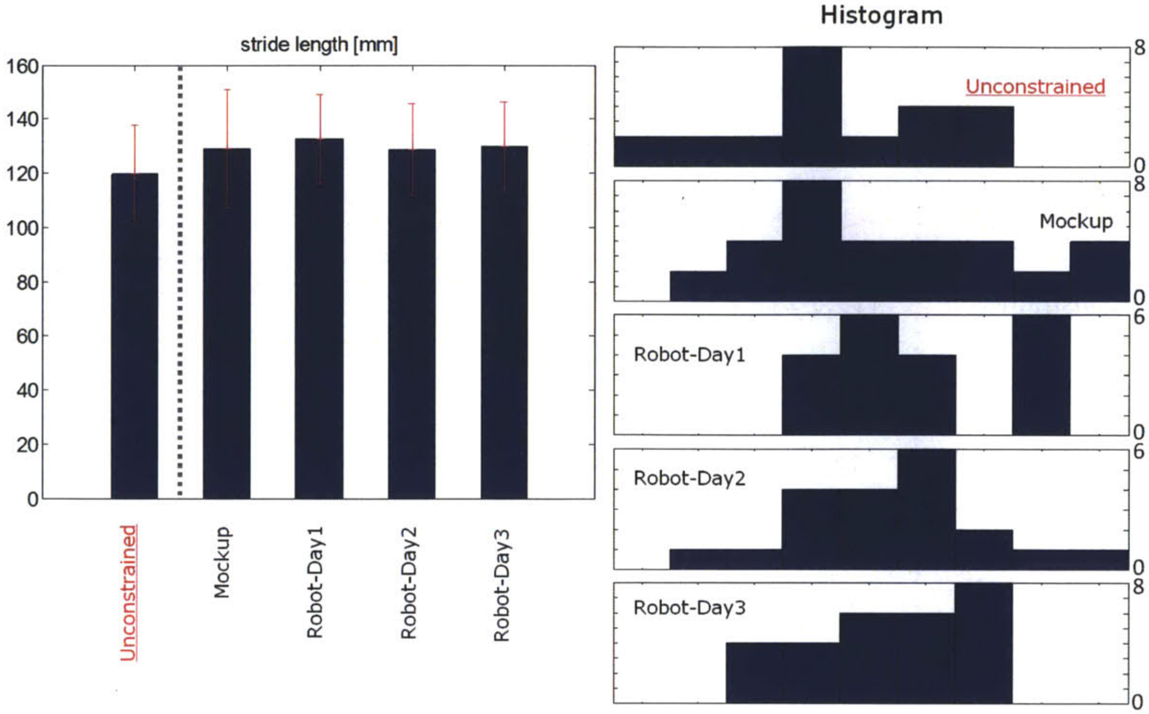

Fig. 8-4. Stride Length data. Left: Mean ±STD. There is no significant difference between cases. Right: Data histograms.

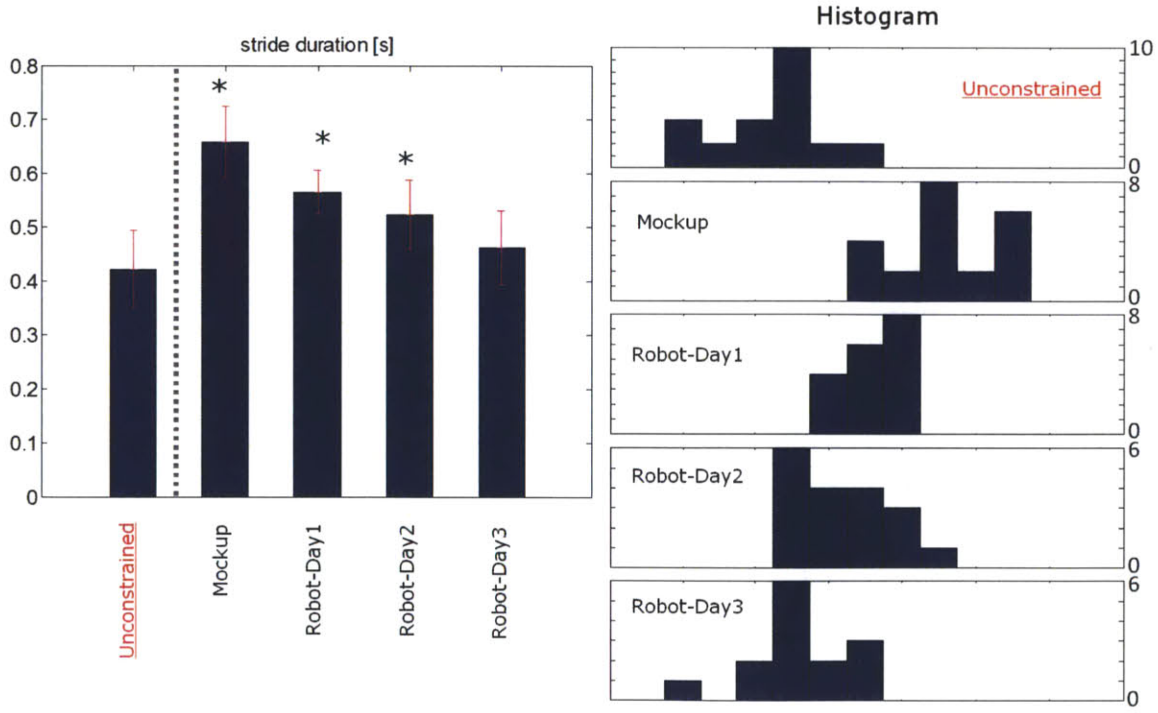

Fig. 8-5. Stride Duration data. Left: Mean ±STD. Significant differences from the unconstrained case are marked with * ($p < 0.05$). Right: Data histograms.

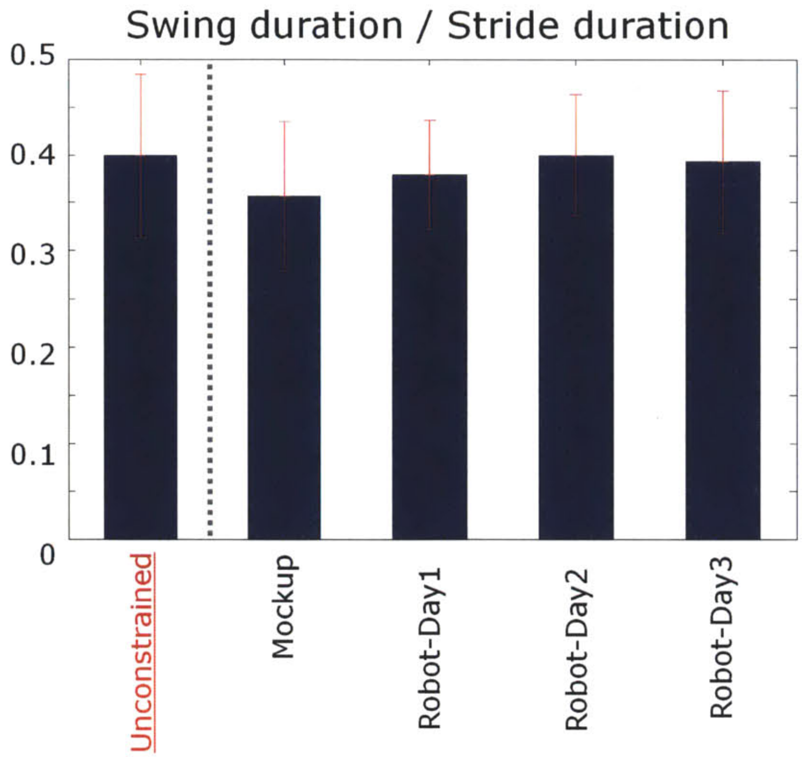

Fig. 8-6. Ratio of swing duration to stride duration (Mean ±STD). No significant differences from the unconstrained case were observed.

8.2.5 Interaction Force

Because the force transducers were coupled to the animal's hindlimb via semi-elastic string the forces measured by the sensors were the forces the animal exerted to the robot. In other words, they were the 'interaction forces' required to back-drive the manipulators on the Rat Module. They provided useful data to assess the robot's back-drivability, as well as the animal's adaptation to the apparatus. The interaction force remained well below 0.2 N with occasional peaks during fast movements. Moments when the animal exerted over 0.2 N were rare.

Figure 8-7 shows the mean interaction force during sustained forward locomotion. Time windows containing only sustained forward locomotion of at least one stride (two steps) were gathered for each day. These time windows (with different durations) were combined to form a single time history of force for each day. The time-average of force during this time history is plotted in blue. In red is the value of the maximum interaction force measured during the entire day.

The time-average of interaction force during movement was lower than 0.07 N (7 gram-force) on the right side, and lower than 0.13 N (13 gram-force) on the left side. The occasional peaks of interaction force were around 0.15 to 0.2 N on the right side, and 0.3 to 0.4 N on the left side. While the left side exhibited larger interaction forces than the right side, there was no apparent trend or statistically significant difference between the data sets recorded during the three days when the active robot was attached.

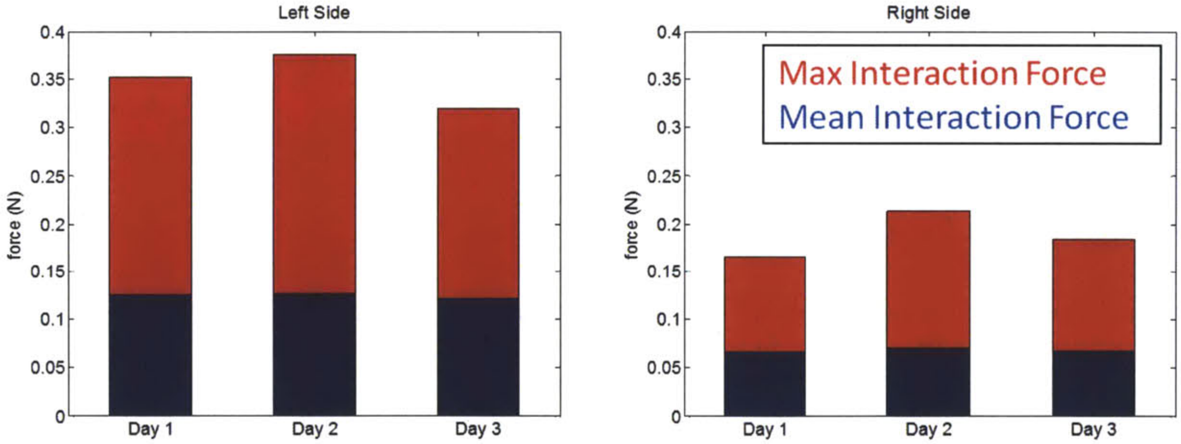

Fig. 8-7. Time-averages of interaction force magnitude during forward locomotion (blue), and the average peak interaction force. The left side showed larger interaction forces.

8.2.6 End Effector Trajectory

The two manipulator arms of the Rat Module were coupled to the tibia, a few millimeters above the animal's hindlimb ankle joints. The encoders monitor the angular positions of the motor shafts. Due to imperfections (notably backlash, 2.2°) in the gearheads, these angles may differ from the angles of the manipulator links with respect to the base of the Rat Module. In addition, the base of the Rat Module is mounted on the animal's fur and thus can translate or rotate about the animal's back. Nevertheless, the coupling point motion derived from the encoders provided data consistent with forward locomotion kinematics.

Fig. 8-8 shows the trajectory of the tip of the manipulator arms of the Rat Module during forward locomotion. The figure contains the right end effector trajectory for nine separate forward locomotion occurrences during the 2nd day when the active robot was attached. Overall, the end effector trajectory was consistent with the ankle joint trajectory of similar sized rats walking on a treadmill **[109][110]**. Although treadmill walking may be different from overground walking **[91]**, the difference is small and the general trajectory of ankle joint is similar.

The apparent 'arcs' seen in Fig. 8-8 are the cases where the angular displacement of one of the motor shafts was very much greater than the other. While this may appear to be an artifact due to static friction in the mechanism or gearheads, in fact, this is due to the animal's voluntary movement of the ankle, as shown by the low interaction force (Fig. 8-7).

The trajectories of the animal's ankles may also be obtained from video. However, the images extracted from the camera used in this experiment had insufficient resolution to capture ankle position during swing.

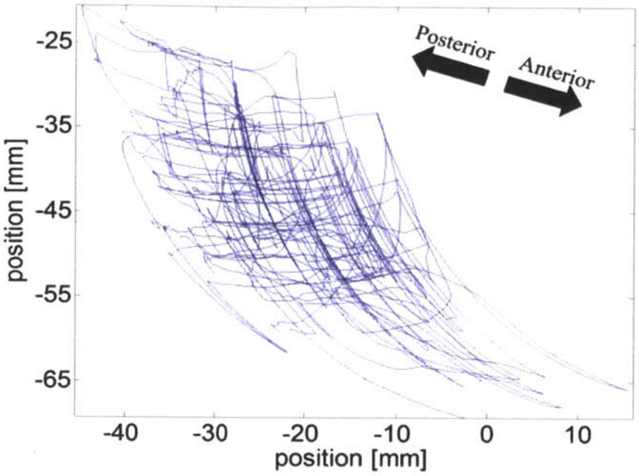

Fig. 8-8. End effector trajectories derived from encoder recordings during nine occurrences of forward locomotion are superimposed.

8.3 Discussion

Although the apparatus was designed to allow the animal to move freely and voluntarily in a more open area, the experiments were conducted using a 1-D arena shown in Fig. 8-2. The narrow 'hallway' was introduced exclusively to facilitate evaluation and is not an essential requirement for the use of this equipment.

Throughout the experiment, the animal showed no sign of anxiety or agitation due to the equipment. The animal did not react to the added inertia, couplings, or ankle motion constrained to parallel sagittal planes due to wearing the Rat Module. Also, a variety of movements that are typically seen in the unconstrained animal were also seen when the active robot was attached, identical to previous observations (Fig. 7-3). This suggested that the animal attached to the active robot was as comfortable as when it was unconstrained.

The animal quickly grew accustomed to the preparation processes, during which the couplings and the apparatus were donned and doffed. The time required for two people to attach the active robot to the rat was less than five minutes. Removing the apparatus from the animal required no more than two minutes.

After three days of exposure to the active rat robot, stride length, stride duration and duty cycle (swing duration per stride duration) measured during overground forward locomotion while attached to the active rat robot and when unconstrained were not statistically distinguishable. Possible adaptation of stride duration occurred during the three days of the active robot condition. The trend is even more visible if we consider the mockup condition as 'day-0' of the active Rat Module experiment, suggesting that the main cause of adaptation may be the kinematic constraint. While other possible causes of this phenomenon have not been completely ruled out, (where possible causes include the added inertia, non-zero interaction force, etc.), it can be concluded that three days of 30-minute training with this apparatus was sufficient to achieve forward locomotion indistinguishable from that of a freely-moving rat, at least as indicated by these measures.

On the other hand, for all three days when the animal was attached to the active Rat Module, it partially dragged its tail on the ground (Fig. 8-3). This behavior did not decline with exposure. This phenomenon was also observed in the mockup condition, although the frequency of occurrence was lower. In contrast, during unconstrained locomotion the tail was constantly raised. Factors such as added inertia, the sagittal plane constraint, or the waist and ankle couplings may have affected tail position during locomotion. Further investigation is required to discriminate among these and other possibilities. Using the BBB Locomotor Rating Scale [**92**], the animal locomotion attached to the active robot would have been scored roughly 20.5 out of

21 (i.e. 98% of fully normal locomotion). However, this number must be interpreted with caution since the BBB scale was designed primarily to address rat locomotion during recovery from spinal cord injury rather than to assess impediments due to attached apparatus.

One remarkable observation was that this apparatus allowed stride duration as low as 0.4 seconds even with the active robot attached. Other studies using a treadmill-based device reported stride durations as long as 1.5 seconds [**95**] for animals similar to those used in this study (same strain, gender, age, weight and health condition).

Studies using healthy female Wistar rats of comparable size (~200 gram) walking on a treadmill with no constraint reported results comparable to those obtained with the active rat robot [**111**]. At 30 cm/s, the Wistar rats performed forward locomotion with stride duration of 0.432 ms and stride length of 141 mm, similar to our observations. The ratio of swing duration to stride duration during overground walking was reported as 36% (28% while on treadmill), compared to almost 40% observed in our study, which is also quite comparable.

The interaction force measured during forward locomotion when the active robot was attached was below 0.07 N (7 gram-force) on the right hindlimb. While this is less than 3% of the animal's body weight, it is not zero and thus may affect features of locomotion not assessed in this study. For example, changes in muscle activation patterns may have occurred over time as the animal adapted to the equipment. Further investigation is required to assess the effect of non-zero interaction force during locomotion. However, to assess the performance of the apparatus, it is clear that the interaction force was sufficiently low to allow forward locomotion essentially identical to that of an unconstrained animal as measure by the BBB scale. When required by the experimenter, larger interaction forces may purposefully be applied to the animal depending on the design of experiment.

The coupling to the waist kept the base of the Rat Module on the lower back of the animal. While the attachment between the animal's fur and the Rat Module was sufficiently secure, any point on the animal's skin can move relative to the muscles and bones underneath it for as much as several centimeters. As the base of the Rat Module carried the motors and encoders, the skin movement prevented the encoder readings from representing the end-effector position with respect to a landmark on the animal's skeleton (e.g. the pelvis), or with respect to a global reference frame (for example, defined by the BWSS robot). While the end-effecter trajectory (Fig. 8-8) reconstructed from the encoder data was consistent with overground walking [**109**][**110**], a better estimate would be available with a more secure waist coupling. Nonetheless, the encoder data collected from the current evolution of the apparatus may potentially be used to detect the initiation of swing, touch-down, or left-right hindlimb coordination. This topic is left for future research.

While skin movement complicated the interpretation of the encoder data, it did not affect the force reading since the force transducer was connected in series with the animal's hindlimb. Also note that skin movement is less pronounced near the ankle joint [**110**], justifying the choice to couple the end-effector to the skin at the lower tibia close to the ankle joint.

The apparatus developed in this work is not perfect - it has non-zero inertia, non-zero interaction force, kinematic constraints and elastic couplings. Walking with such a device cannot be identical to walking with zero-encumbrance. In fact, evidence showed that movement with the Rat Module was not perfectly natural. For example, the animal's locomotion with the Rat Module did not score 21 on the BBB scale. Also, stride duration data (Fig. 8-5) showed a possible adaptation occurring over three days, suggesting that on day 1 and 2, the animal may not have been fully accustomed to walking with the apparatus. While these are signs of limitations, results reported in this chapter such as the stride length, stride duration (day-3), and duty cycle provide quantitative assessment of the naturalness of animal locomotion with Rat Module, compared to unconstrained voluntary movement of the same animal. These data suggest that our apparatus enables animal movement statistically indistinguishable from unconstrained overground movement – a vast improvement over what is allowed in other devices built on treadmills such as the Rat Stepper. While this device does not allow animal locomotion to score 21 on the BBB scale and may require adaptation, the resulting locomotion is still remarkably close to natural overground locomotion and the range of possible movements is significantly greater in this apparatus compared to other alternatives.

Chapter 9

Conclusion

9.1 Implication for the Field of Research

The current apparatus enables studies of overground quadrupedal locomotion in rats in ways that were not possible in the past. First, the apparatus allows a full repertoire of overground movement (Fig. 7-3). Behaviors such as turning or rearing up which are not permitted by more restrictive apparatus are allowed with this device. Also, being 'on the ground' is a more natural state for the animal as opposed to being in often intimidating artificial conditions, such as inside a cage with a treadmill and an electric shocker at one end. In the apparatus described in this thesis, the animal is allowed to choose its own movement unless the device is programmed otherwise. In future experiments with the current device, the base of comparison or the 'reference' is the unconstrained, natural movement of the animal in an open space, and not a heavily constrained movement on a treadmill. For example, BBB scale can be applied to experiments using the proposed device as demonstrated in the previous chapter. Since the BBB scale is for overground locomotion assessment, it cannot be applied to locomotion on treadmill-type devices such as the Rat Stepper.

Secondly, while the animal is on open ground, the apparatus allows investigation not only of movement kinematics but also the dynamics of overground locomotion. The two active manipulators with position and force sensors enable various interaction schemes to be programmed in software. For example, one may implement the novel locomotor training scheme developed in **[112]** on this apparatus to address the effect of that scheme on overground locomotion. Alternatively, one may program the apparatus to simulate an assistive device for hindlimb locomotion.

The new apparatus may be used in conjunction with existing experimental arrangements such as an open area [**113**], 2D Mazes [**114**][**115**], or a more complex 3D maze [**116**]. The apparatus can add an additional degree of control to these experiments, by providing preprogrammed perturbation and/or assistance as needed.

9.2 Future Prototypes

Although the apparatus developed in this thesis allows a wide range of overground movements, physical constraints imposed by the apparatus cannot be completely ignored. In the near future, the exoskeletal robot for overground rodent locomotion may benefit from:

1) A back-drivable BWSS with a larger workspace and programmable weight support. An active weight support system, when fully implemented, may be used to provide partial to full body weight support as well as to pull the animal in a certain direction if desired by the user.

2) Reducing the number of wires between the Rat Module and the supporting hardware. Having too many wires may add unnecessary encumbrance to the Rat Module and may also become problematic if the animal turns in place for multiple cycles, twisting the wire bundle. An early prototype of the apparatus attempted a fully wireless design (Fig. 3-5) but the wireless communication lag was inadequate for real time control and the inertia and volume of the required onboard battery was excessive. Given the improved wireless technology of today's electronics, it may be possible to reduce the number of wired connections between the Rat Module and the supporting hardware, though it may still be necessary to transmit power through a wired connection.

3) Alternative waist coupling method: The current waist coupling method is easy to put on and off the animal and simplifies the preparation. However, it is not secure enough to prevent the Rat Module from shifting or tilting on the animal's body. An alternative waist coupling may use bone pins [**117**] – an invasive method which may complicate animal preparation. Nonetheless, that would greatly enhance the system's ability to track the position or force of the animal's ankle joint with respect to, for example, the hip joint. This would allow previously unavailable manipulations such as applying prescribed knee-hip joint torques, or a prescribed trajectory of the ankle joint with respect to the pelvic bone.

In this work, we have chosen a tethered exoskeletal configuration whose performance was demonstrated in chapter 8. This selection was partially motivated by the limitations of existing alternatives as well as previous design iterations (Fig. 3-5). However, the general requirement of the apparatus, as presented in Table 2.1 and in section 3.1, may be realized through other designs. For example, one may install two 6-DOF, highly back-drivable robotic arms outside the area of activity, with their end effectors coupled to and interacting with the ankles of the animal (Fig. 9-1). While specific pros and cons of such design are not addressed in this work, future developers of apparatus with similar goal may consider such alternatives.

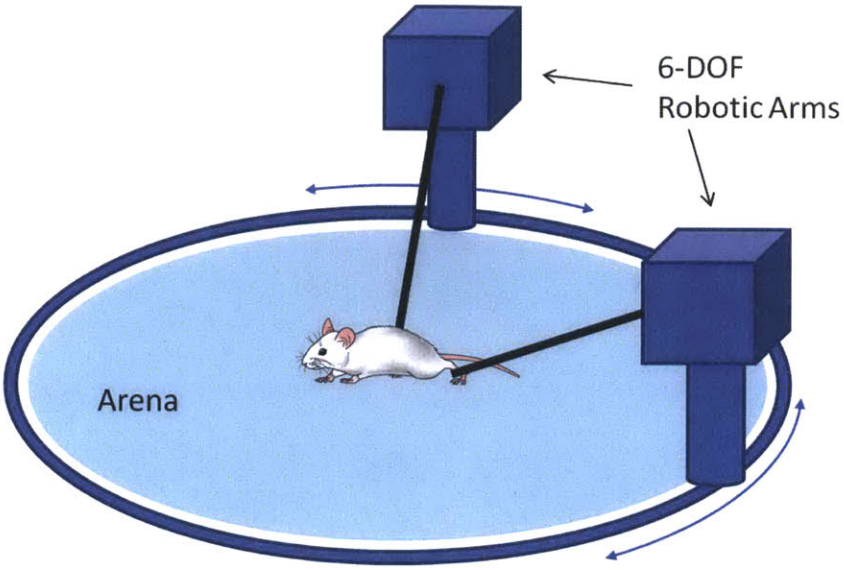

Fig. 9-1. An alternative design. Two robotic arms placed outside the area of activity (arena) are coupled to the ankles of the animal.

9.3 Summary

The work reported here developed and demonstrated an exoskeletal robot that allows free oveground movement of a rat that appears almost as natural as its unconstrained, voluntary movement, while also providing controlled physical interaction with the animal. The device opens up a vast uncharted territory of possible experiments – far beyond those allowed by existing devices. In the future, the new device may be used as a test-bench for similar robots for humans, stimulating research on robot-assisted therapy, wearable robots for amputees, or general lower-limb locomotion research.

Appendix A

Linkage Forward Kinematics and Jacobian

In Fig. 4-9, the 5-bar linkage used in the Rat Module is presented. The end point position can be calculated from the two motor positions. From the configuration in Fig. 4-9, we can calculate

$$A_\mathrm{x} = l_1 \sin\theta_1$$

$$A_\mathrm{y} = -l_1 \cos\theta_1$$

$$B_\mathrm{x} = x_1 + l_2 \sin\theta_2$$

$$B_\mathrm{y} = y_1 - l_2 \cos\theta_2$$

$$\mathrm{AB} = \sqrt[2]{(A_\mathrm{x} - B_\mathrm{x})^2 + \left(A_\mathrm{y} - B_\mathrm{y}\right)^2}$$

$$\varphi_\mathrm{ABP} = \mathrm{atan}\left(\frac{B_\mathrm{y} - A_\mathrm{y}}{B_\mathrm{x} - A_\mathrm{x}}\right)$$

$$\varphi_\mathrm{BAC} = \mathrm{acos}\left(\frac{AB^2 + {l_4}^2 - {l_3}^2}{2 \cdot AB \cdot l_4}\right)$$

$$\varphi_\mathrm{PCA} = \varphi_\mathrm{ABP} - \varphi_\mathrm{BAC}$$

$$\varphi_\mathrm{PAD} = \varphi_\mathrm{PCA} + \alpha$$

Then,

$$\mathrm{Tip}_\mathrm{x} = A_\mathrm{x} - l_5 \cos(\varphi_\mathrm{PAD})$$

$$\mathrm{Tip}_\mathrm{y} = A_\mathrm{y} - l_5 \sin(\varphi_\mathrm{PAD})$$

Then, the jacobian matrix can be found by taking partial derivatives of Tip_x and Tip_y with respect to θ_1 and θ_2. From forward-kinematics, we have

$$\text{Tip}_x = A_x - l_5\cos(\varphi_{\text{PAD}})$$

$$= l_1\sin\theta_1 - l_5\cos\left(\varphi_{ABP} - \varphi_{BAC} + \alpha\right)$$

$$\text{Tip}_y = A_y - l_5\sin(\varphi_{\text{PAD}})$$

$$= -l_1\cos\theta_1 - l_5\sin\left(\varphi_{ABP} - \varphi_{BAC} + \alpha\right)$$

Finding Jacobian matrix then involves partial differentiation of φ_{ABP} and φ_{BAC} with respect to θ_1 and θ_2. We first denote:

$$\varphi_{\text{ABP}} = A(\theta_1, \theta_2)$$

$$= \text{atan}\big(\alpha(\theta_1, \theta_2)\big)$$

where

$$\alpha(\theta_1, \theta_2) = \frac{\alpha_n(\theta_1, \theta_2)}{\alpha_d(\theta_1, \theta_2)} = \frac{B_y - A_y}{B_x - A_x} = \frac{y_1 - l_2\cos\theta_2 + l_1\cos\theta_1}{x_1 + l_2\sin\theta_2 - l_1\sin\theta_1}$$

Then, we can compute

$$\frac{\partial\varphi_{\text{ABP}}}{\partial\theta_1} = \frac{\partial A(\theta_1, \theta_2)}{\partial\theta_1} = \frac{1}{1 + (\alpha_n/\alpha_d)^2} \cdot \frac{\alpha_n l_1\cos\theta_1 - \alpha_d l_1\sin\theta_1}{{\alpha_d}^2} \quad \cdots \; (1)$$

$$\frac{\partial\varphi_{\text{ABP}}}{\partial\theta_2} = \frac{\partial A(\theta_1, \theta_2)}{\partial\theta_2} = \frac{1}{1 + (\alpha_n/\alpha_d)^2} \cdot \frac{\alpha_d l_2\sin\theta_2 - \alpha_n l_2\cos\theta_2}{{\alpha_d}^2} \quad \cdots \; (2)$$

Where α_n and α_d are both functions of θ_1 and θ_2.

Next, to find partial differentiation of φ_{BAC}, we define:

$$\varphi_{\mathrm{BAC}} = B(\theta_1, \theta_2)$$

$$= \mathrm{acos}\big(\beta(\theta_1, \theta_2)\big)$$

where

$$\beta(\theta_1, \theta_2) = \frac{\beta_n(\theta_1, \theta_2)}{\beta_d(\theta_1, \theta_2)} = \frac{\overline{AB}^2 + {l_4}^2 - {l_3}^2}{2 \cdot \overline{AB} \cdot l_4} = \frac{{\alpha_n}^2 + {\alpha_d}^2 + {l_4}^2 - {l_3}^2}{2 \cdot \sqrt{{\alpha_n}^2 + {\alpha_d}^2} \cdot l_4}$$

Note that β_{n} and β_{d} are both functions of θ_1 and θ_2. Then, we have

$$\frac{\partial \varphi_{\mathrm{BAC}}}{\partial \theta_1} = \frac{\partial B(\theta_1, \theta_2)}{\partial \theta_1} = \frac{-1}{\sqrt{1 - (\beta_n/\beta_d)^2}} \cdot \frac{1}{{\beta_d}^2} \cdot \left(\frac{\partial \beta_n}{\partial \theta_1} \cdot \beta_d - \frac{\partial \beta_d}{\partial \theta_1} \cdot \beta_n\right) \quad \cdots \quad (3)$$

$$\frac{\partial \varphi_{\mathrm{BAC}}}{\partial \theta_2} = \frac{\partial B(\theta_1, \theta_2)}{\partial \theta_2} = \frac{-1}{\sqrt{1 - (\beta_n/\beta_d)^2}} \cdot \frac{1}{{\beta_d}^2} \cdot \left(\frac{\partial \beta_n}{\partial \theta_2} \cdot \beta_d - \frac{\partial \beta_d}{\partial \theta_2} \cdot \beta_n\right) \quad \cdots \quad (4)$$

where

$$\frac{\partial \beta_n}{\partial \theta_1} = l_4({\alpha_n}^2 + {\alpha_d}^2)^{-\frac{1}{2}} \cdot \left(\frac{\partial({\alpha_n}^2)}{\partial \theta_1} + \frac{\partial({\alpha_d}^2)}{\partial \theta_1}\right)$$

$$\frac{\partial \beta_d}{\partial \theta_2} = l_4({\alpha_n}^2 + {\alpha_d}^2)^{-\frac{1}{2}} \cdot \left(\frac{\partial({\alpha_n}^2)}{\partial \theta_2} + \frac{\partial({\alpha_d}^2)}{\partial \theta_2}\right)$$

where

$$\frac{\partial({\alpha_d}^2)}{\partial \theta_1} = 2 \cdot {l_1}^2 \cdot \sin\theta_1 \cos\theta_1 - 2 \cdot x_1 \cdot l_1 \cos\theta_1 - 2 \cdot l_1 \cdot l_2 \sin\theta_2 \cos\theta_1$$

$$\frac{\partial({\alpha_d}^2)}{\partial \theta_2} = 2 \cdot {l_2}^2 \cdot \sin\theta_2 \cos\theta_2 + 2 \cdot x_1 \cdot l_2 \cos\theta_2 - 2 \cdot l_1 \cdot l_2 \sin\theta_1 \cos\theta_2$$

$$\frac{\partial({\alpha_n}^2)}{\partial \theta_1} = -2 \cdot {l_1}^2 \cdot \sin\theta_1 \cos\theta_1 - 2 \cdot y_1 \cdot l_1 \sin\theta_1 + 2 \cdot l_1 \cdot l_2 \sin\theta_1 \cos\theta_2$$

$$\frac{\partial(\alpha_n{}^2)}{\partial\theta_2} = -2 \cdot l_2{}^2 \cdot \sin\theta_2\cos\theta_2 + 2 \cdot y_1 \cdot l_2\sin\theta_2 + 2 \cdot l_1 \cdot l_2\sin\theta_2\cos\theta_1$$

Also,

$$\frac{\partial\beta_d}{\partial\theta_1} = -2 \cdot l_1(\alpha_d \cdot \cos\theta_1 + \alpha_n \cdot \sin\theta_1)$$

$$\frac{\partial\beta_n}{\partial\theta_2} = 2 \cdot l_2(\alpha_d \cdot \cos\theta_2 + \alpha_n \cdot \sin\theta_2)$$

Hence, given (1)~(4), we can finally compute the Jacobian matrix, $J(\theta_1, \theta_2)$,

$$J(\theta_1, \theta_2) = \begin{bmatrix} \frac{\partial \mathrm{Tip_x}}{\partial\theta_1} & \frac{\partial \mathrm{Tip_x}}{\partial\theta_2} \\ \frac{\partial \mathrm{Tip_y}}{\partial\theta_1} & \frac{\partial \mathrm{Tip_y}}{\partial\theta_2} \end{bmatrix}_{\theta_1=\theta_1, \theta_2=\theta_2}$$

where

$$\frac{\partial \mathrm{Tip_x}}{\partial\theta_1} = l_1 \cdot \cos\theta_1 + l_5 \cdot \sin\left(\varphi_{\mathrm{ABP}} - \varphi_{\mathrm{BAC}} + \alpha\right) \cdot \left\{\frac{\partial\varphi_{\mathrm{ABP}}}{\partial\theta_1} - \frac{\partial\varphi_{\mathrm{BAC}}}{\partial\theta_1}\right\}$$

$$\frac{\partial \mathrm{Tip_x}}{\partial\theta_2} = l_5 \cdot \sin(\varphi_{\mathrm{ABP}} - \varphi_{\mathrm{BAC}} + \alpha) \cdot \left\{\frac{\partial\varphi_{\mathrm{ABP}}}{\partial\theta_2} - \frac{\partial\varphi_{\mathrm{BAC}}}{\partial\theta_2}\right\}$$

$$\frac{\partial \mathrm{Tip_y}}{\partial\theta_1} = l_1 \cdot \sin\theta_1 - l_5 \cdot \cos(\varphi_{\mathrm{ABP}} - \varphi_{\mathrm{BAC}} + \alpha) \cdot \left\{\frac{\partial\varphi_{\mathrm{ABP}}}{\partial\theta_1} - \frac{\partial\varphi_{\mathrm{BAC}}}{\partial\theta_1}\right\}$$

$$\frac{\partial \mathrm{Tip_x}}{\partial\theta_1} = -l_5 \cdot \cos\left(\varphi_{\mathrm{ABP}} - \varphi_{\mathrm{BAC}} + \alpha\right) \cdot \left\{\frac{\partial\varphi_{\mathrm{ABP}}}{\partial\theta_2} - \frac{\partial\varphi_{\mathrm{BAC}}}{\partial\theta_2}\right\}$$

Appendix B

Programming the R19 Robot

B.1 Roboforth

Robots from ST-Robotics can be programmed using the company's own robot control language, called RoboForth. Developed by an engineer in ST-Robotics, RoboForth is a rather low-level language that resembles Assembly language in many ways. The user is given a vocabulary of predefined 'words'. One can then write a command line as a list of numbers and words, which are executed in the strict sequence of their appearance. In other words, the numbers and words, separated by tokens such as space or new line, are placed into the stack database structure where the most recently presented command word gets executed.

The code written in RoboForth is compiled and executed through software called Robwin63.exe, also provided by the manufacturer.

A few examples of command lines written in RoboForth are presented below:

Ex1) Managing numbers

RoboForth command line: `2 3 + .` (enter)

What it does: when the compiler sees the '+' operator, it fetches the two top-most numbers in the stack, adds them and leaves the result on top of the stack. In this example, the two top-most numbers which are on the stack just before '+' are 2 and 3. The '+' operator fetches (and removes) these two numbers from stack, adds them, and then leaves the result 5 on the top of the stack. The operator '.' fetches the value currently at the top of the stack and displays its value on the screen.

Result: The user will see 5 on the screen.

Ex2) Moving the robot

RoboForth command line: TELL WAIST 500 MOVE (enter)

What it does: TELL command clears all previous joint selections, making the system ready for new selection of joint by its name. WAIST is the name of the joint predefined in the RoboForth. Up to this point, the system is ready to take action on the WAIST joint. The following number 500 is stored in the top of the stack. The next command MOVE moves the selected joint (WAIST) by the value currently stored at the top of the stack (500).

Result: The waist joint of the robot is rotated by 500 steps (roughly 2.5 degrees)

Remarks: The velocity profile at which the waist joint operates is preset in the system. One has limited freedom to manipulate this velocity profile. More on this will be discussed in a later section.

B.2 Position Control of R19

The motors of the R19 robot are stepper motors, the exact rotation of which can be controlled by the RoboForth code. In routine laboratory tasks, robots such as R19 perform movements along pre-programmed trajectories. Applied as a BWSS for the Rat Module, the R19 robot must be supplied the current position of the animal as the target position. Obtaining the current position of the animal was implemented through the use of a video camera, further described in a later section. In this section, the RoboForth code for the position control loop is presented.

The current X and Y coordinate of the animal with respect to the current position of the end effector was obtained from a video camera in the Linux computer. These scalar values were converted into voltages between -10V and +10V (corresponding to -20 cm ~ +20 cm error in x or y) and are sent out through the DAC port of the Linux machine. These ports were wired to the two ADC ports of the R19 controller (seen in Fig. BB-1, left, (a)). The ADC card in the R19 controller converts the analog voltage into values between 0 and 4095 (12-bit resolution), where 2048 corresponds to zero volt input, 0 corresponds to -10 V, and 4095 roughly to 10 V. In our particular case, a 1-volt input corresponded to a 2 cm difference in position between the rat and the end effector in x or y. Hence, the converted value minus 2048, multiplied by 0.1 corresponded to the distance in x or y in mm.

The portion of the RoboForth code that reads and stores the values read by ADC is shown below:

```
: ADCGO                    ···(1)
0 ADC 2048 - X2 !          ···(2)
1 ADC 2048 - -1 / Y2 !     ···(3)
NEWDIRN                    ···(4)
;                          ···(5)
```

Lines 1 and 5 envelop lines 2 to 4 and forms a new 'word' in the RoboForth dictionary, named ADCGO, to be used elsewhere in the code. Line 2 reads from channel #0 of the ADC, subtracts 2048, and then stores the resulting value to a variable X2. Line 3 reads from the ADC channel #1, subtracts 2048, and then reverses sign before storing it to a user-defined variable, Y2.

The sign change is implemented because the camera coordinate frame has the y-axis pointing opposite to the end-effector coordinate frame.

Figure B-1 shows the different coordinate frames mentioned above. The x-y coordinate, also called the robot frame, is a frame fixed to the base of the robot. The current position of the end-effector of the robot is stored in the pre-defined, designated variables in RoboForth. The x'-y' frame is a moving frame attached to the end effector. The orientation of the end-effector is maintained constant, such that the two axes x and x' are always parallel. The video camera attached to the end of the manipulator shares the same x' axis, but the y" axis is opposite in direction to y'.

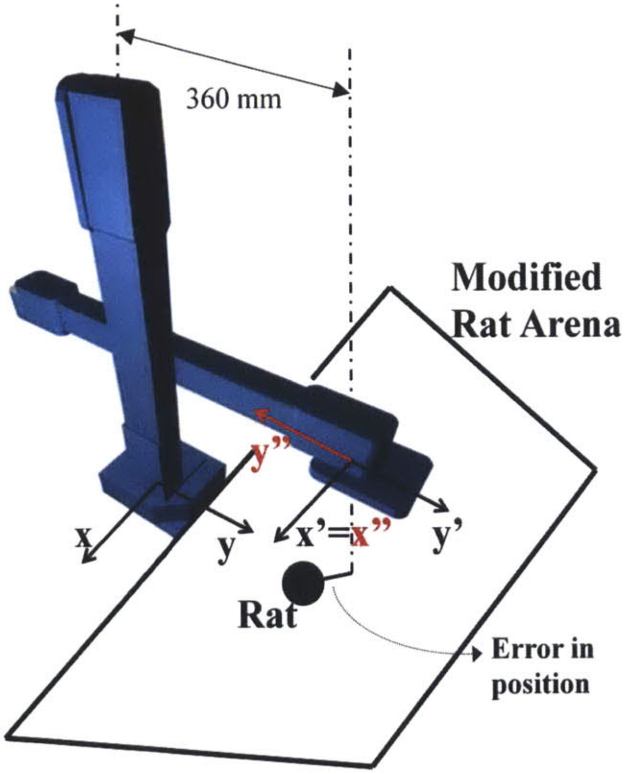

Fig. B-1. Coordinate frames of the BWSS robot in the "home-position". The x-y frame (black), also called the robot frame, is the fixed coordinate for the position of the end-effector of the robot. The x'-y' frame (brown) is attached to the end-effector. The x"-y" frame is also attached to the end-effector (more specifically, to the camera attached at the end-effector). The positive y" axis is opposite to the positive y' axis. In this "home-position", the x'-y' frame is offset 360 mm in the y-direction from the robot frame.

Line 4 of the above code executes a new word named NEWDIRN which is explained below.

```
: NEWDIRN                                                          ···(1)
  STOP ( ." STOP "                                                 ···(2)
  BEGIN ?RUN 0= UNTIL ( ." STOPPED " ASK DROP                      ···(3)
  DSPASSUME COMPUTE                                                ···(4)
  ( SPEED CHANGE )                                                 ···(5)
  ( X2 @ X @ - Y2 @ Y @ - HYP 5 * 2000 + SPEED ! )                 ···(6)
  ( SPEED @ 5 / 200 + ACCEL ! )                                    ···(7)
  X @ 8 / 2048 + DACA                                              ···(8)
  Y @ 8 / 2048 + DACB                                              ···(9)
  X2 @ X @ + X ! Y2 @ Y @ + Y ! ANGLE W ! TRANSFORM DSPSMOOTH (10)
  DROP                                                             ···(11)
;                                                                  ···(12)
```

Lines 1 and 12 envelop lines 2 to 11 to define a new word in the RoboForth dictionary, called NEWDIRN. Line 2 stops the current movement of the robot, if it was still in the process of moving to the previous target position. Otherwise, the robot would already be at zero velocity. Line 3 detects whether the emergency stop button, located at the front panel of the robot controller, has been pressed. If so, the robot stops running the code further. This line comes after line 2, because otherwise, even if the stop button was pressed, the robot would still attempt to finish moving to the previous target location if it was still in the process of doing so.

Line 4 then reads the encoders of all the robot motors and updates the current x-y coordinate (in the robot frame). These values are stored in the pre-defined, designated variables in RoboForth, which are X and Y.

Line 5 to 7 are in parentheses, and RoboForth will ignore these lines. They are in the code in case one wishes to change the speed of the robot depending on the distance between the current position and the target position. Otherwise, the controller will use pre-set values for the maximum speed and acceleration. Line 8 and 9 reads the current position of the robot end-effector, X and Y, and outputs these values through the DAC ports. These values are logged by the Linux machine

Line 10 is the core of the new word NEWDIRN. It updates the target position according to the current position (X and Y) and the relative displacement from it (X2 and Y2), then commands the robot to move to the new target location. Variable W contains the rotation of the end-effector with respect to the robot arm. W is updated by the user-defined word ANGLE such that the x' and y' axes are parallel to the x and y axes, respectively.

Line 11 erases any remaining item in the stack. If all codes were written correctly, there would be no data remaining in the stack. However, due to an unknown bug in the implementation of the pre-defined word TRANSFORM, the code leaves a garbage value in the stack (confirmed by an ST-Robotics engineer). The DROP command flushes the stack. Otherwise, the stack will eventually overflow after multiple executions of the word NEWDIRN, thereby halting the program.

The complete code of the position control loop is presented below:

```
USER X2 USER Y2 USER H2
DECIMAL
CARTESIAN
DISABLE STOP-TIMER

: HYP H2 ! DUP M* H2 @ DUP M* D+ MSQR ;

: ANGLE X @ 10000 M* X @ Y @ HYP M/ ASIN -10 / ;

: NEWDIRN
  STOP ( ." STOP "
  BEGIN ?RUN 0= UNTIL ( ." STOPPED " ASK DROP
  DSPASSUME COMPUTE
  ( SPEED CHANGE )
  ( X2 @ X @ - Y2 @ Y @ - HYP 5 * 2000 + SPEED ! )
  ( SPEED @ 5 / 200 + ACCEL ! )
  X @ 8 / 2048 + DACA
  Y @ 8 / 2048 + DACB
  ( X2 @ X @ + X ! ANGLE W ! TRANSFORM DSPSMOOTH
  X2 @ X @ + X ! Y2 @ Y @ + Y ! ANGLE W ! TRANSFORM DSPSMOOTH
  DROP
;

: ADCGO
0 ADC 2048 - X2 !
1 ADC 2048 - -1 / Y2 !
( X2 ?
( Y2 ?
NEWDIRN
;

: ADCINT
BEEP ADCGO
RETURN
;

: INIT
30000 SPEED !
4000 ACCEL !
SET INTVEC ADCINT
400 INT-TIME !
START-TIMER
;
```

Appendix C

Experiment Procedure

HARDWARE TEST

1. Place the cart in an open space
2. Connect power
3. Make sure Rat Module is fully wired. Put it on a blue block for now.
4. Turn on the power supply
    a. Both Ch1 (~23 V) and Ch2 (5.0 V) should be ON
5. Turn on Black desktop (wait till it boots up completely)
6. Open two terminals
7. In one terminal, Run ./crob/tools/display
    a. Check the status of the four encoders using pcienc 0~3
    b. Check the status of the force sensors using adcvolts[1][0~3]
8. Open (using gedit) /tools/ratexp
    a. Make sure rat_fn = 0, reset_encoder = 1
9. Run ratexp → this will test the four motors
10. Edit ratexp
    a. rat_fn = 1, reset_encoder = 1

   b. measure time = 10 sec, exp time = 10 sec

11. Put the Rat Module's robotic arms to HOME position
12. Run ratexp, test its functionality
13. Do ./tools/all2a and check the logged files and make sure it looks okay
14. Turn off the power supply
15. On the second terminal window, go to /package/code/code
16. Run ./startup
17. Run luvcview and see if there is anything strange. Make sure 30 fps
18. Open uvccapture.c and make sure NOL = high and no file save.
19. Back to editing ratexp
    a. Make sure rat_fn = 1, encoder_zero = 1
20. If you changed ANY C-code during 1~19, be sure to 'make' them again.
21. Leave the computer ON.
22. Disconnect Rat Module of any wires. Move it away from R19 (This is because R19 has to be calibrated)
23. Turn on the laptop
24. Make sure RS-232 is connected
25. Run Robwin63.exe
26. Turn on the R19 controller
27. Do the following in robwin:

   a. ROBOFORTH
   b. START
   c. (make sure R19 is close to HOME position)
   d. CALIBRATE
   e. (when done) HOME
   f. DECIMAL CARTESIAN
   g. Load project: YSS_V1.ed2
   h. File→Open project ed2, check for any strangeness
   i. Upload the project (click on the red down-arrow)
   j. Move R19 to X=0, Y=~3000, appropriate Z

28. In desktop, 2nd terminal, run ./startup again just to make sure
29. Run uvccapture
30. In the other terminal, run ratexp (make sure PSU = off)
31. In Laptop Robwin63, execute INIT
32. Make sure R19 follows the green.
33. In Robwin, type STOP-TIMER
34. Put R19 back to X=0, Y=~3000, W=0
35. halt ratexp and uvccapture

(END OF HARDWARE TEST)

RAT EXPERIMENT STEP-BY-STEP

1. Hardware-wise
    a. PSU is OFF (for now)
    b. Laptop is running Robwin63, loaded project
    c. R19 is at good position (x=0, Y=~3000, W=0)
    d. Desktop is ON
    e. 1st terminal window
        i. Ready to run ratexp
            1. Make sure rat_fn =1, enc_zero = 1 (for now)
            2. Make sure measure_time and exp_time is okay
    f. 2nd terminal window
        i. Do ./startup again
        ii. Ready to run ./uvccapture
2. Rat Preparation
    a. Disconnect Rat Module completely of any wires
    b. Anesthetize the rat
    c. Get the rats on the Elastikon tape belt
    d. Tie the two couplings on the ankles
    e. Put the 'Base' of the Rat Module on the Elastikon belt
    f. Place the rat in the center of the arena

g. *(while the rat is waking up – do these steps quickly)*
    i. Connect the Rat Module wires
    ii. Turn on the PSU (both channels)
    iii. Make the Rat Module on its HOME position
    iv. Desktop, 1st terminal: run ratexp, then quickly turn off
        1. This will zero the encoders

3. ***IT IS IMPORTANT THAT THE DESKTOP AND PSU CH-1 ARE MAINTAINED ON TILL THE END OF THE EXPERIMENT***
4. Experiment is ready to be conducted now
    a. 2nd terminal: run ./startup then run ./uvccapture
    b. 1st terminal: run ratexp
    c. Laptop, Robwin: run INIT
        i. Type (but don't execute) STOP-TIMER

END OF ONE EXPERIMENT

1. ***ASAP***: Robwin: execute STOP-TIMER
2. 1st terminal: stop ratexp
3. 2nd terminal: halt uvccapture

REDO EXPERIMENT

1. Place R19 and the rat at appropriate positions
2. Run ./startup, uvccapture
3. Edit ratexp and make sure all parameters are correct
    a. Especially, make sure enc_zero = 0
4. Run ratexp
5. Laptop: run INIT, get ready to execute STOP-TIMER

END OF ALL EXPERIMENT

1. ***ASAP*****:** laptop: execute STOP-TIMER or even power off R19
2. Halt ratexp, and uvccapture
3. Turn off PSU
4. Disconnect the Rat Module with wires
5. Bring the Rat to a better position
6. Cut-off the ankle couplings
7. Remove the Rat Module from the harness

8. Take off the harness
9. Turning off the hardware:
    a. R19 turn-off
        i. De-energize R19
        ii. Quit Robwin63
        iii. Turnoff R19 controller
    b. Desktop turn-off
        i. Do ./all2a now if leaving the gear in the lab
        ii. Otherwise, nevermind
        iii. Turn off the terminals
        iv. Turn off the PC
    c. Turn off the PSU if not yet done
    d. Unplug the power cord

(END OF ALL EXPERIMENT)

References

[1] ML Tainter and GMA Marcelli, "The Rise of Synthetic Drugs in the American Pharmaceutical Industry," *Bull N Y Acad Med.*, vol. 35, pp. 387–405, 1959.

[2] KG Kinsella, "Changes in Life Expectancy 1900-1990," *Am. J. Clin. Nutrition*, vol. 55, pp. 1196-1202, 1992.

[3] www.nscisc.uab.edu, Spinal Cord Injury Facts and Figures at a Glance, 2011.

[4] J McDonald and C Sadowsky, "Spinal-cord Injury," *The Lancet*, vol. 359, pp. 417-425, 2002.

[5] A Behrman and S Harkema, "Locomotor Training After Human Spinal Cord Injury; A Series of Case Studies," *Physical Therapy*, vol. 80, pp. 688-700, 2000.

[6] S Thuret, LDF Moon, and FH Gage, "Therapeutic interventions after Spinal Cord Injury," *Nature Reviews Neuroscience*, vol. 7, pp. 628-643, 2006.

[7] RD de Leon, JA Hodgson, RR Roy, and VR Edgerton, "Full weight-bearing hindlimb standing following stand training in the adult spinal cat," *J Neurophysiol*, vol. 80, pp. 83-91, 1998.

[8] RD de Leon, JA Hodgson, RR Roy, and VR Edgerton, "Locomotor capacity attributable to step training versus spontaneous recovery after spinalization in adult cats," *J Neurophysiol*, vol. 79, pp. 1329-1340, 1998.

[9] V Dietz, M Wirz, A Curt, and G Colombo, "Locomotor pattern in paraplegic patient: training effects and recovery of spinal cord function," *Spinal Cord*, vol. 36, pp. 380-390, 1998.

[10] RR Roy, RD Sacks, KM Baldwin, M Short, and VR Edgerton, "Interrelationships of contraction time, Vmax and myosin ATPase after spinal transection," *J Appl Physiol*, vol. 56, pp. 1594-1601, 1984.

[11] RR Roy and L Acosta, "Fiber type and fiber size changes in selected thigh muscle six months after low thoracic spinal cord transection in adult cats: exercise effects," *Exp Neurol*, vol. 92, pp. 675-685, 1986.

[12] RR Roy, KM Baldwin, and VR Edgerton, "The plasticity of skeletal muscleL effects of neuromuscular activity," *Exerc Sports Sci Rev*, vol. 19, pp. 269-312, 1991.

[13] RR Roy et al., "Training effects on soleus of cats spinal cord transected (T12-T13) as adults," *Muscle Nerve*, vol. 21, pp. 63-71, 1998.

[14] RR Roy et al., "Differential response of fast hindlimb extensor and flexor muscles to exercise in cats spinalized as adults," *Muscle Nerve*, vol. 22, pp. 230-241, 1999.

[15] S Griller, "Neurobiological bases of rhythmic motor acts in vertebrates," *Science*, vol. 228, pp. 143-149, 1985.

[16] S Grillner et al., "Intrinsic function of a neuronal network – a vertebrate central pattern generator," *Brain Res Rev*, vol. 26, pp. 184-197, 1998.

[17] S Rossignol et al., "The cat model of spinal cord injury," *Prog Brain Res*, vol. 137, pp. 151-168, 2002.

[18] CP de Guzman, RR Roy, JA Hodgson, and VR Edgerton, "Coordination of motor pools controlling the ankle musculature in adult spinal cats during treadmill walking," *Brain Res*, vol. 555, pp. 202-214, 1991.

[19] H Forssberg, S Grillner, and S Rossignol, "Phase dependent reflex reversal during walking

in chronic spinal cats," *Brain Res*, vol. 85, pp. 103-107, 1975.

[20] A Wernig and S Muller, "Improvement of walking in spinal cord injured persons after treadmill training," in *Plasticity of Motoneuronal Connections*, A Wenig, Ed.: Elsevier, 1991, pp. 475-485.

[21] J Duysens and KG Pearson, "Inhibition of flexor burst generation by loading ankle extensor muscles in walking cats," *Brain Res*, vol. 187, pp. 321-332, 1980.

[22] RG Lovely, RJ Gregor, RR Roy, and VR Edgerton, "Effects of training on the recovery of full-weight bearing stepping in the adult spinal cat," *Exp Neurol*, vol. 92, pp. 421-435, 1986.

[23] RG Lovely, RJ Gregor, RR Roy, and VR Edgerton, "Weight-bearing hindlimb stepping in treadmill-exercised adult spinal cats," *Brain Res*, vol. 514, pp. 206-218, 1990.

[24] S Swinnen and J Duysens, *Neuro-Behavioral Determinants of Interlimb Corrdination.*: Kluwer Academic Publishers, 2004.

[25] Stein RB, Ladouceur, M Wieler M et al., "Multicenter evaluation of electrical stimulation systems for walking," *Arch Phys Med Rehabil*, vol. 80, pp. 495-500, 1999.

[26] NJ Tillakaratne et al., "Use-dependent modulation of inhibitory capacity in the feline lumbar spinal cord," *J Neurosci*, vol. 22, pp. 3130-3143, 2002.

[27] V Avelev, N Anissimova, E Khoroshikh, and Y Gerasimenko, "Activation of central pattern generator in cat by epidual spinal cord stimulation," in *Proceedings of the International Symposium on Brain and Movement*, St. Petersburg, Moscow, p. 26.

[28] R Herman, J He, S D'Luzansky, W Willis, and S Dilli, "Spinal cord stimulation facilitates functional walking in a chronic incomplete spinal cord injured," *Spinal Cord*, vol. 40, pp.

65-68, 2002.

[29] RD de Leon, i H Tamak, JA Hodgson, RR Roy, and VR Edgerton, "Hindlimb locomotor and postural training modulates glycinergic inhibition in the pinal cord of the adult spinal cat," *J Neurophysiol*, vol. 82, pp. 359-369, 1999.

[30] JP Kesslak, V So, J Choi, CW Cotman, and F Comez-Pinilla, "Learning upregulates brain-derived neurotrophic factor messenger ribonucleic acid: a mechanism to facilitate encoding and circuit maintenance?," *Behav Neurosci*, vol. 112, pp. 1012-1019, 1998.

[31] R Molteni, Z Ying, and F Gomez-Pinilla, "Differential effects of acute and chronic exercise on plasticity-related genes in the rat hippocampus revealed by microarray," *Eur J Neurosci*, vol. 16, pp. 1007-1116, 2002.

[32] F Gomez-Pinilla, Z Ying, P Opazo, RR Roy, and VR Edgerton, "Differential regulation by exercise of BDNF and NT-3 in rat spinal cord and skeletal muscle," *Eur J Neurosci*, vol. 13, pp. 1078-1084, 2001.

[33] F Gomez-Pinilla, Z Ying, RR Roy, R Molteni, and VR Edgerton, "Voluntary exercise induces a BDNF-mediated mechanism that promotees neuroplasticity," *J Neurophysiol*, vol. 88, pp. 2187-2195, 2002.

[34] YS Lee, I Hsiao, and V Lin, "Peripheral nerve grafts and aFGF restore partial hindlimb function in adult paraplegic rats," *J Neurotrauma*, vol. 19, pp. 1203-1216, 2002.

[35] AJ Fong et al., "Spinal Cord-Transected Mice Learn to Step in Response to Quipazine Treatment and Robotic Training," *J. Neuroscience*, vol. 25, pp. 11738-1747, 2005.

[36] ML Aisen, HI Krebs, N Hogan, F McDowell, and BT Volpe, "The Effect of Robot-Assisted Therapy and Rehabilitative Training on Motor Recovery Following Stroke,"

Arch. Neurol., vol. 54, no. 4, pp. 443-446, 1997.

[37] SE Fasoli and HI, Stein, J, Frontera, WR, Hogan, N Krebs, "Effects of Robotic Therapy on Motor Impairment and Recovery in Chronic Stroke," *Archives of Phys. Medicine & Rehab.*, vol. 84, pp. 477-482, 2003.

[38] M Ferraro et al., "Robot-aided sensorimotor arm training improves outcome in patients with chronic stroke," *Neurology*, vol. 61, pp. 1604-1607, 2003.

[39] L Dipietro et al., "Customized interactive robotic treatment for stroke: EMG-triggered therapy," *IEEE Trans. on Neural Systems and Rehab. Eng.*, vol. 13, no. 3, pp. 325-334, 2005.

[40] S Jezernik, G Colombo, T Keller, H Frueh, and M Morari, "Robotic Orthosis Lokomat: A Rehabilitation and Research Tool," *Neuromodulation: Technology at the Neural Interface*, vol. 6, pp. 108-115, 2003.

[41] SK Banala, SH Kim, SK Agrawal, and JP Scholz, "Robot Assisted Gait Training With Active Leg Exoskeleton (ALEX)," *IEEE Trans. on Neural Systems and Rehab. Eng.*, vol. 17, pp. 2-8, 2009.

[42] DJ Reinkensmeyer et al., "Tools for understanding and optimizing robotic gait training," *J. Rehab. Res. & Development*, vol. 43, pp. 657-671, 2006.

[43] MYC Pang and JF Yang, "The initiation of the swing phase in human infant stepping; the importance of hip position and leg loading," *J Physiol*, vol. 528, pp. 389-404, 2000.

[44] J Ahn et al., "Feasibility of entrainment with ankle mechanical perturbation to treat locomotor deficit of neurologically impaired patients," in *Eng. in Medicine and Biology Society*, 2011, pp. 7474-7477.

[45] MR Dimitrijevic, Y Gerasimenko, and MM Pinter, "Evidence for a spinal central pattern generator in humans," *Ann. N Y Acad. Science*, vol. 860, pp. 360-376, 1998.

[46] SP Rossignol et al., "Intralimb and Interlimb coordination in the cat during real and fictive rhythmic motor programs," *Semin Neurosci*, vol. 5, pp. 67-75, 1993.

[47] CA Giuliani and JL Smith, "Stepping behaviors in chronic spinal cats with one hindlimb deafferented," *J Neurosci*, vol. 7, pp. 2537-2546, 1987.

[48] H Cruse and H Warneck, "Coordination of the legs of a slow-walking cat," *Exp Brain Res*, vol. 89, no. 1, pp. 147-156, 1992.

[49] S Miller, J Van Der Burg, and FGA Van der Meche, "Coordination of movements of the hindlimbs and forelimbs in different forms of locomotion in normal and decerebrate cats," *Brain Res*, vol. 91, pp. 217-237, 1975.

[50] S Miller, J Van Der Burg, and FGA Van der Meche, "Locomotion in the cat: basic programmes of movement," *Brain res*, vol. 91, pp. 239-253, 1975.

[51] AW English and PR Lennard, "Interlimb coordination during stepping in the cat: in-phase stepping and gait transitions," *Brain Res*, vol. 245, pp. 353-364, 1982.

[52] D Yanagihara, M Udo, I Kondo, and T Yoshida, "A new learning paradigm: adaptive changes in interlimb coordination during perturbed locomotion in decerebrate cats," *Neurosci Res*, vol. 18, no. 3, pp. 241-244, 1993.

[53] O Andersson, H Forssberg, and S Grillner, "Phasic gain control of the transmission in cutaneous reflex pathways to motoneurones during 'fictive' locomotion," *Brain Res*, vol. 149, no. 2, pp. 503-507, 1978.

[54] O Andersson and S Grillner, "Peripheral control of the cat's step cycle I. Phase dependent

effects of ramp-movements of the hip during “fictive locomotion”," *Acta Physiol Scand*, vol. 113, pp. 89-101, 1981.

[55] O Andersson and S Grillner, "Peripheral control of the cat’s step cycle. II. Entrainment of the central pattern generators for locomotion by sinusoidal hip movements during “fictive locomotion”," *Acta Physiol Scand*, vol. 118, pp. 229-239, 1983.

[56] C Perret and JA Cabelguen, "Main characteristics of the hindlimb locomotor cycle in the decorticate cat with special reference to bifunctional muscles," *Brain res*, vol. 187, pp. 333-352, 1980.

[57] A Prochazka, JA Stephens, and P Wand, "Muscle spindle discharge in normal and obstructed movements," *J Physiol*, vol. 287, pp. 57-66, 1979.

[58] D Wisleder, RF Zernicke, and JL Smith, "Speed-related changes in hindlimb intersegmental dynamics," *Exp. Brain Res.*, vol. 79, pp. 651-660, 1990.

[59] HWAA Van de Crommert, M Faist, W Berger, and J Duysens, "Biceps fermoris tendon jerk reflexes are enhanced at the end of the swing phase," *Brain Res*, vol. 734, pp. 341-344, 1996.

[60] D Orsal, JM Cabelguen, and C Perret, "rlimb coordination during fictive locomotion in the thalamic cat," *Exp Brain Res*, vol. 82, no. 3, pp. 536-546, 1990.

[61] M Faist, C Blahak, J Duysens, and W Berger, "Modulation of the biceps fermoris tendon jerk reflex during human locomotion," *Exp Brain Res*, vol. 125, pp. 265-270, 1999.

[62] LH Ting, CC Raasch, DA Brown, SA Kautz, and FE Zajac, "Sensorimotor state of the contralateral leg affects ipsilateral muscle coordination of pedaling," *J Neurophysiol*, vol. 80, no. 3, pp. 1341-1351, 1998.

[63] MYC Pang and JF Yang, "Sensory gating for the initiation of the swing phase in different directions of human infant stepping," *J Neurosci*, vol. 22, no. 13, pp. 5734-5740, 2002.

[64] MY Pang, T Lam, and JF Yang, "Infants adapt their stepping to repeated trip-inducing stimuli," *J Neurophysiol*, vol. 90, pp. 2731-2740, 2003.

[65] T Lam and JF Yang, "Could different directions of infact stepping be controlled by the same locomotor central pattern generator?," *J Neurophysiol*, vol. 83, pp. 2814-2824, 2000.

[66] JE Misiaszek, MJ Stephens, JF Yang, and KG Pearson, "Early corrective reactions of the leg to perturbations at the torso during walking in humans," *Exp Brain Res*, vol. 131, no. 4, pp. 511-523, 2000.

[67] SF Donker, "Flexibility of Human Walking: A study on Interlimb Coordination," RUG, Groningen, The Netherlands, 2002.

[68] P Tang and MH Woollacott, "Phase-Dependent Modulation of Proximal and Distal Postural Responses to Slips in Young and Older Adults," *The Journals of Gerontology: Series A*, vol. 54, no. 2, pp. M89-102, 1998.

[69] P Tang, MH Wollacott, and RKY Chong, "Control of reactive balance adjustments in perturbed human walking: roles of proximal and distal postural muscle activity," *Exp Brain Res*, vol. 119, no. 2, pp. 141-152, 1998.

[70] JC Smith and JL Feldman, "In vitro brainstem-spinal cord preparations for study of motor systems for mammalian respiration and locomotion," *J Neurosci Methods*, vol. 21, pp. 321-333, 1987.

[71] JR Cazalets, i Y Sqalli-Houssain, and F Clarac, "Activation of the central pattern generators for locomotion by serotonin and excitatory amino-acids in neonatal rats," *J*

Physiol, vol. 455, pp. 187-204, 1992.

[72] O Kjaerulff and O Kiehn, "Crossed rhythmic synaptic input to motoneurons during selective activation of the contralateral spinal locomotor network," *J Neurosci*, vol. 17, pp. 9433-9447, 1997.

[73] B Ballion, D Morin, and D Viala, "Forelimb locomotor generators and quadrupedal locomotion in the neonatal rat," *Eur J Neurosci*, vol. 14, pp. 1727-1738, 2001.

[74] M Iikuza, H Nishimaru, and N Kudo, "Development of the spatial pattern of 5-HT induced locomotor rhythm in the lumbar spinal cord of rat fetuses in vitro," *Neurosci Res*, vol. 31, pp. 107-111, 1998.

[75] D Morin and D Viala, "Coordination of locomotor and respiratory rhythms in vitro are critically dependent on hindlimb sensory inputs," *J Neurosci*, vol. 22, pp. 4756-4765, 2002.

[76] Clarac F Jamon M, "Early walking in the neonatal rat: a kinematic study," *Behav Neurosci*, vol. 112, pp. 1218-1228, 1998.

[77] JC Norreel et al., "Reversible disorganization of the locomotor pattern after neonatal spinal cord transection in rat," *J Neurosci*, vol. 23, pp. 1924-1932, 2003.

[78] J Altman and S Bayer, *The Development of the Rat Spinal Cord, Advances in Anatomy Embryology and Cell Biology.*: Springer-Verlag, 1984.

[79] EP Zehr and R Chua, "Modulation of human cutaneous reflexes during rhythmic cyclical arm movement," *Exp.l Brain Ress*, vol. 135, pp. 241-250, 2000.

[80] EP Zehr and A Kido, "Neural control of rhythmic, cyclical human arm movement: task dependency, nerve specificity and phase modulation of cutaneous reflexes," *J Physiol*, vol.

537, pp. 1003-1045, 2001.

[81] V Dietz, "Spinal cord lesion: effects of and perspectives for treatment," *Neural Plasticity*, vol. 8, pp. 83-90, 2001.

[82] V Dietz, K Nakazawa, M Wirz, and T Erni, "Level of spinal cord lesion determines locomotor activity in spinal man," *Exp Brain Res*, vol. 128, pp. 405-409, 1999.

[83] V Dietz, "Do human bipeds use quadrupedal coordination?," *Trends Neurosci*, vol. 25, pp. 462-467, 2002.

[84] A Lundberg, "Half-centres revisited. In Regulatory Functions of the CNS. Motion and Organization Principles," *Adv. Physiol. Sci.*, vol. 1, pp. 155-167, 1980.

[85] H Haken, JAS Kelso, and H Bunz, "A theoretical model of phase transitions in human hand movements," *Biol Cybern*, vol. 51, pp. 347-356, 1985.

[86] Ö Ekeberg and K Pearson, "Computer Simulation of Stepping in the Hind Legs of the Cat: An Examination of Mechanisms Regulating the Stance-to-Swing Transition," *J. Neurophysiol.*, vol. 94, pp. 4256-4268, 2005.

[87] JA Nessler et al., "A Robotic Device for Studying Rodent Locomotion After Spinal Cord Injury," *IEEE Trans. on Neural Systems and Rehab. Eng.*, vol. 13, no. 4, pp. 497-506, 2005.

[88] DJ Reinkensmeyer et al., "A Robotic Stepper for Retraining Locomotion in Spinal-Injured Rodents," in *IEEE Int. Conf. on Robotics and Automation*, 2000, pp. 2889-2894.

[89] RD de Leon et al., "U sing robotics to teach the spinal cord to walk," *Brain Res. Rev.*, vol. 40, pp. 267-273, 2002.

[90] S Buerger, "Stable, High-Force, Low-Impedance Robotic Actuators for Human-Interactive

Machines," Massachusetts Institute of Technology, Dissertation 2005.

[91] JE Pereira et al., "A Comparison Analysis of Hindlimb Kinematics During Overground and Treadmill Locomotion in Rats," *Behavioural Brain Research*, vol. 172, pp. 212-218, 2006.

[92] DM Basso, MS Beattie, and JC Bresnahan, "A sensitive and Reliable Locomotor Rating Scale for Open field Testinng in Rats," *J. Neurotrauma*, vol. 12, pp. 1-21, 1995.

[93] M Djawdan and T Garland, "Maximal Running Speeds of Bipedal and Quadrupedal Rodents," *J. Mamm.*, vol. 69, pp. 765-772, 1988.

[94] R Hruska, S Kennedy, and EK Silgergeld, "Quantitative Aspects of Normal Locomotion in Rats," *Life Sciences*, vol. 25, pp. 171-180, 1979.

[95] G Courtine et al., "Transformation of Nonfunctional Spinal Circuits into Functional State after the Loss of Brain Input," *Nature*, vol. 12, no. 10, pp. 1333-1342, 2009.

[96] NH Cook and E Rabinowicz, *Physical Measurement and Analysis.*: Addison-Wesley, 1963.

[97] T Yasuhara et al., "Lack of Exercise, Via Hindlimb Suspension, Impedes Endogenous Neurogenesis," *Neuroscience*, vol. 149, pp. 182-191, 2007.

[98] S Buerger and N Hogan, "Complementary Stability and Loop Shaping for Improved Human-Robot Interaction," *IEEE Transactions on Robotics*, vol. 23, no. 2, pp. 232-244, 2007.

[99] JE Colgate, "The Control of Dynamically Interacting Systems," MIT, Dissertation 1988.

[100] M Zhuang and DP Atherton, "Automatic Tuning of Optimum PID Controller," *IEE Proc. Part D*, pp. 216-224, 1993.

[101] FG Shinskey, *Process Control Systems, Application, Design and Tuning*, 3rd ed. New York: McGraw-Hill, 1988.

[102] JJE Slotine and W Li, *Applied Nonlinear Control*. New Jersey: Prentice Hall, 1991.

[103] M Kermani, M Wong, R Patel, M Moallem, and M Ostojic, "Friction compensation in low and high-reversal-velocity manipulators," in *Proceedings of the International Conference on Robotics and Automation*, 2004, pp. 4320-4325.

[104] B Bona and M Indri, "Friction compensation in robotics: an overview," in *Proceedings of the IEEE Conference on Decision and Control*, 2005, pp. 4360-4367.

[105] B Armstrong-Hélouvry, P Dupont, and CC De Wit, "A Survey of Models, Analysis Tools and Compensation Methods for the Control of Machines with Friction," *Automatica*, vol. 30, no. 7, pp. 1083-1138, 1994.

[106] K Youcef-Toumi and O Ito, "A Time Delay Controller for Systems with Unknown Dynamics," in *American Control Conference*, 1988, pp. 904-913.

[107] M Jin, SH Kang, and PH Chang, "Robust Compliant Motion Control of Robot With Nonlinear Friction Using Time-Delay Estimation," *IEEE Transactions on Industrial Electronics*, vol. 55, no. 1, pp. 258-269, 2008.

[108] SF Giszter, MR Davies, and V Graziani, "Motor Strategies Used by Rats Spinalized at Birth to Maintain Stance in Response to Imposed Perturbations," *Journal of Neurophysiology*, vol. 97, pp. 2663-2675, 2007.

[109] V Filipe et al., "Effect of Skin Movement on the Analysis of Hindlimb Kinematics During Treadmill Locomotion in Rats," *J. of Neuroscience Methods*, vol. 153, pp. 55-61, 2006.

[110] JM Bauman and YH Chang, "High-speed X-ray Video Demonstrates Significant Skin

Movement Errors with Standard Optical Kinematics During Rat Locomotion," *J of Neuroscience Methods*, vol. 186, pp. 18-24, 2010.

[111] LM Costa et al., "The Effect of Gait Speed on Three-Dimentional analysis of Hindlimb Kinematics during Treadmill Locomotion in Rats," *Reviews in the Neuroscience*, vol. 21, pp. 487-497, 2010.

[112] LL Cai, AJ Fong, Y Liang, and J Burdick, "Assist-as-needed Training Paradigms for Robotic Rehabilitations of Spinal Cord Injuries," in *Proc. IEEE Int. Conf. on Robotics and Automation*, 2006, pp. 3504-3511.

[113] W Enard et al., "A Humanized Version of Foxp2 Affects Cortico-Basal Ganglia Circuits in Mice," *Cell*, vol. 137, pp. 961-971, 2009.

[114] WE DeCoteau et al., "Learning-related coordination of striatal and hippocampal theta rhythms during acquisition of a procedural maze task," *Proc. of the National Academy of Science (PNAS)*, vol. 104, pp. 5644-5649, 2007.

[115] V Ego-Stengel and M Wilson, "Disruption of Ripple-Associated Hippocampal Activity During Rest Impairs Spatial Learning in the Rat," *Hippocampus*, vol. 20, pp. 1-10, 2010.

[116] A Ennaceur, S Michalikova, R van Rensburg, and PL Chazot, "Models of Anxiety: Responses of Mice to Novelty and Open Spaces in a 3D maze," *Behavioural Brain Research*, vol. 174, pp. 9-38, 2006.

[117] U Udoekwere, A Ramakrishnan, L Mbi, and SF Giszter, "Robot Application of Elastic Fields to the Pelvis of the Spinal Transected Rat: a Tool for Detailed Assessment and Rehabilitation," in *Proc. IEEE EMBS Annual International Conference*, 2006, pp. 3684-3687.